BATTERY IDENTIFICATION METHODS BASED

ON EQUIVALENT CIRCUIT MODEL

by

MATTHEW RAGSDALE

Presented to the Faculty of the Graduate School of

The University of Texas at Arlington in Partial Fulfillment

of the Requirements

for the Degree of

MASTER OF SCIENCE IN ELECTRICAL ENGINEERING

THE UNIVERSITY OF TEXAS AT ARLINGTON

August 2009

ACKNOWLEDGEMENTS

I would like to thank my graduate advisor, Dr. Babak Fahimi, for his endless patience and sound advice throughout the researching and writing of this thesis.

I would like to thank my committee members, Dr. Wei-Jen Lee and Dr. Rasool Kenarangui for their valuable support and continued patience.

I would also like to thank my family and friends for their loving but irreverent support and encouragement.

July 31, 2009

ABSTRACT

BATTERY IDENTIFICATION METHODS BASED

ON EQUIVALENT CIRCUIT MODEL

Matthew Ragsdale, M.S.

The University of Texas at Arlington, 2009

Supervising Professor: Babak Fahimi

Development of an intelligent battery diagnostic system is a necessity for future transportation industry. These technologies will have the potential to create profound impact in other industries such as portable electronics. This theses reports on a pattern recognition method that is primarily engineered to detect the chemistry, number of cells, and state of charge in an unknown package of batteries. The proposed method has the potential to be used for condition monitoring in a known set of batteries thereby, creating a health monitoring apparatus that can be an integral part of a battery management system using any of the prominent lead acid, lithium-ion, and Nickel Metal Hydride batteries. The proposed method is based on distinct signatures that one can identify in a relatively straightforward equivalent circuit of a battery. These signatures are extracted using time domain diagnostics and are used in combination

with nonlinear mappings such as exponential regression and artificial neural networks for pattern recognition purposes

This thesis presents the design and development of three battery identification methods based on a single RC equivalent circuit model. The first method compares measured circuit parameters with lookup tables using MSE analysis to identify chemistry, cell count, and SOC of the battery. The second method uses an artificial neural network to identify battery chemistry based on measured circuit parameters. The final method uses an artificial neural network to identify battery chemistry and SOC based on raw voltage waveforms, bypassing the need to calculate equivalent circuit parameters.

TABLE OF CONTENTS

LIST OF ILLUSTRATIONS

LIST OF TABLES

CHAPTER 1

INTRODUCTION

1.1 Importance of Battery Management

As time goes on, we become more reliant on technology, and we have more demands on the functionality and longevity of our technology. From cell phones and laptops to electric vehicles and renewable energy systems, all of these devices are becoming more dependent on batteries and battery management to function effectively. Batteries serve an important role in many different markets and each has their own specific and unique requirements for battery design and battery management; these markets can be broadly split into three categories:

1). *Portable Electronics*: Portable electronics, such as cell phones and laptops, keep getting smaller while their power demands grow larger because of advanced features like touch screens and HD video. Because of the variable power loads these devices are subjected to, accurate SOC estimation becomes more challenging and more critical. In addition, with the continual development of new batteries combined with a lack of standardization, a number of portable devices have a range of possible battery chemistries; this is gradually creating demand for universal battery chargers [1].

2). *Electric and Hybrid Electric Vehicles*: Hybrid electric vehicles (HEV) and Plug-in hybrid electric vehicles (PHEV) are making a strong entrance into the automotive market. The ultimate success of these technologies depends on development

1

of a reliable, durable, compact, cost effective, and efficient energy storage system. In this context, determination of state-of- health, and state-of-function in batteries is of paramount significance for successful development of reliable electric and hybrid electric vehicles. Despite this critical role, the research and development on battery monitoring and identification is far from exhausted.   For instance, development of a universal battery monitoring and management system can make it possible for a variety of batteries to be used in a single EV/HEV platform. In fact, with the development of a universal battery charger, devices can be designed for universal battery acceptance without worrying about how to charge or maintain those batteries.   Incorporating universal battery chargers in EV/HEVs will provide the same functionality that FlexFuel systems provide for conventional IC's in Brazil, allowing the customer to choose the best fuel option based on current market prices [2]. An automotive universal battery charger would allow customers to use cheap lead acid batteries for short workday commutes then switch to longer lasting Li-Ion batteries for weekend drives.

3). *Renewable Energy Generation*: Rising oil prices and advances in power electronics are making green technology viable. This has spawned development in a multitude of green technologies, besides HEV and EV development, a significant amount of research is focused on alternative energy sources such as solar and wind. As renewable energy becomes more viable, demand for renewable generators is growing in both residential and commercial sectors. While these generators have the potential to provide cheap or free energy, they are heavily reliant on batteries to provide power during peak time when renewable energy is often less plentiful, such as at nighttime or

2

when there isn't any wind. Because of this critical function, renewable generation is heavily reliant on efficient and robust battery technology to maintain stable operation. Because batteries for this technology are large, expensive and critical to performance, it is exceedingly important to have reliable and accurate SOC and SOH information

1.2 Review of Battery Identification and Battery Monitoring Methods

As the purpose of this thesis is battery identification and battery monitoring, it is important to understand these concepts and to review the work done previously in these fields.

For the purposes of this thesis, battery identification refers to the detection and classification of a battery's electrical properties without prior knowledge; in general terms, this means identifying at least the chemistry and cell count of an unknown battery so that proper charging algorithms can be applied, though more advanced battery identification could include capacity and internal resistance. At present, no useful or significant battery identification methods exist.

Battery monitoring refers to methods that continuously monitor a battery's status using voltage and current measurements; in general, battery monitoring involves measuring a battery's SOC and occasionally their SOH. The current state of battery monitoring includes several different monitoring techniques, but these generally detect either SOC or SOH for fixed battery chemistries.

1.2.1 *Review of SOC Methods*

State of charge (SOC) is a measurement of a battery's remaining energy. This is often expressed as a ratio of the battery's remaining charge vs. the total amp hour (Ah) capacity of the battery, usually expressed as a percentage. This definition bypasses aging effects that lower a battery's total capacity as these are expressed in state of health (SOH). There are dozens of methods to detect SOC but the four most common are discharge test, coulomb counting, open circuit voltage test, and impedance spectroscopy:

1) *Coulomb Counting*: Coulomb counting is the most common method for measuring SOC in high priced systems; it works by keeping track of all the current entering and leaving the battery through integration. Coulomb counting is so popular because it is able to give accurate SOC on demand as long as it knows the battery's initial SOC. Coulomb counting has several main disadvantages: first, it requires expensive current sensors to maintain its accuracy; second, it requires a processor with nonvolatile memory in order to calculate and store the SOC; finally, coulomb counting requires regular recalibration to account for integration errors and current losses. Often systems that use coulomb counting will use one of the other SOC methods for recalibration.

2) *Discharge Test*: The discharge test is the simplest and most reliable method to measure SOC. This method involves discharging the battery down to its minimum safe voltage then recharging it to full capacity and 100% SOC. While the discharge test has the advantage of being the most accurate, it is also useful for removing memory effects

on nickel based batteries and calibrating the coulomb counting method; however, the discharge test is rarely used by itself because it is a wasteful and time consuming process that usually requires taking the battery offline.

3) *Open Circuit Voltage Test*: The second most common SOC method is the open circuit voltage (OCV) test. This method draws a linear relationship between a battery's SOC and its terminal voltage while no load is present. This method's main drawback is waiting for the battery's terminal voltage to settle before measurements can be taken, which is especially cumbersome with lead acid batteries whose settling time is several hours. The OCV method is mainly used on low budget or less critical systems that don't warrant using the other more expensive methods; these budget systems may also sacrifice accuracy by not waiting for the batteries to fully settle. This can cause sudden changes in SOC readings when heavy loads are applied.

4) *Impedance Spectroscopy*: The last method, impedance spectroscopy, uses a small AC current to measure the impedance of the battery, which is then compared to lookup tables to determine SOC. Although this method is heavily researched, it is rarely practiced in actual battery systems due to poor stability in regard to temperature fluctuations and the requirement for special equipment to measure impedance.

1.2.2   *Review of SOH Methods*

The state of health (SOH) of a battery is very loosely defined as the battery's ability to continue performing compared to a new battery. Unlike SOC, SOH has no consistent definition or testing procedure, instead most developers use a definition that

is most suited for the system they are designing. The two most common definitions of SOH are based on internal resistance and usable capacity.

1) *Capacity Test:* The capacity test calculates a battery's SOH by comparing its current maximum capacity with the rated maximum capacity of a new battery. This test is often used with coulomb counting systems to measure a battery's maximum capacity during a full charge/discharge recalibration. This is usually the more preferred method because it doesn't require any added hardware when combined with coulomb counting for SOC measurements.

2) *Impedance Test*: The impedance test uses impedance spectroscopy to measure a battery's internal resistance, which increases over time and heavy use; the current internal resistance is compared to the battery's original value to determine SOH. Since internal resistance directly affects a battery's maximum power output; this is often expressed as a percentage of maximum power. This method depends on knowing a battery's internal resistance when new; this requires measuring a battery's impedance when it's first installed and saving it for future tests.

1.3 Objectives of Current Research

The goal of this thesis is to develop novel battery identification methods for use in intelligent battery management systems for all battery chemistries. In principle, a battery management system based on battery identification would not only allow unrestricted battery use but would also be more reliable and accurate because it factors in more battery parameters. In order to develop universal battery charger/monitors, one needs reconfigurable software that can accurately monitor and identify the kinds of

batteries being used in a specific configuration. Deterioration of the fundamental parameters in a known chemistry can be interpreted as an alarming sign in the state-of health in a battery. This thesis is focused primarily on chemistry detection and SOC estimation; as such SOH is regarded as a secondary objective and is only considered in extreme cases when poor SOH results in false chemistry detection in a known battery, a more complete SOH investigation is simply beyond the scope this research and is reserved for future work.

1.4 Review of Proposed Methods

Over the course of research, three distinct identification methods were designed and investigated, a Statistical Analysis method, a Neural Network method, and a Hybrid method developed as an intermediate step from the Statistical Analysis method to the neural network method. All of these methods are based on the principle that any battery can be modeled as a simple Thevenin equivalent RC circuit with a unique set of circuit parameters; figure 1.1 shows the circuit used for this research. Each method functions by analyzing the charging and settling voltage waveforms of the unknown battery during a controlled pulse charge. The Statistical Analysis method was designed first; all others are refinements on this original method.
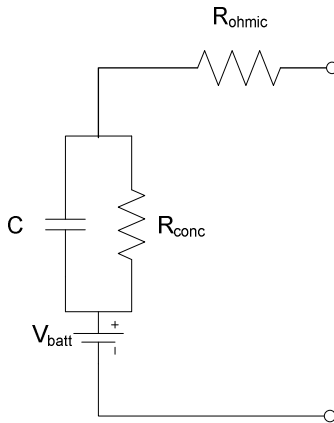
Figure 1.1: Simple RC Equivalent Circuit

1.4.1 *Statistical Analysis Method*

The original method was the Statistical Analysis method, which derived equations for the four circuit parameters in figure 1.1 using KVL and KCL analysis at the transient and boundary conditions present during a pulse charge. The Statistical Analysis method is a multistage process. The first step uses a line fitting function to derive line equations for the charging and settling voltage waveforms, and then the coefficients of the line equations are fed into the derived circuit equations to generate a set of equivalent circuit parameters. In order to complete the identification, the four circuit parameters are compared with lookup tables using MSE analysis. In order to calibrate the detection process, weigh terms are applied to all the inputs to the MSE analysis stage.

Since the equivalent circuit model in figure 1.1 is linear while battery properties are nonlinear, the derived circuit parameter vary with respect to SOC, so the reference lookup tables must be a function of chemistry and SOC. Fortunately, initial thesis

8

research showed that for a given battery chemistry, the circuit parameters scaled linearly in regards to capacity and cell count, so the lookup tables need not be a function of these parameters as well.

Fully testing the Statistical Analysis method revealed several advantages and disadvantages. The Statistical Analysis method's main selling points are its accuracy, expandability, and completeness. Because this method is based on firm circuit model theory implemented in a series of easily understood steps; the results are calibrated for accuracy and the process reveals insight into the nature and operation of batteries. In addition, the equation based modular design facilitates expanding the outputs to provide additional useful information such as specific gravity, electrolyte resistance, or SOH. Unfortunately, most of these advantages are academic in nature while the disadvantages are not. The Statistical Analysis method is lacking in efficiency, simplicity, and accuracy when compared to the neural network method. This is mainly due to the lengthy and computationally expensive line fitting techniques and the difficulty of calibrating the weight terms, which require advances input correlation analysis and loss functions augmented with experience. The correlation analysis is used to determine which inputs are most important and the loss functions are used to properly scale the weight terms. Due to time and resource constraints, the correlation analysis was never performed and the loss functions were never fully implemented before the research shifted to neural network analysis, even without these last steps the Statistical Analysis method performed admirably but suffered from stability issues.

1.4.2 *Hybrid Method*

The Hybrid method began as a modification to the Statistical Analysis method, in which the MSE step was replaced with a neural network. This modification would replace the correlation analysis and loss functions requirements with a simple training procedure. This intermediate method proved to be an effective solution for the accuracy problems of the incomplete Statistical Analysis method, but it did little to reduce the complexity or computational expense inherited from the Statistical Analysis method. Moreover, the Hybrid method suffered its own stability issues due to software errors in the line fitting algorithm, revealing the ultimate limitations of this method. Efforts to correct these issues led to the development of the Neural Network method.

1.4.3 *Neural Network Method*

The Neural Network method employs a novel use for neural networks because it operates directly on the voltage waveforms. Traditional neural networks generally use a small number of inputs whose values directly correlate with the outputs; in terms of this project that would relate to using the derived circuit parameters as inputs or a combination of terminal voltage, current, temperature, and coulomb count capacity as was done in other neural network projects [3]. Instead, the Neural Network method accepts the entire 90 point voltage waveform as its inputs, in this way the Neural Network method mimics the Statistical Analysis method except that the neural network performs the line fitting, derives the circuit parameters, and identifies all of the battery characteristics in a single step. The main advantages of the Neural Network method are its simple and compact design, computational efficiency, easy calibration, and superior

accuracy. The only slight disadvantages are its lack of insight and the randomness inherent in training. As shown in figure 1.2, the neural network is composed of interconnected nodes with seemingly random values; because of this, the Neural Network method offers no insight into how or why the current output is generated. Also, because the training processes are based on random numbers, the training time and overall accuracy of a particular training session are unknown, and the system may require several trainings to achiever the desired accuracy. Ultimately however these disadvantages are academic in nature and are far outweighed by the advantages of this method.
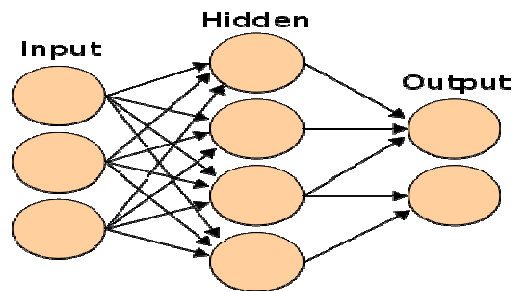
Figure 1.2: Generic Neural Network Model.

CHAPTER 2

BATTERY BACKGROUND

2.1 List of Included Batteries

Although this research is based on battery identification, some limits need to be placed on the range of possible battery chemistries. Currently, several dozen different battery chemistries are in use but only a handful are used extensively enough to warrant inclusion as possible battery candidates. Out of all the possible battery chemistries, only lithium ion (Li-Ion), lead acid, and nickel-metal hydride (NiMH) were included in this research. A fourth chemistry, nickel cadmium (NiCd), was briefly considered but was ultimately excluded because of its impending obsolete status and insufficient data was available for that chemistry.

2.2 Lead Acid Batteries

2.2.1 *History and Review of Lead Acid Batteries*

Lead acid batteries are the oldest and the most well defined rechargeable batteries. There are two types, the wet cell and the gel cell. The wet cell, also known as the flooded lead acid battery or simply the lead acid battery, was invented by Gaston Planté in 1859 [4]; this is the battery most commonly used for traditional automotive applications. The gel cell, most often referred to as SLA (sealed lead acid) or VRLA (valve regulated lead acid) are a class of maintenance free lead acid batteries developed

12

during the 70's. SLA batteries differ from flooded lead acid because they are completely sealed, except for a safety vent, and their electrolyte is gelled so that they are spill proof. These differences make SLA batteries maintenance free. Lead acid batteries generally come in two different types, SLI (starter, lights, and ignition) for automotive purposes and deep cycle batteries for long term power use, golf carts, UPS (uninterruptable power supplies), energy storage, etc. Both batteries share the same chemistry and construction but the SLI batteries are optimized for the higher power output required for a starter motor, while the deep cycle batteries are optimized for capacity and cycle life required for primary power applications.

2.2.2   *Lead Acid Chemistry*

Each cell contains (in the charged state) electrodes of lead metal (Pb) and lead (IV) dioxide (PbO_2) in an electrolyte of about 33.5% *v/v* (6 Molar) sulphuric acid (H_2SO_4). In the discharged state both electrodes turn into lead(II) sulfate ($PbSO_4$) and the electrolyte loses its dissolved sulphuric acid and becomes primarily water. Due to the freezing-point depression of water, as the battery discharges and the concentration of sulphuric acid decreases, the electrolyte is more likely to freeze.

$$Pb + PbO_2 + 2H_2SO_4 \underset{\text{charge}}{\overset{\text{discharge}}{\rightleftharpoons}} 2PbSO_4 + 2H_2O$$

(2.1)
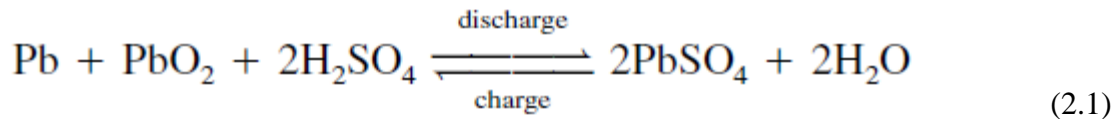
Because of the open cells with liquid electrolyte in most lead-acid batteries, overcharging with excessive charging voltages will generate oxygen and hydrogen gas by electrolysis of water, forming an explosive mix. The acid electrolyte is also corrosive.

Practical cells are usually not made with pure lead but have small amounts of antimony, tin, calcium or selenium alloyed in the plate material. [5]

2.2.3 *Lead Acid Construction*

All lead acid batteries are made of lead and lead dioxide plates suspended in an electrolyte of sulphuric acid with a separator to isolate the positive and negative plates. The positive plates are made of lead dioxide while the negative plates are made of regular lead. The plates of SLI batteries are about 0.040" (1mm) thick, while the typical deep cycle battery will have plates that are between 0.07-0.11" (1.8- 2.8mm) thick. Each plate consists of a rectangular lead grid alloyed with antimony or calcium to improve the mechanical characteristics. [5]. The holes of the grid are filled with a paste mad of red lead and dilute sulphuric acid, this paste allows the sulphuric acid to react with the lead inside the plate, increasing the surface area many fold. The paste material used to make battery plates also contains carbon black, blanc fixe (barium sulfate) and lignosulfonate. The blanc fixe acts as a seed crystal for the lead to lead sulfate reaction. The blanc fixe must be fully dispersed in the paste in order for it to be effective. The lignosulfonate prevents the negative plate from forming a solid mass of lead sulfate during the discharge cycle. It enables the formation of long needle like crystals. The long crystals have more surface area and are easily converted back to the original state on charging. Carbon black counteracts the effect of inhibiting formation caused by the lignosulfonates. [6]. One of the problems with the plates is that the plates increase in size as the active material absorbs sulfate from the acid during discharge and decrease as they give up the sulfate during charging. This causes the plates to gradually shed the

paste during their life. It is important that there is plenty of room underneath the plates to catch this shed material. If this material reaches the plates a shorted cell will occur.

2.2.4   *Applications for Lead Acid Batteries*

Lead acid batteries used to be the exclusive rechargeable battery, but today they are only used in three specific markets that favor low price over small size.

1) *Starter Batteries*: Lead acid batteries are used primarily in automotive and stationary power applications. The majority of lead acid batteries are of the SLI type used in almost every automobile. And not just automobiles, boats planes and just about anything with an engine uses SLI type lead acid batteries. Even with more attractive battery options, lead acid batteries are still used in automotive applications due to their low price, reliability, and well known operation and maintenance.

2) *Standby Power Supply*: Lead acid batteries remain popular for standby power applications, for both small scale home applications and large scale power grid applications. Smaller-sized batteries are used for energy storage in systems employing renewable but interruptible energy sources, such as wind and solar energy. These systems are usually located on the customer side of the utility power grid. Golf-cart-type lead-acid batteries and modified electric-vehicle designs are widely used in these small stationary energy-storage systems because they are the least expensive design in commercial production. For large scale applications, lead acid batteries are now being considered for load leveling in electric utility systems as an alternative to meet peak power demands currently provided with energy-expensive oil- or gas-fueled turbines. Large batteries, on the order of 50 MWh at 1000 V, are required. The goal is to obtain

in excess of 2000 cycles or 10 year of operation at a cost of about $90 per kilowatt-hour.

3) *Uninterruptable Power Supply*: Another popular market for lead acid batteries is for uninterruptable power supplies (UPS). These are commonly used with computers to provide a continuity of service in the event of an interruption of the utility power. UPS's function as surge protectors and short term backup power supplies, converting the input AC power to DC to charge the battery then back to AC to provide pure clean AC power to sensitive devices. Upon power interruption, DC power is drawn from the battery and converted to AC to supply emergency power to critical loads. Depending on the size of the battery and the number of devices connected, commercially available UPS systems can provide power for 5 to 30 minutes on average. SLA batteries of 6 to 12 Ahs are the preferred choice for UPS systems because of their low cost and maintenance free operation.

2.2.5 *Pros and Cons of Lead Acid Batteries*

Lead acid batteries are the oldest form of rechargeable batteries, and despite their disadvantages they are still viable for standby and automotive applications. The main disadvantages of lead acid batteries are their low energy density and poor cycle life; these disadvantages make lead acid batteries unsuitable for most portable applications except for automotive, where size is less of an issue. The primary advantages of lead acid batteries are their relatively low cost, high rate capacity, and maintenance free operation; these advantages make lead acid batteries perfectly viable for standby power

and UPS operations, where bulky but cheap high capacity batteries can sit unattended for extended periods of time.

2.3 Nickel Metal Hydride Batteries

2.3.1 *History and Review of Nickel-Metal Hydride Batteries*

The Nickel Metal Hydride battery (NiMH) was the most common portable electronics battery; it powered everything from flashlights, cell phones, even a few electric vehicles. The NiMH battery was developed in 1989 as an improvement of the Nickel Hydrogen Cell commonly used in spacecraft and satellites [7]. Chemically, the NiMH battery is similar to the nickel cadmium (NiCd) battery except that the cadmium is replaced with a metal hydride alloy, which is non toxic and has a higher energy density. Because of NiMH's moderate energy density and reasonable cost, it rapidly became the portable battery of choice, replacing NiCd in all but the higher power devices. This trend continued until Li-Ion batteries became more acceptable and dominated the high end electronics market [7]. Today, NiMH batteries are still the most popular standalone rechargeable battery, available in the standard AA, AAA, C, and D cells. NiMH has a number of advantages that make it such a popular battery, namely the second highest energy density available combined with the second lowest cost; its main disadvantages are high self discharge, low current delivery, and low cycle life, though improvements over the years have reduced or eliminated most of these defects.

2.3.2 *Nickel-Metal Hydride Chemistry*

The negative electrode reaction occurring in a NiMH cell is

$$H_2O + M + e^- \rightleftharpoons OH^- + MH. \tag{2.2}$$

The electrode is charged in the right direction of this equation and discharged in the left direction. On the positive electrode, nickel oxyhydroxide (NiOOH) is formed,

$$Ni(OH)_2 + OH^- \rightleftharpoons NiO(OH) + H_2O + e^-. \tag{2.3}$$
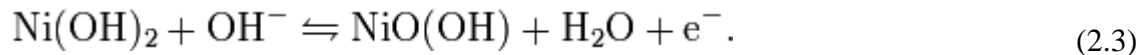
The "metal" M in the negative electrode of a NiMH cell is actually an intermetallic compound. Many different compounds have been developed for this application, but those in current use fall into two classes. The most common is AB_5, where A is a rare earth mixture of lanthanum, cerium, neodymium, praseodymium and B is nickel, cobalt, manganese, and/or aluminium. Very few cells use higher-capacity negative material electrodes based on AB_2 compounds, where A is titanium and/or vanadium and B is zirconium or nickel, modified with chromium, cobalt, iron, and/or manganese, due to the reduced life performances. Any of these compounds serves the same role, reversibly forming a mixture of metal hydride compounds [8].

When overcharged at low rates, oxygen produced at the positive electrode passes through the separator and recombines at the surface of the negative. Hydrogen evolution is suppressed and the charging energy is converted to heat. This process allows NiMH cells to remain sealed in normal operation and to be maintenance-free. NiMH cells have an alkaline electrolyte, usually potassium hydroxide [8].

2.3.3 *Nickel-Metal Hydride Construction*

1) *Cylindrical Batteries*: The assembly of the cylindrical unit is shown in Fig. 2.1. The electrodes are spirally wound and the assembly is inserted into a cylindrical nickel-plated steel can. The electrolyte is added and contained within the pores of the electrodes and separator.
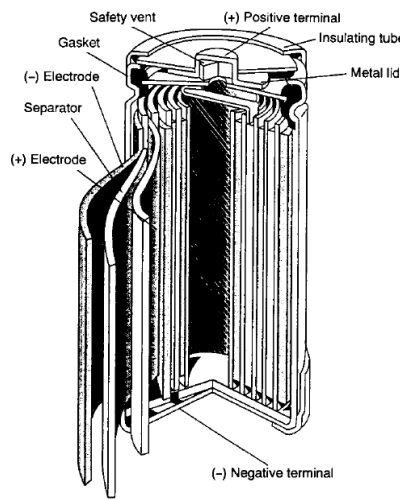

Figure 2.1: Diagram of Cylindrical Nickel Metal Hydride Battery.

The cell is sealed by crimping the top assembly to the can. The top assembly consists of a lid, which includes a resealable safety vent, a terminal cap, and a plastic gasket. The can serves as the negative terminal and the lid as the positive terminal, both insulated from each other by the gasket. The vent provides additional safety by releasing any excessive pressure that may build up if the battery is subjected to abuse.

2) *Prismatic Batteries*: The thin prismatic batteries are designed to meet the needs of compact equipment. The rectangular shape permits more efficient battery

assembly, eliminating the voids that occur with the assembly of cylindrical cells. The volumetric energy density of the battery can be increased by a factor of about 20%. The prismatic cells also offer more flexibility in the design of batteries, as the battery footprint is not controlled by the diameter of the cylindrical cell. Figure 29.2c shows the structure of the prismatic battery.
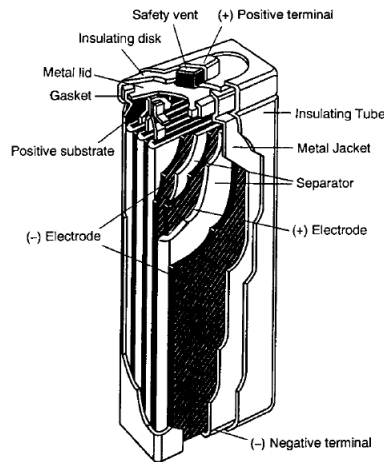

Figure 2.2: Diagram of Prismatic Nickel Metal Hydride Battery.

The electrodes are manufactured in a similar manner as the electrodes for the cylindrical cell, except that the finished electrodes are flat and rectangular in shape. The flat electrodes are then assembled, with the positive and negative electrodes interspaced by separator sheets, and welded to the cover plate. The assembly is then placed in the nickel-plated steel can and the electrolyte is added. The cell is sealed by crimping the top assembly to the can. The top assembly is a lid which incorporates a resealable safety vent, a terminal cap, and a plastic gasket, similar to the one used on the cylindrical cell. An insulating heat-shrink tube is placed over the metal can (jacket). The bottom of the

metal can serves as the negative terminal and the top lid as the positive terminal. The gasket insulates the terminals from each other [9].

2.3.4 *Applications for Nickel-Metal Hydride Batteries*

1) *Portable Electronics*: Shortly after their development in 1989, NiMH replaced the NiCd battery as the number one rechargeable battery for portable consumer electronics in all areas except power tools. As consumer demand for longer battery life grew, the more durable NiCd battery was replaced with the NiMH due to its 40% greater capacity [10]. Currently, NiMH batteries dominate the low end consumer electronics market, where NiMH batteries of the common AA, AAA, C, and D sizes are often used in place of the disposable alkaline batteries. In fact, NiMH batteries are so common in this market share that special orders are required to obtain any other rechargeable battery chemistry in the AA, AAA, C, and D sizes. Li-Ion batteries have replace NiMH batteries in the high end consumer electronics such as cell phones and laptops, which often feature integrated battery chargers that can handle the special charging needs of Li-Ion. Advancements in electrode design and packaging have allowed NiMH batteries to meet and even exceed NiCd current rates, though their cycle life is still poor at these high rates. Because of this, NiMH batteries gained acceptance in high drain electronics such as power tools and RC vehicles; although they are soon to be replaced by high rate Li-Ion batteries [10] [11].

2) *Stationary Power Supply*: Despite the long dominance of flooded lead acid batteries, the stationary power and UPS markets have begun to switch over to NiMH batteries. Despite the fact that NiMH batteries exceed lead acid in every way except

cost, lead acid has been the preferred choice due to customer familiarity and concerns about NiMH's long term performance because they were new to the market. However, commercially available UPS systems require a fourth of the floor space, a tenth of the weight, last up to ten times as many cycles and require a fraction of the maintenance and safety protocols as flooded lead acid batteries due to their low maintenance and environmentally friendly materials [12]. NiMH batteries have yet to fully catch on but changeover is very likely.

3) *EV and HEV*: NiMH batteries are currently the most popular batteries for HEV and EV applications due to their low cost, moderate energy density, and reliable operation. However, talk amongst automakers is that the next generation of EV and HEV vehicles will use Li-Ion. Although Li-Ion batteries have better energy density, the NiMH batteries have reliably given EV's 110 mile ranges with over 80,000 service miles, while the Li-Ion batteries have only limited testing in the Tesla roadster and a projected service lifetime of 50,000 miles [13].

4) *Small scale portable*: NiMH batteries are so popular for the AA and AAA market that it is often hard to find any other rechargeable batteries in these sizes

2.3.5 *Pros and Cons of Nickel-Metal Hydride Batteries*

Nickel metal hydride batteries are a good midrange battery, in terms of cost and energy density they fall right between lead acid and Li-Ion batteries. Their main advantages are relatively low price, 50+% higher capacity than a comparable lead acid battery, and they are constructed from environmentally friendly materials. Their main

22

disadvantage is their low durability; they cannot handle high discharge current, deep cycling, hot temperature, and overcharging.

2.4 Lithium Ion Batteries

2.4.1 *History and Review of Lithium Ion Batteries*

Li-Ion batteries are one of the most popular battery types, with one of the best energy-to-weight ratios, no memory effect, and a slow loss of charge when not in use. In addition to uses for consumer electronics, lithium-ion batteries are growing in popularity for defense, automotive, and aerospace applications due to their high energy density. Currently, numerous competing Li-Ion chemistries are available, each with their own advantages and disadvantages compared to each other. While all modern Li-Ion batteries use the same materials for the anode and electrolyte, they vary widely in cathode material and are usually classified by cathode material alone. The three most common are lithium cobalt oxide ($LiCoO_2$), lithium manganese oxide ($LiMn_2O_4$), and lithium iron phosphate ($LiFePO_4$).

In the 1970s, Lithium ion batteries were first proposed by M.S. Whittingham (Binghamton University), then at Exxon. Whittingham used titanium(II) sulfide as the cathode and lithium metal as the anode [14].

In 1980, the electrochemical properties of the lithium intercalation in graphite were first discovered by Rachid Yazami et al. at the Grenoble National Polytechnic Institute (INPG) and National Center for Scientific Research (CNRS) in France. They showed the reversible intercalation of lithium into graphite in a Lithium/polymer electrolyte/graphite half-cell.

Lithium batteries in which the anode is made from metallic lithium pose severe safety issues. As a result, lithium-ion batteries were developed in which the anode, like the cathode, is made of a material containing lithium ions.

In 1983, Michael Thackeray, John Goodenough, and coworkers identified lithium manganese oxide as a cathode material (spinel) [15]. Spinel showed great promise, since it is a low-cost material, has good electronic and lithium ion conductivity, and possesses a three-dimensional structure which gives it good structural stability.

In 1991, Sony released the first commercial lithium-ion battery, a lithium cobalt oxide chemistry. These batteries revolutionized consumer electronics.

In 1996, Padhi, Goodenough and coworkers identified the lithium iron phosphate ($LiFePO_4$) as cathode material for lithium ion batteries [16].

In 2002, Yet-Ming Chiang and his group at MIT published a paper in which they showed a dramatic improvement in the performance of Li batteries by boosting the material's conductivity by doping it with aluminium, niobium and zirconium, though at the time, the exact mechanism causing the increase became the subject of a heated debate [7].

In 2004, Chiang again increased performance by utilizing iron-phosphate particles less than 100 nanometres across. This miniaturized the particle density by almost 100 fold, increased the surface area of the electrode and improved the battery's ability to store and deliver energy. Commercialization of the iron-phosphate technology

led to a competitive market and a patent-infringement battle between Chiang and Goodenough, two of the leading developers of the technology [7].

2.4.2   *Lithium Ion Chemistry*

Lithium-ion (Li-Ion) batteries are comprised of cells that employ lithium intercalation compounds as the positive and negative materials. As a battery is cycled, lithium ions (Li_) exchange between the positive and negative electrodes. They are also referred to as rocking chair batteries as the lithium ions ''rock'' back and forth between the positive and negative electrodes as the cell is charged and discharged. When a cell is discharging, the lithium is extracted from the anode and inserted into the cathode. When the cell is charging, the reverse process occurs: lithium is extracted from the cathode and inserted into the anode [17].

The anode of a conventional Li-Ion cell is made from carbon, the cathode is one of several metal oxides or other materials, and the electrolyte is a lithium salt in an organic solvent [18].

Useful work can only be extracted if electrons flow through an external circuit. Therefore the half reactions are enlightening. The following equations are written in units of moles, making it possible to use the coefficient *x*. The cathode half reaction (with charging being forwards) is:

$$LiCoO_2 \leftrightarrows Li_{1-x}CoO_2 + xLi^+ + xe^- \tag{2.4}$$
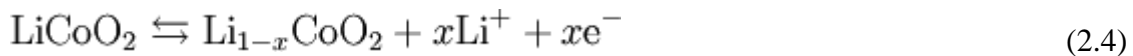
The anode half reaction is:

$$xLi^+ + xe^- + 6C \leftrightarrows Li_xC_6 \tag{2.5}$$

25

The overall reaction has limits. Over discharge will supersaturate lithium cobalt oxide, leading to the production of lithium oxide, possibly by the following irreversible reaction:

$$Li^+ + LiCoO_2 \rightarrow Li_2O + CoO \qquad (2.6)$$

Overcharge up to 5.2V leads to the synthesis of cobalt(IV) oxide, as evidenced by x-ray diffraction

$$LiCoO_2 \rightarrow Li^+ + CoO_2 \qquad (2.7)$$

2.4.3   *Differences between Lithium Ion Chemistry*

1) *Lithium Cobalt LiCoO₂*: Lithium Cobalt is a mature, proven, industry-standard battery technology that provides moderate cycle life and energy density compared to other lithium ion chemistries. The cell voltage is 3.7 Volts. Cells using this chemistry are available from a wide range of manufacturers. The use of Cobalt is unfortunately associated with environmental and toxic hazards [19].

Table 2.1 Lithium Cobalt Statistics

Chemistry	Voltage	Energy Density	Working Temp.	Cycle Life	Safety	Cost vs. SLA
LiCoO2	3.7V	>200 wh/kg	-20 - 60 °C	> 500	Unsafe without PCB or PCM	1.5-2.0

2) *Lithium Manganese Spinel LiMnNi*: Lithium Manganese Spinel provides a higher cell voltage than Cobalt based chemistries at 3.8 to 4 Volts but the energy density is about 20% less. It also provides additional benefits to Lithium-ion chemistry, including lower cost and higher temperature performance. This chemistry is more stable than Lithium Cobalt technology and thus inherently safer but the trade off is lower

26

potential energy densities. Lithium Manganese Spinel cells are also widely available but they are not yet as common as Lithium Cobalt cells. Manganese, unlike Cobalt, is a safe and more environmentally benign cathode material [19].

Table 2.2 Lithium Manganese Spinel Statistics

Chemistry	Voltage	Energy Density	Working Temp.	Cycle Life	Safety	Cost vs. SLA
LiMnxNiyCozO2	3.7V	>160 wh/kg	-20 - 40 °C	>500	Unsafe without PCB or PCM	1.5-2.0

3) *Lithium Iron Phosphate*: The key advantages for $LiFePO_4$ when compared with $LiCoO_2$ are improved safety through higher resistance to thermal runaway, longer cycle and calendar life, higher current or peak-power rating, and use of iron and phosphate which have lower environmental impact than cobalt. Phosphates significantly reduce the drawbacks of the Cobalt chemistry, particularly the cost, safety and environmental characteristics. Once more the trade off is a reduction of 14% in energy density, but higher energy variants are being explored.[19] While $LiFePO_4$ cells have lower voltage and energy density than normal, $LiCoO_2$ Li-Ion cells, this disadvantage is offset by the greater calendar-life of $LiFePO_4$ when compared with all other lithium-ion battery chemistries. After one year, a $LiFePO_4$ cell is likely to have higher energy density than a normal, $LiCoO_2$ Li-Ion cell due to the differences in their respective calendar-lives.

Table 2.3 Lithium Iron Phosphate Statistics

Chemistry	Voltage	Energy Density	Working Temp.	Cycle Life	Safety	Cost vs. SLA
$LiFePO_4$	3.2V	>120 wh/kg	-0-60 °C	>2000	Safe	0.15-0.25

2.4.4 *Applications for Lithium Ion Batteries*

Currently lithium ion batteries are suitable in all applications that require high energy density, such as portable electronics or electric vehicles, and with further advances they could eventually encompass all battery use.

1) *Portable electronics*: Lithium ion batteries are the dominant and most preferred battery for portable electronics, due to their high energy density and constant power throughout discharge. The current level of battery technology makes lithium ion equally suitable for laptops and power tools and all other portable devices. The only area of portable electronics that lithium ion batteries are excluded from is the disposable battery market, where rechargeable batteries replace alkaline batteries, this is because it is to difficult and impractical to construct 1.5 V lithium ion batteries in general and it is dangerous to construct lithium ion batteries in common AA, AAA, C, and D sizes which customers might inadvertently use the wrong charger and explode the batteries.

2) *HEV and EV*: Currently the hottest growth market for lithium ion batteries is the EV and PHEV market, where high energy density outweighs almost every other battery factor. Rapid improvements in lithium ion technology combined with intellectual property issues with other battery chemistries have made lithium ion

batteries the preferred choice for vehicular applications, such as the Tesla Roadster and the Chevy Volt [13].

2.4.5 *Pros and Cons of Lithium Ion Batteries*

Lithium ion batteries are extremely popular and their market is growing because of their advantages over all other chemistries. Lithium ion's main advantage is its high energy density, highest among all competing rechargeable batteries. This advantage allows for extremely light batteries for portable applications or extremely powerful and oversized batteries compared to other chemistries of similar weight and volume. The next major advantage is higher cell voltage, which allows lithium ion batteries to achieve required pack voltages with fewer cells in series. This is very advantageous in high power systems like EV's because fewer cells in series reduce the electronics needed for cell balancing and battery management. Also, having fewer cells in series increases pack longevity because it is less likely that one of the batteries will fail. Small change in voltage during discharge is another small but important advantage because it allows full power output over entire SOC range while SLA and NiMH batteries power drop off after 50% SOC [10]. This feature reduces the need for DC/DC converters to regulate voltage but it does make SOC harder to measure. In addition, lithium ion batteries have the lowest self discharge of all rechargeable batteries. In fact, the batteries by themselves have almost no self discharge but the protection circuits packaged inside the batteries and battery packs often create a 1-5% discharge per month [cite this], which is still far lower than NiMH, lithium ion's closest competitor, which has a self discharge as high as 30% a month. Finally, lithium ion batteries do not suffer

29

from the memory effect, commonly associated with NiMH and NiCd batteries, which lowers battery capacity after repeated shallow cycles. This lack of a memory effect allows lithium ion batteries to accept thousands of shallow cycles without any adverse effects. All of these advantages are shared by all lithium ion chemistries, but certain specific chemistries like lithium iron phosphate have the added advantage of high current rate and the highest cycle life of all rechargeable batteries [19] at a small cost to energy density compared to other lithium ion chemistries.

Despite all of these advantages, lithium ion batteries have a few disadvantages that prevent them from immediate acceptance in all markets. The foremost disadvantage is safety and durability, lithium ion batteries are far less tolerant of abuse than the other rechargeable batteries and they have a tendency to catch fire or explode if abused, this is the main reason that lithium ion batteries require protection circuits. Although some lithium chemistries are more tolerant than others, namely lithium iron phosphate, the potential for catastrophic failure still exists. The main cause for explosive lithium ion failure is a short circuit, which can be caused by a number of preventable and unpreventable events. A short circuit generates a lot of heat which causes thermal runaway. The two most common and preventable events are overcharge and puncturing the separator between the electrodes. Overcharging the battery generates excess heat and plating on the electrodes which can lead to an internal short, and puncturing the separator creates a path between the electrodes. The one unavoidable cause of failure is deposits of lithium metal inside the cell; this rare side effect of the manufacturing process is the leading cause of battery recall [19]. The

second major disadvantage of lithium ion batteries is their cost. Due to complicated cell design and added protection circuits, lithium ion batteries are the most expensive of all rechargeable batteries, almost double of NiMH. Although mass production and rising nickel prices will make lithium ion more attractive, it will probably remain more expensive than the other chemistries. Finally, a lesser known but significant disadvantage is lithium ion's poor shelf life. Lithium ion batteries continuously loose capacity after manufacture, regardless if they are in use or not. This capacity loss is often mistaken for self discharge. Because of this continuous capacity loss, lithium ion batteries generally have a finite shelf life of five years or less [17].

CHAPTER 3

STATISTICAL ANALYSIS METHOD

3.1 Review of Battery Modeling Methods

As mentioned previously, all of this research is derived from an RC equivalent

battery model, which is a well researched and fully validated area of battery research.

Before going into detail about the battery model, a little background into battery models

is called for. In general, battery models provide insight into the inner workings of

batteries and help to predict their external characteristics. Battery models are used

primarily to simulate battery performance or to aid in measuring battery characteristics.

The current research in battery modeling revolves around two distinct types of battery

models, namely electrochemical models and equivalent system models.

1) *Electrochemical Battery Models*: Electrochemical battery models seek to

model the physical and chemical processes of batteries; these models are often

extremely complex and based on partial differentials in one or more dimensions.

Electrochemical models in general have a high degree of accuracy and they provide a

great deal of insight into the inner workings of batteries and how they affect the

battery's external characteristics. Unfortunately, the high degree of complexity in

electrochemical models tends to make them computationally intensive and slow, which

generally makes them suitable only for simulations. One such model requires 112

Gflops of computational power, for which the authors used the nine core processor

inside a playstation 3 [20]. Moreover, most electrochemical models require detailed information about the physical and chemical makeup of target batteries, which isn't always available because of intellectual property issues. Another sample electrochemical model is capable of modeling changes in a battery's physical or chemical structure [21]. This model reasonably describes how changes in cathode material or electrolyte composition will affect the external characteristics of a battery, but like many electrochemical models, it requires numerous specific details such as conductance, concentration, and molar density of electrolyte, diffusion rate of separator, and exact physical dimensions of anode and cathode. Generally, electrochemical models are of more use to battery designers than to automotive or electronics designers because they have more access to detailed battery electrochemical data and a better understanding of battery science, so electrochemical models are more natural and intuitive for them.

2) *Equivalent System Models*: Equivalent system models seek to increase our understanding and control over distinct and complex systems; this is generally accomplished by modeling them with simpler and more generic systems. For batteries, the most common equivalent system models are impulse response, state space description, and equivalent circuit models, with the equivalent circuit models being the most popular. Both impulse response and state space models are purely mathematical representations, and although they are capable of moderately high degree of accuracy, they usually require extremely high quadratic or sinusoidal equations that are extremely difficult to simulate or derive; very little information is available for these types of

33

battery models. Equivalent circuit battery models try to simulate a battery's electrical characteristics by designing a circuit with the same characteristics. Equivalent circuit models tend to range in complexity from simple equivalent Thevenin circuits to complex RLC circuits with cascaded parallel and series architecture as seen in figure 3.1 below.
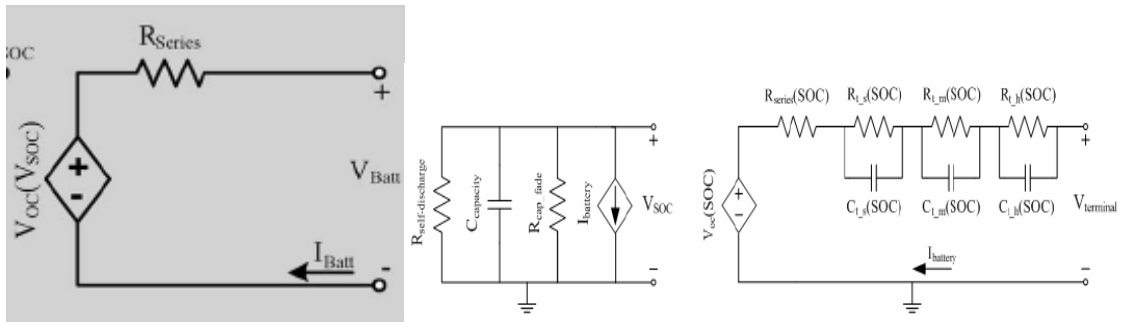
Figure 3.1: Various Equivalent Circuit Models [22].

All of these equivalent circuit models generally have reasonable to excellent accuracy at modeling some or most of a battery's electrical characteristics. Also, because a battery's electrical characteristics usually vary with SOC, most equivalent circuit models have circuit components that are functions of SOC. The simpler models, like the Thevenin in figure xx generally have very good accuracy over a short range of parameters, much like linearized models of nonlinear systems. These simple models rely on complex functions or lookup tables to model component changes based on SOC, discharge rate, and temperature, which all cause significant variations in circuit components. Simple equivalent circuit models have a major advantage in implementation and computation time. Because of their simplicity and small size,

34

simple equivalent circuits require a small amount of computer memory and processing power, and they are usually fast enough for real time applications. Unfortunately, because of their linear nature, they are rarely able to model rapidly changing load conditions, such as regenerative breaking, with any degree of accuracy [23]. Simple equivalent circuits are very useful for modeling batteries under predictable load conditions, such as constant current charging and discharging. Complex equivalent circuit models generally have a higher degree of accuracy over the simple models, and they continue to function over a larger range of operating parameters. Complex equivalent circuit models are essentially improved versions of the simpler equivalent circuit models, anything the simple ones can do, the complex ones can do more accurately, even under unstable circumstances, such as rapidly changing load current or temperature fluctuations. This increased accuracy and functionality comes at a cost, complex model generally have more than twice as many circuit components than a simpler equivalent circuit model and the circuit components often have complex correlations, which require several times the computer memory and processing power to simulate. The majority of the complex equivalent circuit models are only useful for offline simulations because the processing time usually requires two minutes per second of real time simulated [22].

3.2 Discussion of Chosen RC Equivalent Circuit Model

As mentioned previously, the goal of this research is to develop a battery identification and monitoring method, one capable of identifying any unknown battery and accurately monitoring its SOC in real time in order to safely and effectively charge

it. In comparison, all of the discussed modeling methods are designed for simulating or monitoring a specific and well known battery. However, the proposed method is designed for completely unknown batteries, whose chemistry, capacity, SOC, and cell count are never provided and can change without notification. Because of these unknown and changing operating conditions, a static, pre-generated battery model is ill suited at best. This battery identification method requires a battery model that can be actively reconfigured around the unknown battery in order to identify and monitor it

The battery identification methods are based on actively modeling of a battery as an RC equivalent circuit, using the charging and settling voltage waveforms of the battery as it undergoes pulse charging. By comparing the estimated battery parameters with ideal references, all of the battery's properties can be determined, including chemistry, SOC, and even SOH. Because of this, a simple battery model is required whose parameters can be easily extracted in real time using an automated process. To accomplish this, the relatively simple 4 element RC equivalent circuit shown in figure 3.2 was chosen.
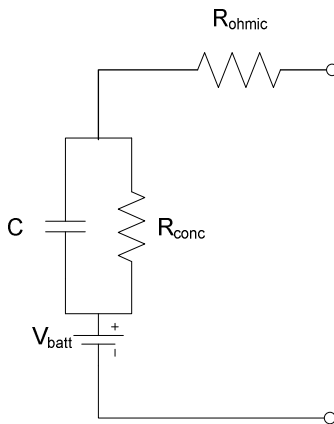
Figure 3.2: Chosen RC equivalent circuit.

This battery equivalent circuit provides a convenient model to quantify all of a battery's characteristics into four circuit parameters, $V_{batt}, C, R_{conc}, and\ R_{ohmic}$ (see figure 3.2). These four circuit parameters represent different parts of a battery. R_{ohmic} represents the electrode and packaging resistance of the battery, R_{conc} represents the battery's internal resistance, which defines the maximum current a battery can deliver and accounts for charging and discharging losses. C is the double layer capacitance of a battery, which accounts for transient effects when the load is changed. V_{batt} represents the battery's open circuit voltage. Generic equations for each of these parameters can be derived from the model using KCL and KVL, one example set is listed below

$$V_{batt} = \left(\frac{V_1 e^{t_1/\tau} - V_2 e^{t_2/\tau}}{e^{t_1/\tau} - e^{t_2/\tau}} \right) \tag{3.1}$$

$$R_{conc} = \frac{e^{t_1/\tau}\left(e^{t_2/\tau}(V_1 - V_2) + V_o'\right) - V_o' e^{t_2/\tau}}{I\left(e^{t_1/\tau} - e^{t_2/\tau}\right)} \tag{3.2}$$

$$C = \frac{\tau}{R_{conc}} \tag{3.3}$$

$$R_{ohmic} = \frac{e^{t_2/\tau}\left(V_{batt} - V_2 + e^{t_1/\tau}(V_2 - V_1) + V_o'\right)}{I\left(e^{t_1/\tau} - e^{t_2/\tau}\right)} - \frac{e^{t_1/\tau}\left(V_{batt} - V_2 + V_o'\right)}{I\left(e^{t_1/\tau} - e^{t_2/\tau}\right)} \tag{3.4}$$

Where I is the current, V_1, V_2 , and V_3 are voltage sample taken at equally spaced times t_1, t_2, and t_3, and V_o' is the voltage across the capacitor, the equations for V_o' are in (3.5) and (3.6) below. Tau is calculated using equation (3.7); the delta t is the difference between t_1 and t_2.

$$V_o' = V_o e^{-t/\tau}$$

(3.5)

$$V_o = \left(\frac{V_2 - V_1}{e^{-t_2/\tau} - e^{-t_1/\tau}} \right)$$

(3.6)

$$\tau = \frac{-\Delta t}{2} \frac{V_3 - V_1}{V_3 + V_1 - 2V_2}$$

(3.7)

3.3 Hardware Setup

For the experimental test bed, the BK precision 9123 programmable power supply shown in figure 3.3 was used; it provides full power supply functionality in the 0 – 5 amp and 0 – 30 volt range. In addition, the power supply incorporates a 12 bit ADC for both voltage and current measurements. The BK power supply can connect to any PC using a standard serial or GPIB interface in order to transmit data collected or to receive new power supply settings. In addition to the power supply, the program LabView was used to manage and control all experiments. The LabView software was chosen because it has built in support for serial communication in order to control the BK power supply as well as the ability save and process all data collected and store it in

38

any desired file type. Additionally, LabView can integrate with a number of other powerful software suites, including MatLab which can be useful for future work. The main benefit of LabView is the ability to control the BK power supply in order to automate the pulse charging process that forms the basis of this research. In order to have consistent results, the pulse charging must be accurately timed in order to have consistent current pulses and evenly spaced sample points, all of which are near impossible to do by hand; moreover, the LabView software can electronically change the power supply settings much faster than could ever be done by hand.

In terms of battery selection, the focus of this research is on small scale, portable electronics batteries of the three most popular chemistries, Li-Ion, NiMH, and SLA. Although the goal is to design a universally applicable battery identification method, the proposed battery identification method is developed in the form of a household universal battery charger in order to simplify the scope of the research. With this simplification in mind, only the most commonly available batteries, of each chemistry was chosen; only batteries suitable for an external battery charger, ideally using the standard AA, AAA, C, and D form factors when available. For the NiMH batteries, a 24 piece set of 2.3Ah AA batteries made by Tenergy was selected; these were divided into battery packs of 1, 2, 4, 6, and 10 cells. For lead acid batteries, only the sealed type (SLA) was used because they are the only type available for small scale portable applications. Four different SLA batteries were selected. First is a 3 piece set of 4 volt, 4.5Ah SLA batteries made by Power Sonic, these were grouped separately and in pairs during testing. Next, there is one 6 volt, 4Ah battery and one 12 volt, 7Ah battery both

made by Genesis, each used individually during testing. Finally, a 3 piece set of 2 volt,

2.5Ah Cyclon batteries made by EnerSys, these were used in 1 to 3 cell battery packs.

The Cyclon batteries are a special 2 volt version of the common SLA battery that comes

in the D cell form factor instead of the box form factor. A sample set of the test

batteries is shown in figure 3.3.
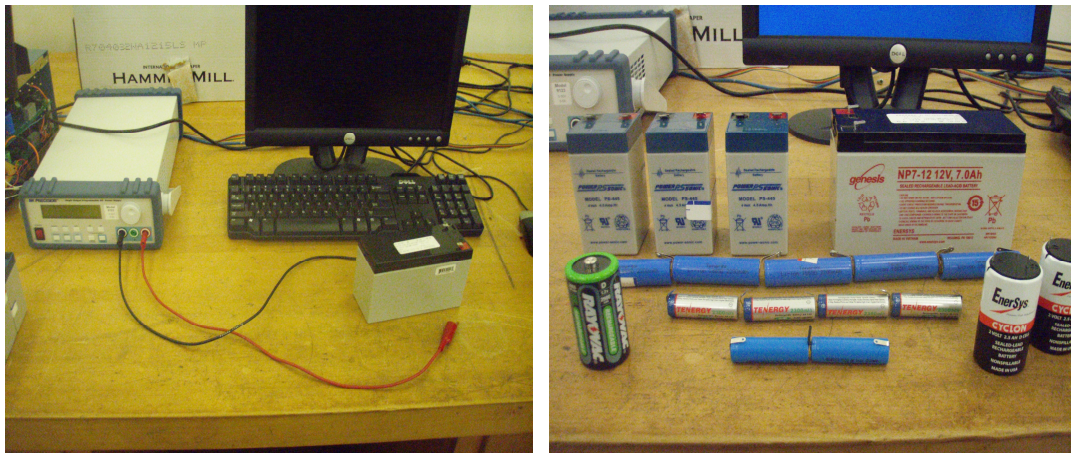
Figure 3.3: BK Power Supply with Controlling PC and Test Batteries.

As mentioned previously, this research began as part of the International Future

Energy Competition (IFEC), where the project was to design a standalone universal

battery charger. BK used while prototype constructed, prototype was programmable

supply with built in microcontroller to execute Statistical Analysis method. Prototype

worked ok but not as good as BK and DSP had no data export so was unsuitable for

data collection, and DSP too weak and cumbersome for experimentation. Only BK

power supply was used during this research, but the prototype is available for final

implementation if desired.

3.4 Implementation of Statistical Analysis Method

3.4.1 *Data Collection and Modified Parameter Equations*

The goal of this project is to continuously remodel the unknown battery using charging and settling voltage waveforms collected during a standard pulse charging. By using a simple RC equivalent circuit model and efficient, easy to use parameter equations, it is possible to model the battery online and in real time. Unfortunately, because the equivalent circuit model and the parameter equations are so simple, any simulation based on them will only be a crude approximation of the battery's output and will only be valid under the same testing conditions that the model was generated. To overcome this limitation, the circuit parameters will not be used for simulation, instead, they will be compared to ideal parameter lookup tables generated from well known batteries under the same testing conditions. In order to simplify the research procedure, all of the batteries are charged using a fixed charging pulse, a 50% duty cycle 1 minute period pulse with a quarter amp amplitude. An automated procedure will use this fixed current pulse to collect a 90 point charging and settling voltage waveform, a sample of which is provided in figure 3.4.
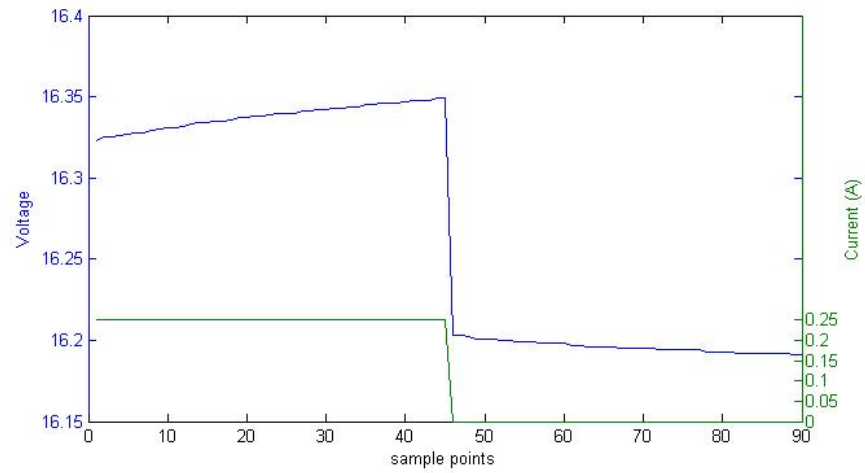
Figure 3.4: Fixed Quarter Amp Charging Pulse with Sample Voltage Waveform.

The equations derived above are included mainly for reference sake, they are based on an ideal equivalent circuit with noise free voltage waveforms, in practice, the voltage waveforms proved too noisy which caused problems choosing specific voltage samples to calculate the circuit parameters. So instead, it was chosen to take advantage of the advance tools in the LabView experimentation platform to adopt a line fitting approach to parameter estimation. Shown in figure 3.5 below are the charging and settling waveforms captured in labview, along with the exponential line fitting, samples are in white line fit in red.
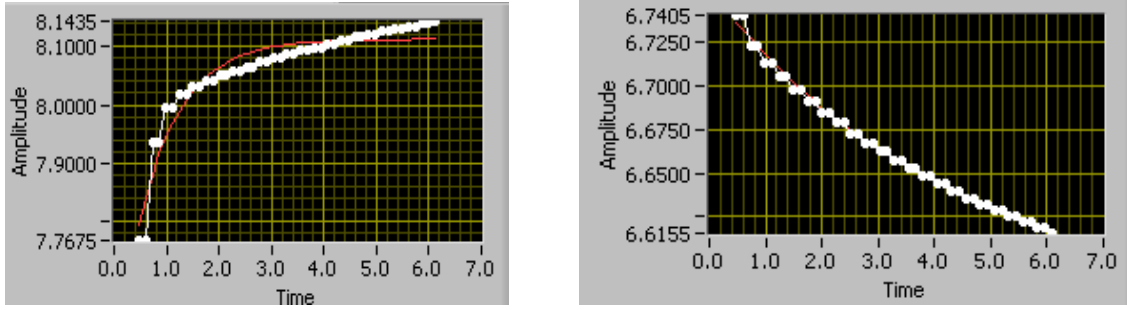
Figure 3.5: Charging and Settling Voltage Waveforms with Line Fit.

A nonlinear lev-mar line approximation algorithm supplied by labview was used; it fit both of the voltage waveforms to the exponential equations below, with all of the a_{x0} terms for the charging plot and a_{x1} terms for the settling plot.

$$Y = a_{00}e^{a_{10} \times x} + a_{20} \qquad\qquad Y = a_0 e^{a_{11} \times x} + a_{21} \qquad\qquad (3.8)$$

Below are a simpler set of circuit parameter equations based on the coefficients from the line fitting equations in (3.8).

$$tay = \frac{\left(\dfrac{-1}{a_{10}} + \dfrac{-1}{a_{11}}\right)}{2} \qquad\qquad (3.9)$$

$$R_{ohmic} = \frac{\left(a_{20} - a_{21} - e^{-t/tay}\left(-a_{00} + a_{01}e^{t/tay}\right)\right)}{I} \qquad\qquad (3.10)$$

$$R_{conc} = \frac{e^{-t/tay}\left(-a_{00} + a_{01}e^{t/tay}\right)}{I} \qquad\qquad (3.11)$$

43

$$V_{batt} = a_{21} \tag{3.12}$$

$$C = \frac{tay}{R_{conc}} \tag{3.13}$$

3.4.2 *Overview of LabView Implementation*

Following is a complete and detailed description of the battery identification method based on RC equivalent circuit parameters, hereto referred to as the Statistical Analysis method. The description is organized around the LabView implementation and includes reference figures and descriptions of all relevant LabView functions and block diagrams. The LabView program is organized into three function blocks, a parameter estimation block, a detection block, and a master control block. The parameter estimation block conducts a single pulse charge when called, during this pulse charge, it simultaneously collects the voltage waveforms and uses them to calculate the battery's RC circuit parameters for that moment of time. The detection block is responsible for filtering and analyzing the array of circuit parameters in order to identify the battery's characteristics, using lookup tables and mean square error (MSE) analysis to accomplish this. The master control block is responsible for overseeing the entire experiment, its main duties are to manage battery charging and handling the flow of data between the two sub blocks. The main control block manages battery charging by continuously calling the parameter estimation block a preset number of times or until

44

an end of charge condition is detected on the battery. The main control block handles data flow by compiling the stream of circuit parameters into an array and feeding it to the detection block when it is called.

3.4.3 *Main Control Block*

Now for a more detailed look at the main control block, the LabView program is shown in figure 3.6. As mentioned previously, the main control block manages battery charging and data flow. For the charging task, the main control block utilizes a simple fifty pulse iteration combined with a manual stop button. While this method provides simple and error free operation, it does require a supervising human operator to issue a manual stop when end of charge is reached. Although several automated EOC routines were designed, they were ultimately excluded due to time constraints and an unfortunate programming error during early development that prompted a more cautious approach to battery charging. The main control block is actually quite basic, this simple routine uses the LabView equivalent of a while loop to repeatedly call the parameter estimation block until the loop counter exceeds forty nine or the stop command is issued.
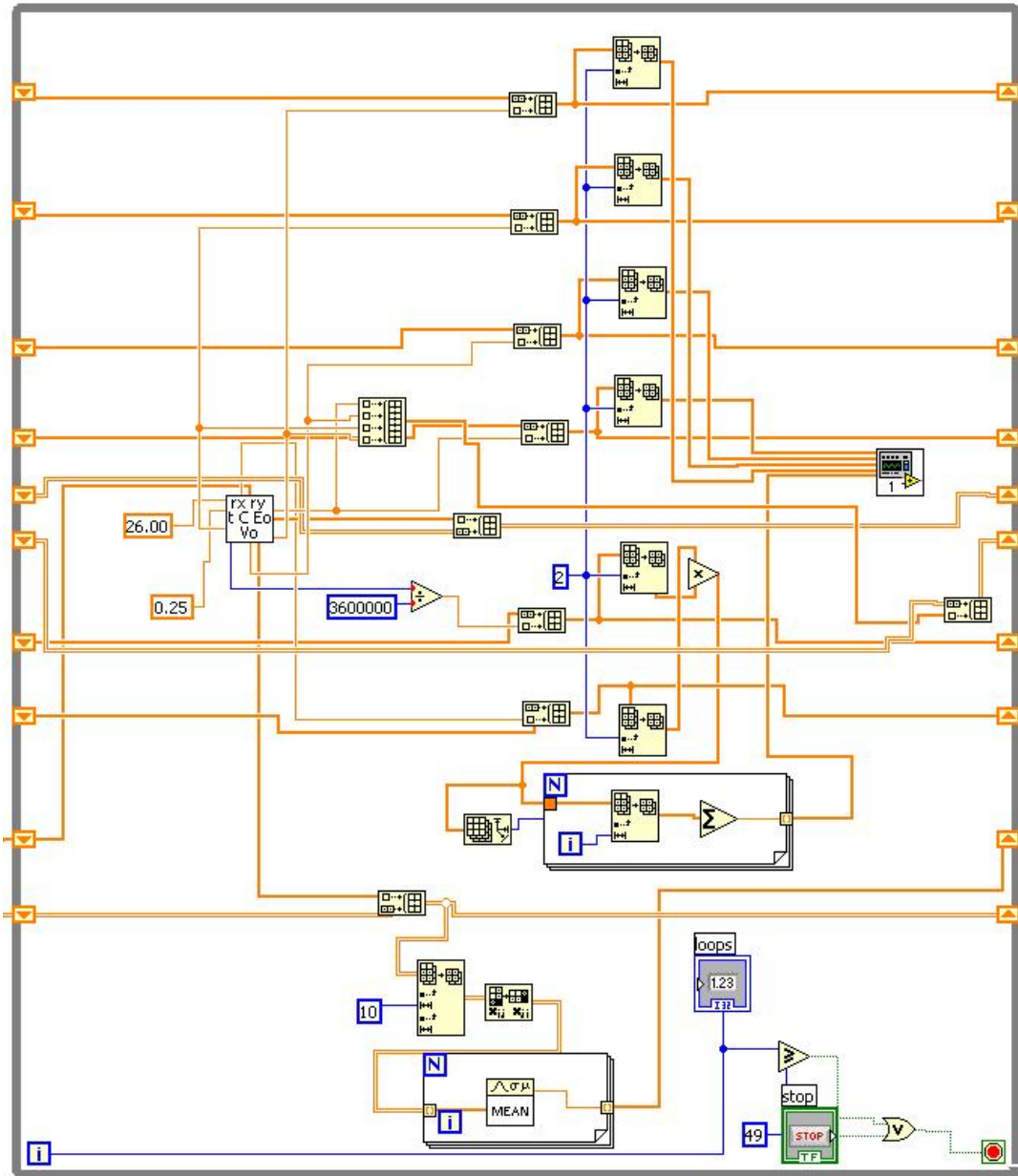
Figure 3.6: LabView Main Control Block Code.

Now to discuss the data flow, all operation inside the main control block are conducted inside the charge control loop. During each iteration, the main control block, calls the parameter estimation block, receives the voltage waveforms and estimated

46

parameters, calculates the coulomb count, updates the growing arrays with current parameters and coulomb count, then feeds the updated arrays to the detection block. With this setup, the main control block generates new battery detections after each current pulse. As a secondary feature, the main control block saves the compiled voltage and parameter arrays to a file after the charge is completed.

3.4.4   *Parameter Estimation Block*

Now for a more detailed look at the parameter estimation block, the LabView program is shown in figures 3.7. The parameter estimation block has three main tasks, performing a single current pulse, measuring the resulting voltage waveforms, and using the collected data to estimate the equivalent circuit parameters. The data collection and pulse generation tasks are combined by using the measurement procedure to time the current pulse. Each current pulse has two phases; a 30 sec on phase followed by a 30 second off phase, each phase uses the exact same procedure. The procedure for each phase is illustrated in the flow chart in figure x, first the appropriate on or off command is sent to the power supply, then a loop of 50 sample and wait commands are issued. This approach compensates for the serial communication time by dividing the 30 second pulse time into a set of 50 spaces voltage samples. After each pulse phase, the measure voltage waveform is sent to the nonlinear Lev-Mar fit block, provided by LabView. The Lev-Mar block uses the Levenberg-Marquardt algorithm to calculate the best set of coefficients for equations (3.8) to fit the voltage waveforms. Finally, after both voltage waveforms are line fitted, the coefficients are sent to a function block which estimates the circuit parameters using equations (3.9) through

47

(3.12) listed previously. After the circuit parameters are calculated, the parameter estimation block ends by sending the estimated parameters and measured voltage waveforms to the main control block.
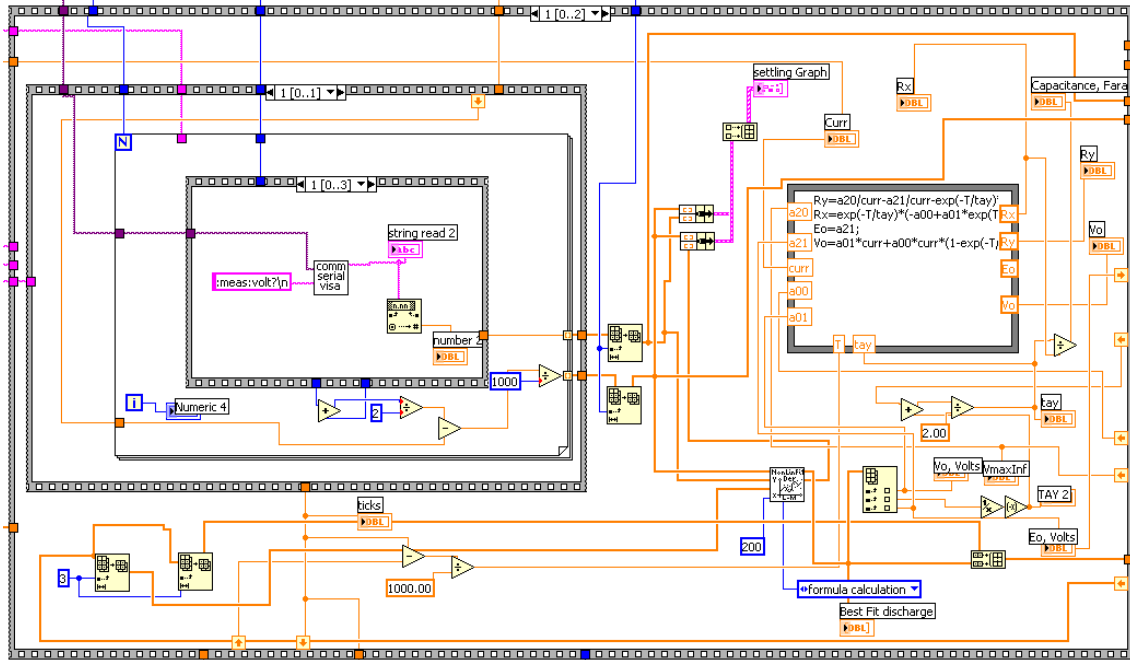
Figure 3.7: LabView Parameter Estimation Block Code.

3.4.5 *Detection Block*

Now for a more detailed look at the detection block. The detection block is responsible for filtering the parameter data then processing it through a series of estimations steps in order to identify the most likely set of battery characteristics. The detection block is based on a set of 12 normalized lookup tables, 4 per chemistry which consist of the 4 circuit parameters; each lookup table is a function of SOC. By studying previously collected sets of estimated parameters, it was discovered that any combination of cell count and Ah capacity of a given battery chemistry could be

normalized to a single set of circuit parameters that vary with SOC. Because of this, any battery configuration can be expressed as a scaled version of the appropriate normalized lookup table using the equations below, where n is cell count and m is capacity in Ah.

$$V_{batt,measured} = n\left(V_{batt,normalized}\right) \tag{3.13}$$

$$C_{measured} = \frac{m}{n}\left(C_{normalized}\right) \tag{3.14}$$

$$R_{conc,measured} = \frac{n}{m}\left(R_{conc,normalized}\right) \tag{3.15}$$

$$R_{ohmic,measured} = \frac{n}{m}\left(R_{ohmic,normalized}\right) \tag{3.16}$$

The first stage of the detection block is the filtering stage, where the incoming parameter arrays are filtered and preprocessed. The filtering stage applies a simple linear fit to each of the incoming arrays, in order to remove noise fluctuations. Then the linearized arrays are averaged to provide a single set of parameters to test. Figure 3.8 shows the LabView program for this stage.
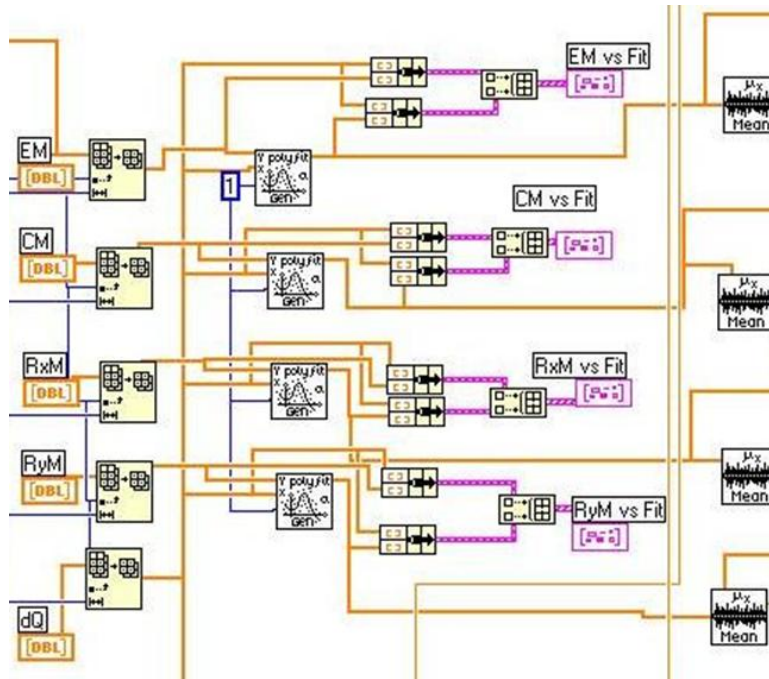
Figure 3.8: LabView Filtering Stage Code.

After the filtering stage is the identification stage, which is composed of three estimation steps, candidate selection, capacity estimation, and mean square error (MSE) analysis. The first step is candidate selection, where the measured V_{batt} is compared with V_{batt} profiles of every possible battery configuration within the experimental parameters, up to 24 volt battery packs which allows a total of 38 battery candidates. This comparison is accomplished by scaling the three V_{batt} lookup table by cell count, using equation (3.13), in order to match the 38 battery candidates. Once the battery comparison task is completed, all of the suitable battery candidates are compiled into an array that list the chemistry, cell count, and SOC of matching V_{batt} for each battery candidate; this array is sent to the next estimation step. Figure 3.9 shows the candidate selection part of the LabView program.

50
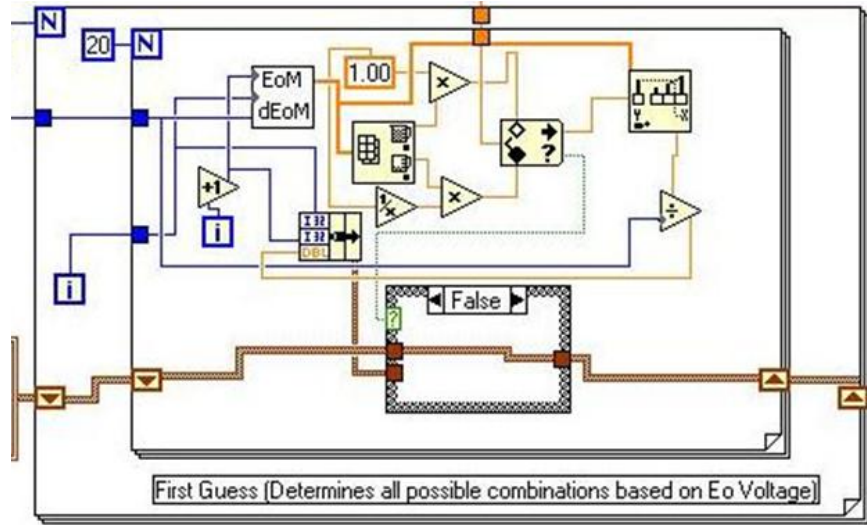
Figure 3.9: LabView Candidate Selection Stage Code.

Nested For loops cycle through chemistry and cell count options and send them to the V_{batt} lookup table function, which returns the properly scaled V_{batt} of the selected chemistry. Next a min/max function determines if the measured V_{batt} is within the range of V_{batt} values of the candidate battery. Lastly, if the measured V_{batt} resides within the V_{batt} range of a candidate battery, a linear interpolation function calculates the closest matching V_{batt} value in the lookup table and returns the corresponding SOC.

The second estimation step is the capacity estimation step, which calculates the appropriate Ah capacity of each battery candidate. This is accomplished by comparing the candidate parameter, at the default 1Ah scale, to the measured parameters using equation (3.17), derived from equations (3.13) through (3.16) listed previously.

$$ m = \frac{1}{3}\frac{V_{batt,measured}}{V_{batt,candidate}}\left(\frac{C_{measured}}{C_{candidate}} + \frac{R_{conc,candidate}}{R_{conc,measured}} + \frac{R_{ohmic,candidate}}{R_{ohmic,measured}} \right) \tag{3.17} $$

The LabView program for this step is shown in figure x., the mdet function block calculates the estimated capacity for each candidate battery, and then candidate array is updated and sent to the next step.
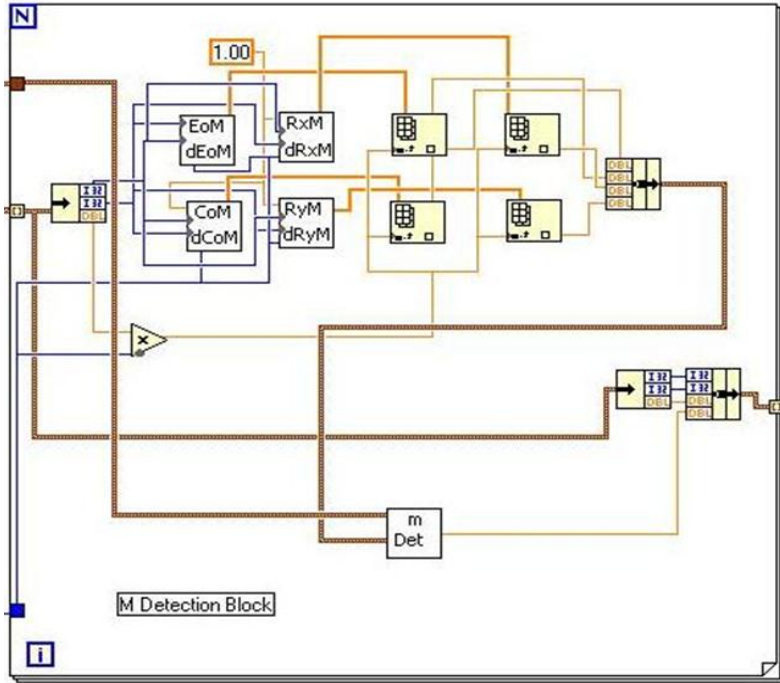
Figure 3.10: LabView Capacity Estimation Stage Code.

The last estimation step is the MSE analysis, which generates an error value for each battery candidate that determines how close the candidate matches the measured parameters. For each of the possible battery configurations, the ideal data is compared with the actual data using equation (3.18) to calculate error terms for each of the four circuit parameters as well as $C*R_{conc}$ and R_{conc}/R_{ohmic}.

$$\left(\frac{X_{ideal} - X_{actual}}{X_{ideal} + X_{actual}} \right)^2 \tag{3.18}$$

Once these error terms are calculated, the results are multiplied by a weights matrix and summed together to form one error term for each battery configuration, with the smallest error representing the most likely battery configuration. The weights matrix establishes the relative importance of each error term; the larger the weight value, the more important it is to keep that error term small in order to minimize the final error term. For this method to work, the weights matrix must be properly calibrated in order to establish the proper relationship between the six error terms. The LabView program for this step is shown in figure 3.11.
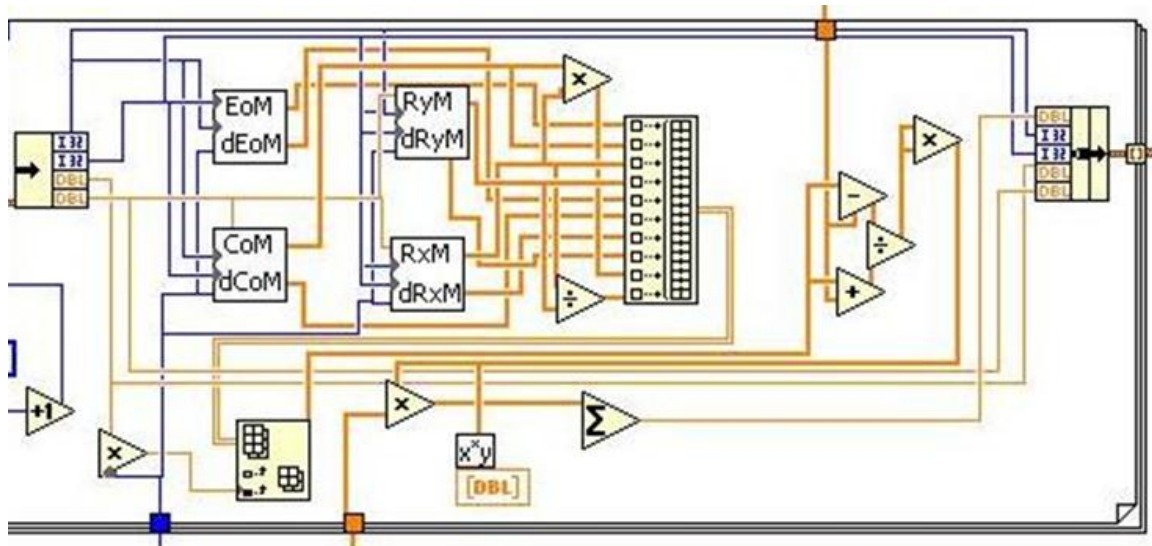
Figure 3.11: LabView MSE Analysis Stage Code.

Once all the estimation steps are complete, the candidate battery with the smallest error is selected as the proper battery identification and displayed in text format on the LabView display panel, as seen in figure 3.12.
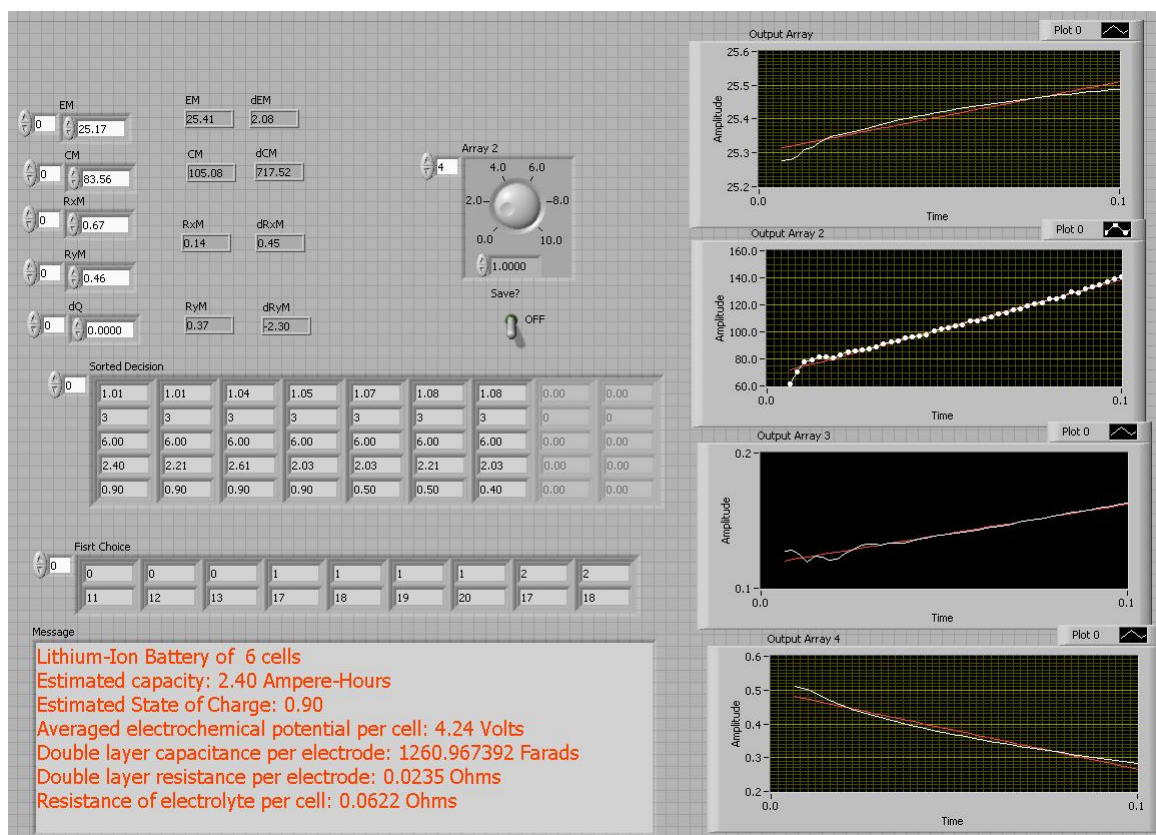
Figure 3.12: LabView Results Front Panel.

The four graphs in figure 3.12 show the four circuit parameter arrays and their linear fit. The message block in the bottom of figure x displays the identified battery characteristics, along with other useful battery characteristics that was never used in this research. The circular dial in figure x is used to adjust the weights matrix and the large array in the middle of figure x displays all of the candidate battery configurations sorted by their error terms.

54

3.4.6 *Results*

Ultimately, the accuracy of this identification method is determined by the MSE analysis step, which depends on the calibration of the weights matrix. A simple correlation analysis was used to calibrate the weights matrix based on the relative changes in error terms due to changes in battery configuration, with trial and error used for fine tuning. The final results were very promising, with a relatively high degree of accuracy in terms of chemistry and cell count detection; unfortunately the tuning process lacked stability as the overall accuracy ranged from 60-80% between testing periods, and a sample testing log is shown in figure 3.13.

Figure 3.13: Log Results for Statistical Analysis Method.

Failure analysis revealed that detection errors were caused by a poor separation between final error terms. In order to maintain accuracy, the correct candidate battery must have a MSE significantly lower than the other battery candidates; without this region of confidence, the detection accuracy is extremely susceptible to temperature fluctuations and measurement errors. This lack of a definitive identification is due to the inadequate tuning process used, and significant accuracy improvements can be achieved using a stronger, minimum cost analysis or other similar methods. Unfortunately, the true potential of this method was never realized; deadlines imposed by the IFEC competition prevented testing of additional calibration procedures.

CHAPTER 4

HYBRID METHOD AND
NEURAL NETWORK BACKGROUND

4.1 Review of Neural Network Based Methods

The second phase of research is based on artificial neural networks (ANN), used to partially or completely replace aspects of the previous Statistical Analysis method (or equivalent circuit method). This phase of research began as an improvement on the Statistical Analysis method; ideally, the previous method's shortcomings in terms of accuracy and stability could be rectified by replacing the inadequately tuned MSE analysis step with an ANN with well known and easily implemented training methods, creating the Hybrid method. However, it was soon realized that ANN's could replace all of the steps of the Statistical Analysis method, since most steps entailed simple arithmetic calculations and the only complex component, the line fitting, is based on the same Levenberg-Marquardt algorithm commonly used in neural network training, thus forming the Neural Network method.

4.2 Neural Network Background

4.2.1 *Basic Neural Network Concept*

Before beginning a detailed discussion of the ANN research, it's important to understand about neural networks in general, their architectures, training procedures, and primary areas of application. Neural networks are composed of simple elements

operating in parallel. These elements are inspired by biological nervous systems. As in nature, the connections between elements largely determine the network function. You can train a neural network to perform a particular function by adjusting the values of the connections (weights) between elements. Typically, neural networks are adjusted, or trained, so that a particular input leads to a specific target output. Figure 4.1 illustrates such a situation. There, the network is adjusted, based on a comparison of the output and the target, until the network output matches the target. Typically, many such input/target pairs are needed to train a network.
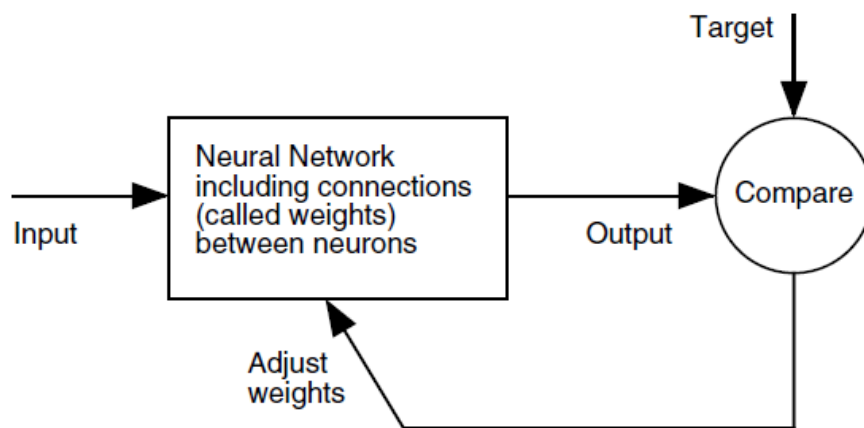
Figure 4.1: Neural network concept model [24].

Neural networks have been trained to perform complex functions in various fields, including pattern recognition, identification, classification, and speech, vision, and control systems. Neural networks can also be trained to solve problems that are difficult for conventional computers or human beings. Neural networks are good at fitting functions and recognizing patterns. In fact, there is proof that a fairly simple neural network can fit any practical function [24].

4.2.2   *Feed Forward Neural Network*

Many different neural network types exist, but the simplest and most commonly used one is the feed forward neural network. The feed forward neural network makes a great example to explain how neural networks work. A sample feed forward neuron with R inputs is shown in figure 4.2. Each input is weighted with an appropriate w. The sum of the weighted inputs and the bias forms the input to the transfer function f. Neurons can use any differentiable transfer function f to generate their output.
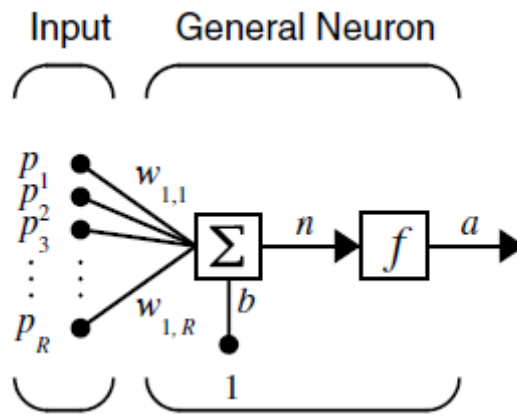
Figure 4.2: Single Feed Forward Neuron Model [24].

Most neural networks contain two or more neurons, operating in parallel branches called layers, and two or more layers can be cascaded together. A generic feed forward neural network is shown in Figures 4.3 and 4.4 below figure 4.4 is a visual model that outlines the overall neural network structure while figure 4.3 is a functional model that describes the mathematical operations used in each layer. Studying figure 4.3, each layer has R inputs and S neurons that form the outputs, the inputs forms an Rx1 input matrix (representing the input training set for one time series) that is

multiplied by an SxR matrix of weight terms to form S intermediate terms in as Sx1

matrix. Next an Sx1 matrix of bias terms is added to the intermediate terms and the

result is used as the input for the transfer function for the layer. The transfer function

shown in figure 4.3 is a log sigmoid function, which accepts any input value and gives

an output between zero and one. The sigmoid function is the primary transfer function

used for feed forward ANN's.
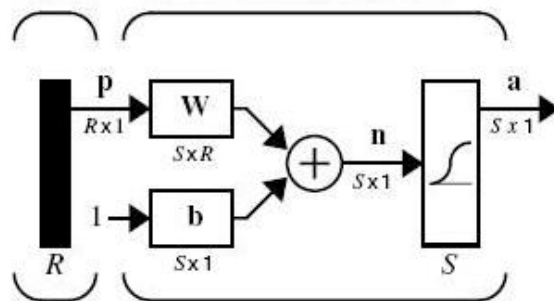
Figure 4.3: Functional Neural Network Model [24]
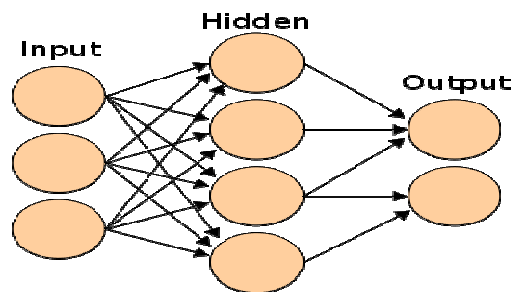
Figure 4.4: Visual Representation of Neural Network [24]

4.2.3   *Radial Basis Neural Network*

Now to look at a more complex neural network, namely the radial basis neural

network. The radial basis ANN is similar to the feed forward ANN except that it uses a

special transfer function and has special rules about the number of neurons in the hidden

layer. Radial basis networks have a separate neuron for each input vector in the training set. Figure 4.5 shows a model for a single radial basis neuron.
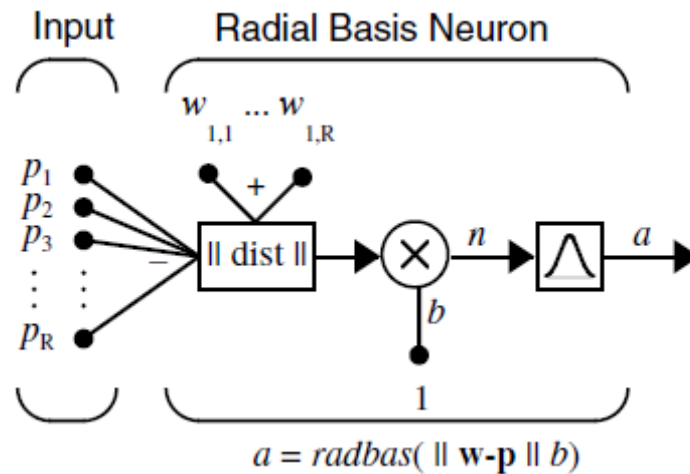
Figure 4.5: Single Radial Basis Neuron Model [24]

Notice that the expression for the net input of a radial basis neuron is different from that of the feed forward neuron. Here the net input to the radial basis transfer function is the vector distance between its weight vector **w** and the input vector **p**, multiplied by the bias b. (The || dist || box in this figure accepts the input vector **p** and the single row input weight matrix, and produces the dot product of the two.) The radial basis function has a maximum of 1 when its input is 0. As the distance between **w** and **p** decreases, the output increases. Thus, a radial basis neuron acts as a detector that produces 1 whenever the input **p** is identical to its weight vector **w** [24]. Figure 4.6 shows a complete radial basis ANN.
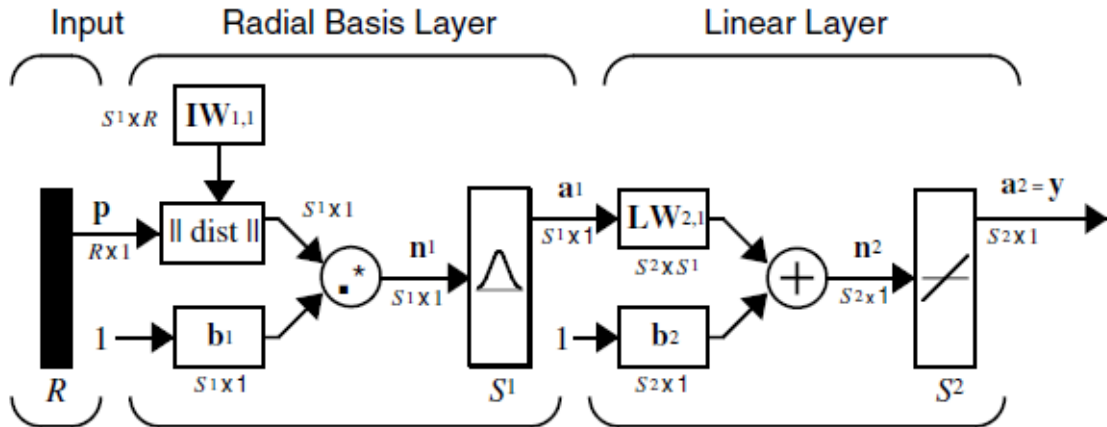
Figure 4.6: Functional Model of a Radial Basis Neural Network [24]

Note that the radial basis layer contains $S1$ elements, where $S1$ is the number of data sets used during training. The || dist || box in this figure accepts the input vector **p** and the input weight matrix **IW**1,1, and produces a vector having $S1$ elements. The elements are the distances between the input vector and vectors i**IW**1,1 formed from the rows of the input weight matrix. The bias vector **b**1 and the output of || dist || are combined with the MATLAB® operation (.*), which does element-by-element multiplication.

4.2.4   *Levenberg-Marquardt Training Algorithm*

The Levenberg-Marquardt algorithm was designed to approach second-order training speed without having to compute the Hessian matrix. When the performance function has the form of a sum of squares (as is typical in training feed forward networks), then the Hessian matrix can be approximated as

$$\mathbf{H} = \mathbf{J}^T \mathbf{J}$$

(4.1)

and the gradient can be computed as

$$\mathbf{g} = \mathbf{J}^T \mathbf{e}$$

(4.2)

Where **J** is the Jacobian matrix that contains first derivatives of the network errors with respect to the weights and biases, and **e** is a vector of network errors. The Levenberg-Marquardt algorithm uses this approximation to the Hessian matrix in the following Newton-like update:

$$\mathbf{x}_{k+1} = \mathbf{x}_k - [\mathbf{J}^T\mathbf{J} + \mu\mathbf{I}]^{-1}\mathbf{J}^T\mathbf{e}$$

(4.3)

When the scalar μ is zero, this is just Newton's method, using the approximate Hessian matrix. When μ is large, this becomes gradient descent with a small step size. Newton's method is faster and more accurate near an error minimum, so the aim is to shift toward Newton's method as quickly as possible. Thus, μ is decreased after each successful step (reduction in performance function) and is increased only when a tentative step would increase the performance function. In this way, the performance function is always reduced at each iteration of the algorithm [24].

4.3 Neural Network Selection

During the early stages of neural network research, all of the available ANN architectures were tested and evaluated for use in battery identification. Of all the different types, only the feed forward and radial basis models were suitable for this research. Throughout this preliminary testing, the radial basis networks had the highest accuracy and the absolute fastest training time, less than one second on average.

63

Unfortunately, the radial basis networks had the absolute highest neuron count, which averaged well above a thousand neurons; this caused excessively long simulation times, requiring at least several seconds per output point. In comparison, the feed forward networks had only slightly less accuracy but with and extremely fast simulation time. Due to their small size, feed forward networks had simulation times measured in the millisecond range or faster; unfortunately, they have a long training time which ranges from 10 to 100 minutes depending on the number of neurons in their hidden layers. This lengthy training time is common among most ANN's except the radial basis networks. In the end, the feed forward network was the preferred choice, because its minor training problems were easily overshadowed by the impractically large size and long simulation time of the radial basis network. Accordingly, the majority of the ANN research used feed forward neural networks, so any references to neural networks in this thesis refers specifically to feed forward neural networks unless stated otherwise.

4.4 Hybrid Method

4.4.1 *Justification of Hybrid Method*

As mentioned previously, this neural network phase of this thesis was originally conceived as an improvement on the Statistical Analysis method, in which the calibration problems of the MSE step would be solved with a simple neural network. The plan was to replace the entire detection block of the LabView program with an ANN designed to work directly with the measured parameter arrays. At the time, the error weight tuning process was proving to be more troublesome and time consuming than expected and a neural network alternative was believed to be a more logical and

efficient choice, and a literature review supported this hypothesis. The literature review revealed that the proposed neural network implementation fits nicely within the traditional uses of neural networks; one example of a traditional ANN use is seen in [25], in which voltage, current, and temperature readings from a photovoltaic panel are used to perform maximum power point tracking. This simple example is analogous to the neural network implementation in the Hybrid method because both use a small set of important measurement data that is required for the task at hand.

4.4.2 *Neural Network Design*

The first step of ANN research was the network evaluation stage, during which all of the various neural network architectures were researched, understood, and evaluated for effective use in battery identification; ultimately selecting feed forward ANN as only valid choice for detection block replacement. Because this method involves combining neural networks with the previous Statistical Analysis, this method was referred to as the hybrid method. The ANN selected was a 2 layer feed forward network with 20 log sig neurons in the hidden layer and 3 binary neurons in the output layer, one for each chemistry type. This early neural network research focused only on chemistry detection as a proof of concept, so the three network outputs represent a three bit chemistry classification where the bit representing the proper chemistry outputs a one while the other two output zeros. For testing and training purposes, the existing parameter data, used to design the lookup tables, was compiled and formatted into a 25,000 point data set. Because of this extremely large amount of data, a radial basis network would have been extremely impractical.

4.4.3 *Testing Results of Hybrid Method*

Initial testing showed very promising results for this method, averaging 94.5% success rate over the entire 25,000 point sample set. The 5.5% failure rate was mostly caused by bad parameter data from damaged batteries. Unfortunately, a LabView software upgrade caused the LabView program to become corrupted halfway through the hybrid method research phase. After the upgrade, the nonlinear Lev Mar fit function inside the parameter estimation block ceased to function properly, often generating linear fits instead of exponential fits. Under these conditions, the constructed neural networks had a 100% failure rate. Although disappointing, the defects in the LabView program reveal some of the inherent defects in the hybrid method, namely that the ANN's accuracy is externally limited by the measurement errors of previous steps.

4.4.4 *Conclusion of Hybrid Method*

On the whole, the hybrid method was a success; it outperformed the Statistical Analysis method over the same data and demonstrated a consistently high 94.5% accuracy when using good data. However, despite the improved accuracy, the hybrid method does little to reduce the complexity or computational expense inherited from the Statistical Analysis method. Moreover, efforts to repair the faulty line fitting function and reduce the complexity of the hybrid method led to the complete neural network method, where the entire LabView program is replaced with a single neural network. This new method required a neural network capable of analyzing the raw voltage waveforms directly in order to identify the battery; this is intuitively possible because

the line fitting program in LabView uses the same Levenberg-Marquardt algorithm commonly used in neural network training. Due to the greater potential of the neural network method, the hybrid method was abandoned without properly documenting the test results, thus explaining the lack of data.

CHAPTER 5

NEURAL NETWORK METHOD

5.1 Design of Neural Network Method

5.1.1   *Neural Network Design*

This last and most significant phase of this research is titled the ANN method, because it uses ANNs to perform all of the analytical steps of the Statistical Analysis method.   The ANN method is designed as an enhanced version of the Statistical Analysis method; as such, it uses the same pulse charging voltage waveforms as the Statistical Analysis method but it replaces the line fitting, circuit parameter calculation, and detection steps with a single neural network.   This enhancement gives the ANN method the same functionality of the Statistical Analysis method but greatly reduces its complexity and computational expense.   Although this method is derived from the Statistical Analysis method and is based on the same RC equivalent circuit theory, it doesn't actually derive any circuit parameter, instead it operates directly on the voltage waveforms that the parameters are derived from, effectively cutting out the middle man so to speak.   The basic setup for the ANN method is to use LabView to generate the charging pulse and measure the voltage waveform, using the same setup as the Statistical Analysis method, then the 90 point measured voltage waveforms are used as inputs into a single neural network implemented in MatLab.

5.1.2   *Novel Network Architecture*

By using the entire 90 point voltage waveform as inputs, the ANN method employs a very novel and unorthodox use of neural networks. Traditionally, ANNs use a relatively small set of inputs, each of which are somewhat distinct from the others and holds some significance to the task at hand. The ANN used in the hybrid method is an example of traditional ANN use; that ANN uses the four distinct equivalent circuit parameters as inputs, each representing a distinct and significant part of the battery model. Some examples such as [crab classification, random other] use a small set of measurements that directly relate to their tasks. Other ANN examples specific to battery monitoring traditionally use battery measurements such as voltage, current, coulomb count, and temperature, as [26], [27], and [28] did or they use impedance measurements like in [29]. In contrast, the ANN for this method uses 90 voltage measurements, more that ten times the number of inputs of any other battery management ANN and each voltage input is almost meaningless without the others.

5.1.3   *Experimental Setup*

Although the goal of the ANN method is to design a single ANN that identifies both chemistry and SOC of the unknown battery, for practicality, each identification task was performed by separate ANNs. It was reasoned that the novel ANN use and the general complexity of the research would confuse matters and that chemistry detection and SOC estimation for each chemistry should be researched separately in order to fully test and evaluate each aspect of the research. Despite this separation, a single ANN is capable of performing all tasks that any separate ANN can complete, though it may

69

require additional neurons up to the combined total of all the separate ANNs. Although

dozens of ANNs were designed and evaluated for each design considerations, only 2 to

3 representative networks will be presented in each design section, any more would be

unreasonable due to the number of figures for each network. Each network result

section will show a training window that displays the training MSE at the top, the

number of training epoch at the bottom (or cycles through the training data), and a

graph of the training, testing, and validation MSE; when a network is setup to train, part

of the training data is set aside to form a testing and validation set that the training

program uses to test the training results and decide when to stop.

<u>5.2 Experimental Results Chemistry Detection</u>

5.2.1   *Chemistry Detection Design Considerations*

First up is chemistry detection, where a single ANN is designed to output the

chemistry of the unknown battery. The datasets used for this research are the combined

datasets for each of the separate SOC estimation ANNs.   Important design

considerations include, determining if input data needs conditioning, designing the most

accurate output format for chemistry classification, and adjusting neuron transfer

functions to suit the output format. In terms of input conditioning, the networks will be

trained and tested on both normalized and unnormalized data. A design criteria specific

to the chemistry detection task is chemistry output format, namely what kind of

numerical output will be used to indicate which chemistry is detected. A simple three

number class system was chosen, where 1 indicates NiMH, 2 indicates SLA, and 3

indicates Li-Ion batteries, the main design considerations is to decide whether a single

numeric output is better or three separate binary outputs that can output the chemistry in a special binary code where 001 indicates NiMH, 010 indicates SLA, and 100 indicates Li-Ion. Initial thought suggests that the linear output will give a smaller network due to fewer outputs and that the output can be directly output to the user, where as the binary output might be more precise due to separate outputs for each chemistry even if some post processing is needed to generate a numeric number. The last design consideration is which output transfer function is most appropriate for each output format; clearly a linear transfer function is best for the numeric output because that function is designed for outputting whole ranges of numbers, however, the binary outputs are only designed to output zero or one, so several useful transfer functions can accomplish this task.

5.2.2   *Chemistry Detection Setup*

Figure 5.1 below shows the three datasets used for chemistry detection, figure 5.1.a is the training set, 5.1.b is the test set that contains mostly clean data, and 5.1.c is the bad set that contains all remaining data sets not used in the first two including irregular ones due to damaged batteries or measurement errors. The plots in figure x are displayed in numeric format even though they are used for both output types, these plots seem rather unremarkable because they are concatenated from the corresponding SOC datasets without randomization.

71
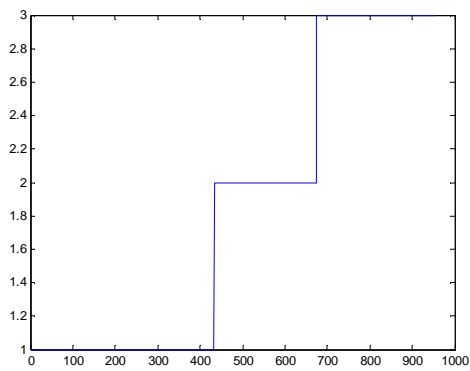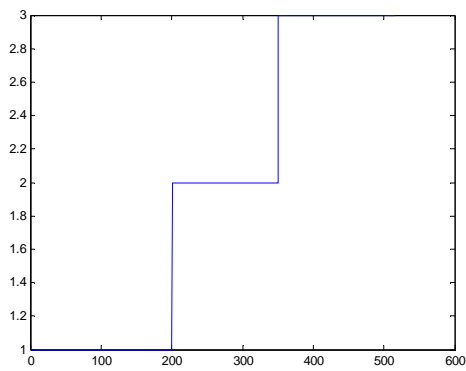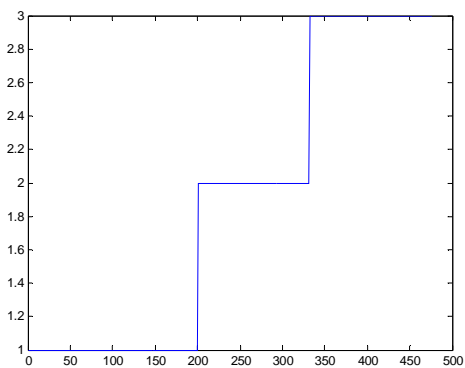
Figure 5.1: Original Chemistry Detection Plots, a) Training set, 956 samples, b) Test set, 517 samples c) Bad set, 476 samples

The numeric output was evaluated first; these networks all use the network model in figure 5.2 but with 5, 10, or 20 neurons in the hidden layer. Separate networks were designed for either normalized or unnormalized data, the normalized data used the mapminmax function in MatLab to normalize the data in a range from zero to one.
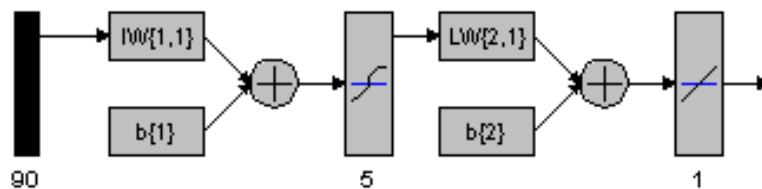
Figure 5.2: Sample Numeric Chemistry Detection Model

In regards to the numeric output networks, because the output are linear they can take on any number, so although the goal is to output an integer number from one to three, in practice errors cause decimal number outputs close to the target integer number. If these errors are small then the result is still a successful classification, but if the error exceeds 0.5 then it is a classification error because the output is closer to one of the other target integers. In regards to binary output networks, each output is designed to generate a one or zero but in practice they rarely generate integer numbers. Extremely well behaved and error free outputs will often have decimal outputs infinitely close to the proper integer number, either .99999 instead of 1 or .001 to $1e^{-34}$ instead of zero; on the other hand, outputs with a high amount of error can output any number from zero to one, or higher in the case of linear outputs. Binary output networks have a post processing step where the output with the highest value is set to one and the rest are set to zero, because of this two different kinds of detection errors can occur, quantization and classification. Classification errors occur when the outputs are well behaved but incorrect, meaning they clearly output a one or a zero but the chemistry indicated is incorrect. Quantization errors occur when the outputs are misbehaved, or noisy, so that the outputs are not "quantized" to either zero or one, when two or more

73

outputs are poorly quantized, whichever has the highest number is treated as the one output and the rest are treated as zero.

With these errors in mind, numeric output networks are evaluated based on absolute value error, with errors greater than 0.5 as detection errors; while binary output networks are evaluated hit or miss, with detections errors identified as either classification or quantization.

5.2.3   *Normalized Numeric Chemistry Detection*

This first section analysis chemistry detection networks using the numeric output format and normalized input data. Network 1 is a representative of the average network built while Network 2 is an above average example; on average, most networks will look like Network 1 after training but a few retraining will generate one like Network 2.

1) *Network 1*: Network 1 is a representative average training result for chemistry detection networks with numeric outputs using normalized data, it training and testing results are displayed in figure 5.3, 5.4, and table 5.1 below. Network 1 has 5 neurons in its hidden layer, it took 251 training epoch to reach a MSE of 0.0108, figure 5.3 displays the last 51 epochs of the training results.
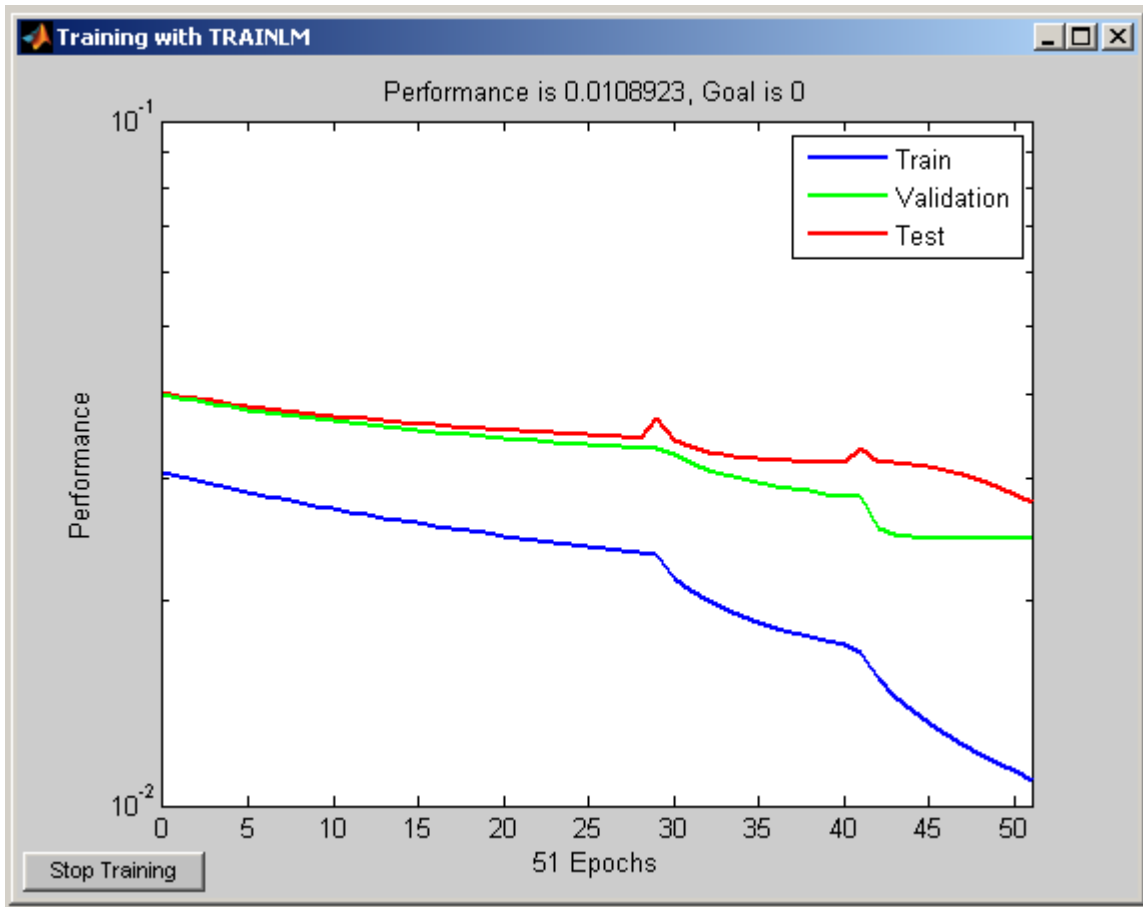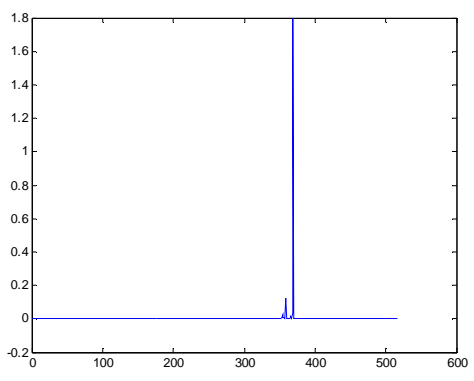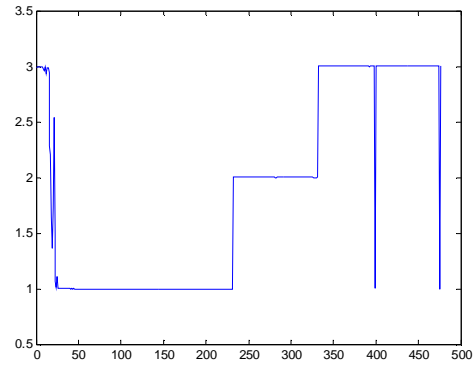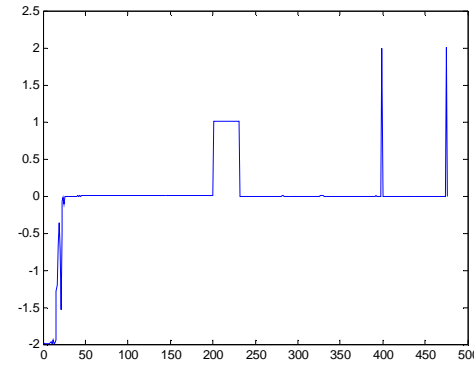
Figure 5.3: Network 1 Training Window
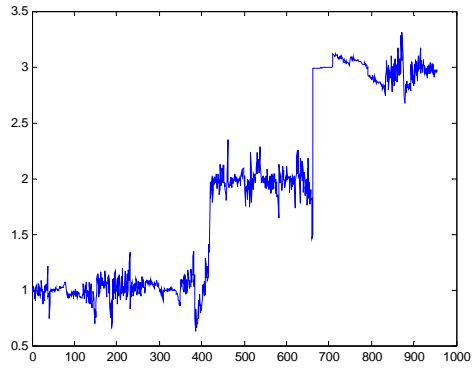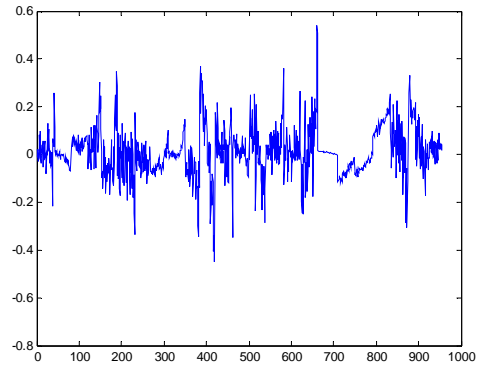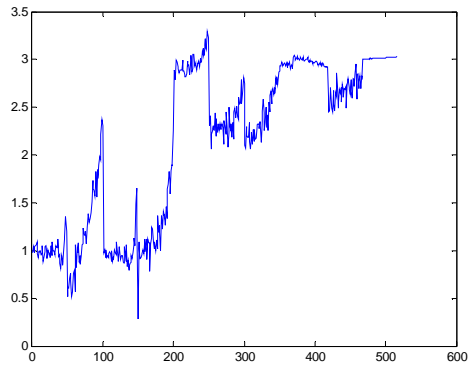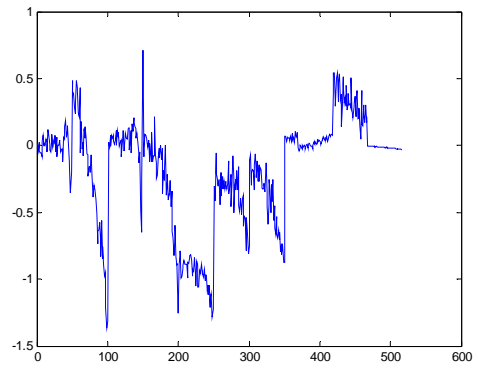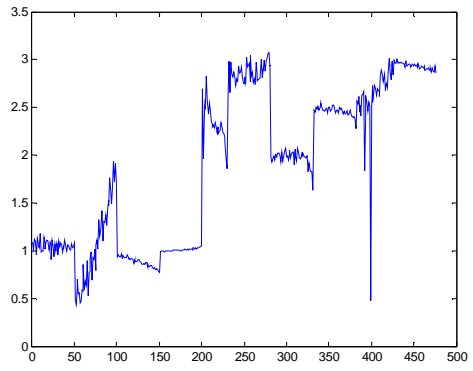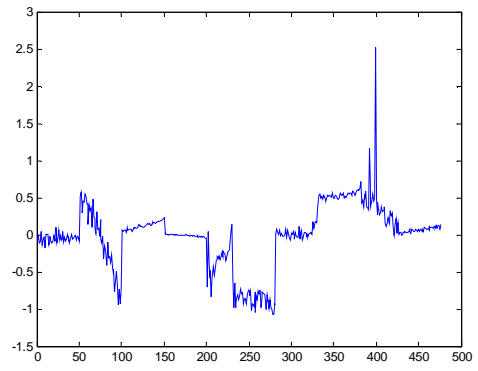
Figure 5.4: Network 1, 5 Neuron Average Normalized Numeric Network, a) training set results, b) training set error, c) test set results, d)test set error, e) bad set results, f) bad set error

76

Table 5.1: Network 1 Error Statistics

Network 1	Mean error	Max error	Accuracy
Training set	0.0732	0.5403	>95%
Test set	0.2903	1.367	>70%
Bad set	0.2794	2.52	>60%

The results of Network 1 are below average at best; although the mean error for each dataset is below the 0.5 error threshold, the max errors show that each set has detection errors and only the Training set is visually close to the original.

2) *Network 2*: Network 2 is a representative good training result for chemistry detection networks with numeric outputs using normalized data, it training and testing results are displayed in figure 5.5, 5.6, and table 5.2 below. Network 2 has 20 neurons in its hidden layer, it took 276 training epoch to reach a MSE of 0.002826, figure 5.5.a displays the first 100 epochs and figure 5.5.b displays the last 76 training epochs, the rest were omitted.

a)   b)
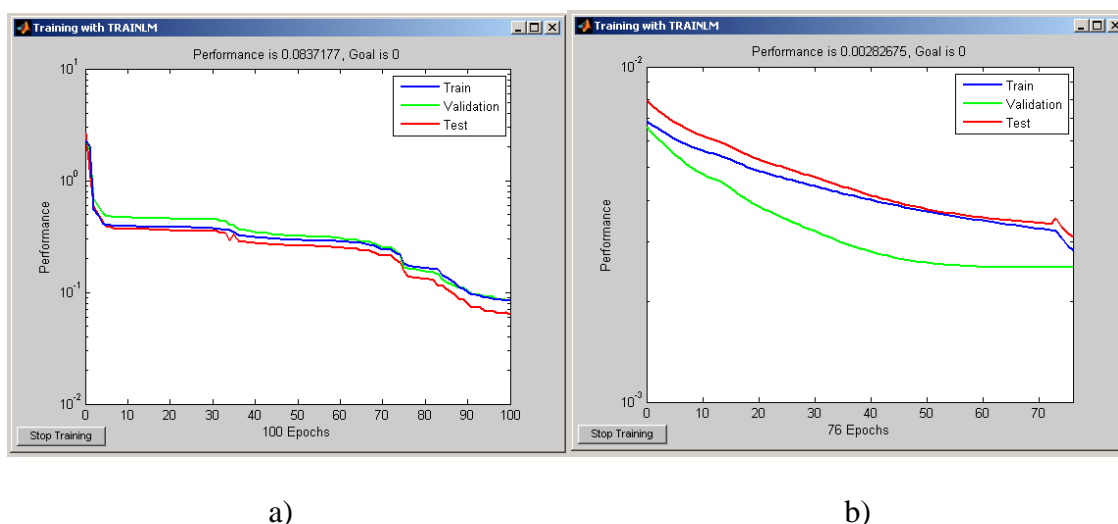
Figure 5.5: Network 2 Training Window, a) First 100 training epochs, b) Last 76 training epochs
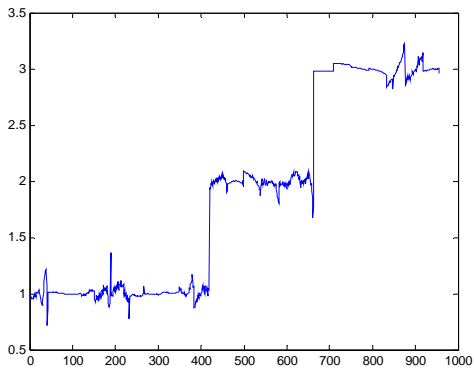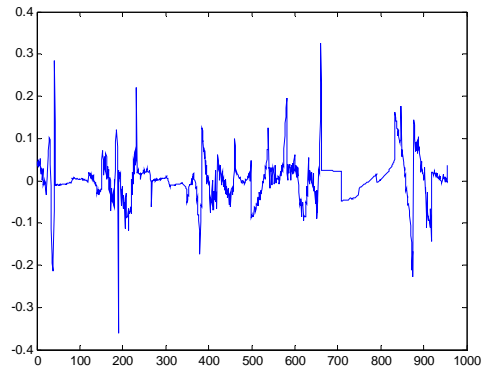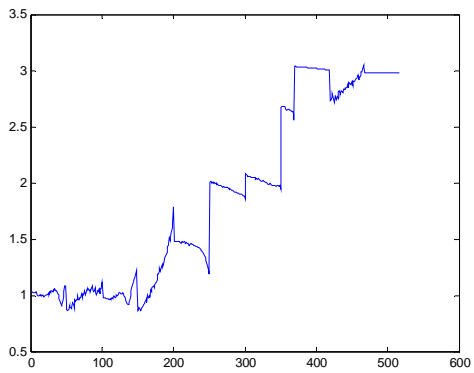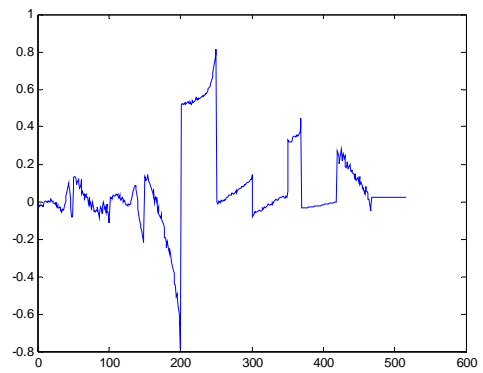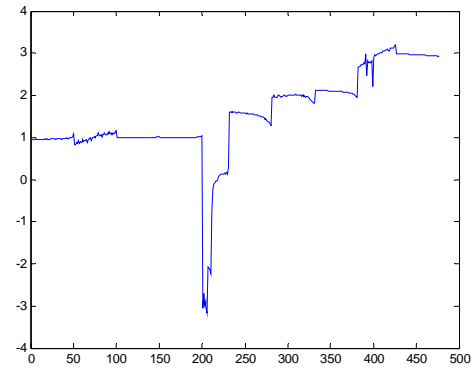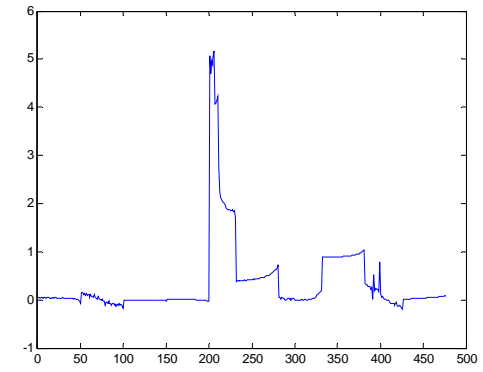
Figure 5.6: Network 2, 20 Neuron Good Normalized Numeric Network, a) training set results, b) training set error, c) test set results, d)test set error, e) bad set results, f) bad set error

Table 5.2: Network 2 Error Statistics

Network 2	Mean error	Max error	Accuracy
Training set	0.0337	0.3621	100%
Test set	0.1282	0.812	>84%
Bad set	0.3681	5.16	>67%

The results of Network 2 are only slightly better than Network 1, the average example, and although this is the best network produces its still offers only above average results. Both visual inspection and error statistics show that Network 2 has superior performance on the Training and Test sets compared to Network 1, the error statistics in table x show that Network 2 has 100% accuracy on the Training set and although the Test set has some detection error, its error statistics are lower that Network 1's and visual inspection shows that it more closely resembles the actual output than Network 1's output does. In terms of Bad set performance, both error statistics and visual inspection appear to indicate poor performance, but this is a misconception caused by an extremely large max error, one which is two numbers higher that the highest allowed value. A close inspection of the error plot in figure 5.6.f shows that Network 2 has almost zero error, except for three spots; this show that Network 2 had 100% accuracy with Bad set NiMH batteries. Also of note, the extremely high error spike occurred on an extremely distorted section from the SLA Bad set which has regularly caused massive errors and will be discussed in the SLA SOC section.

Overall, normalized input data has very poor performance, where even the best network can only offer 60-80% accuracy during testing; the unnormalized section will determine if numeric outputs are viable. Several interesting facts are revealed in the output graphs, first is that the output errors have curves similar to the SOC outputs, shown in their sections. This finding is not explored in the current research but is significant enough for future work. A second fact is that error spikes occur on the boundaries between battery sets; this is most clearly seen in the sudden discontinuities in the output plots and the isolated spikes in the error plots. These result from the concatenation of multiple battery plots and are unlikely to occur in field conditions, and they can be compensated for by a master controller that can detect a change in batteries.

5.2.4   *Unnormalized Numeric Chemistry Detection*

This second section analysis chemistry detection networks using the numeric output format and unnormalized input data. Network 3 is a representative of an average network, Network 4 is an exceptional example, and Network 5 is a rare perfect network, on average, most networks will look like Network 3 after training but a few retraining will generate one like Network 4, Network 5 is very rare and requires dozens of retraining but is far from impossible to generate.

1) *Network 3*: Network 3 is a representative average training result for chemistry detection networks with numeric outputs using unnormalized data, its training and testing results are displayed in figure 5.7, 5.8, and table 5.3 below. Network 3 has 5 neurons in its hidden layer, it took 160 training epoch to reach a MSE of 0.01689, figure 5.7 displays the last 60 training epochs. Unfortunately the remaining epoch figures and

error data were lost, so this network is only presented as a visual example without in depth discussion.
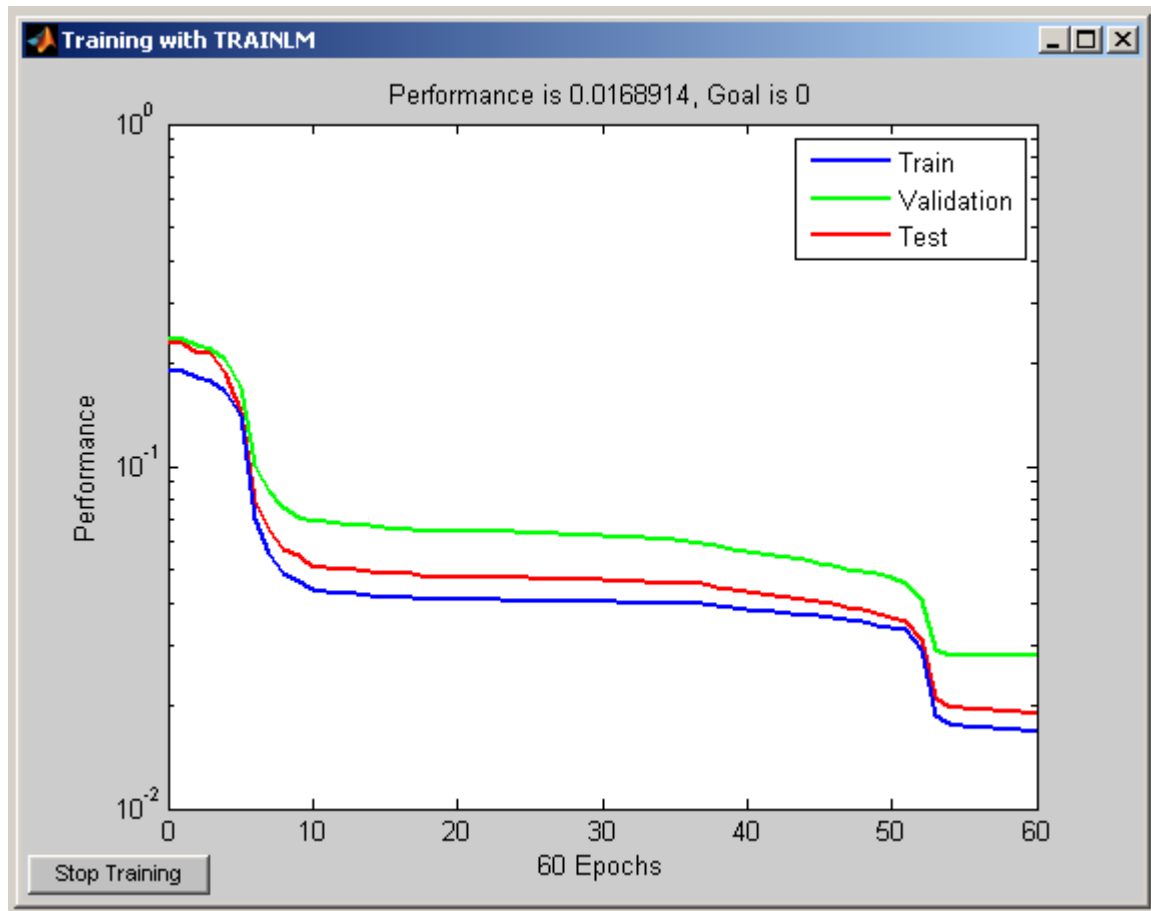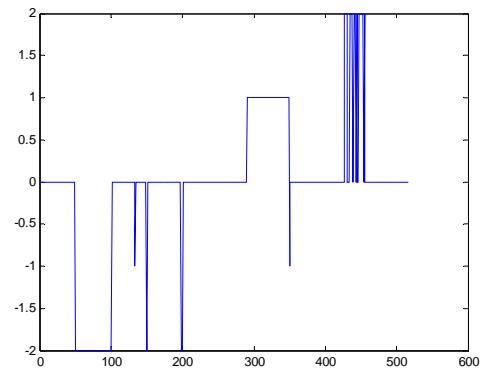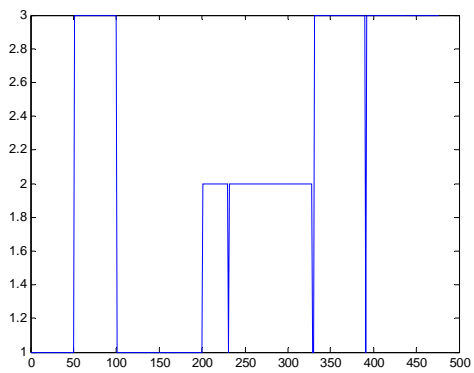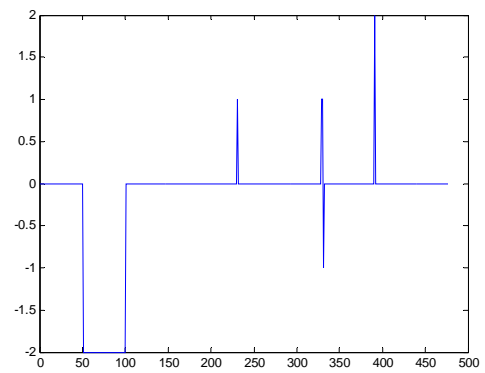

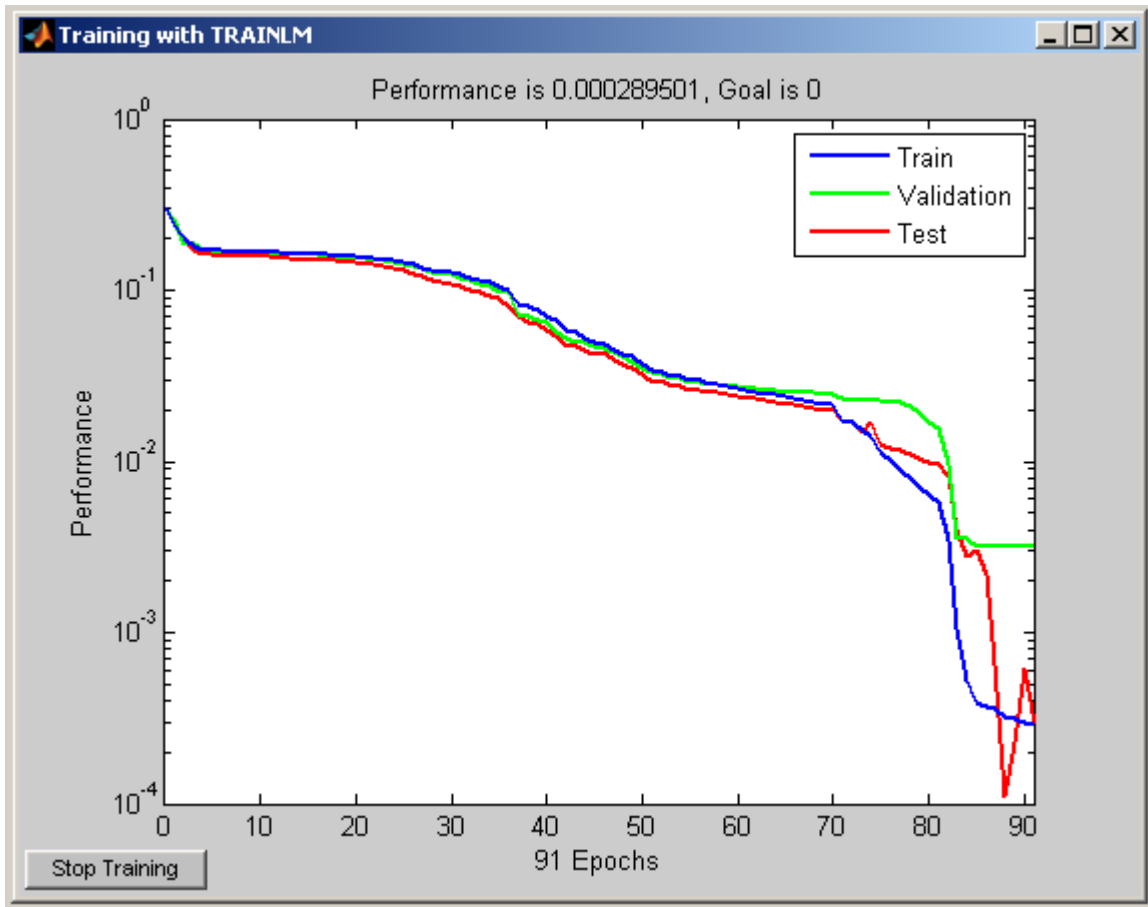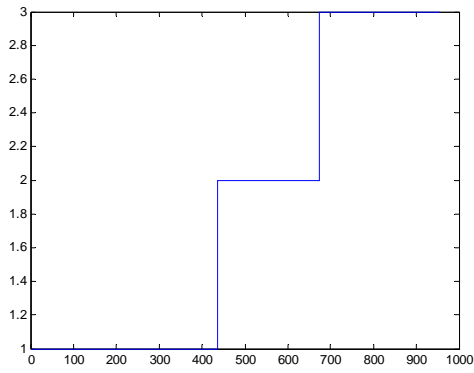Figure 5.7: Network 3 Training Window
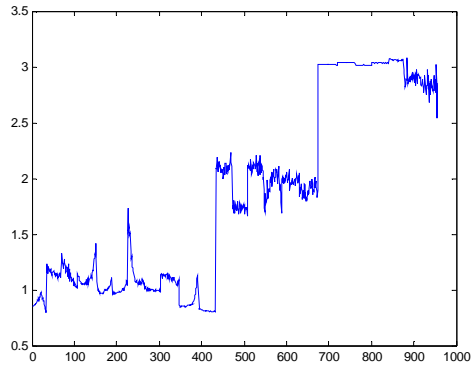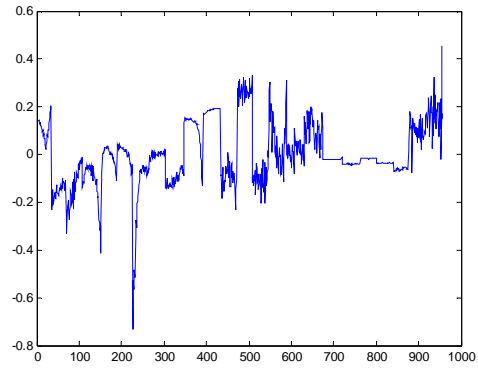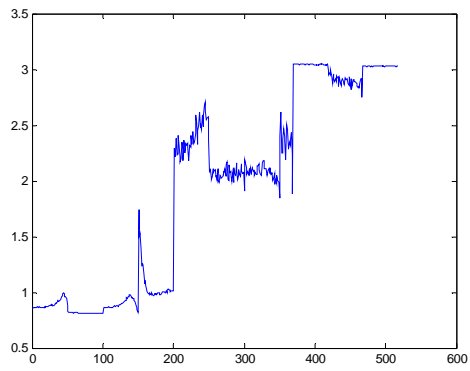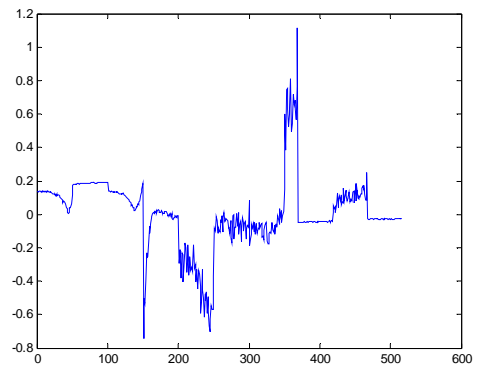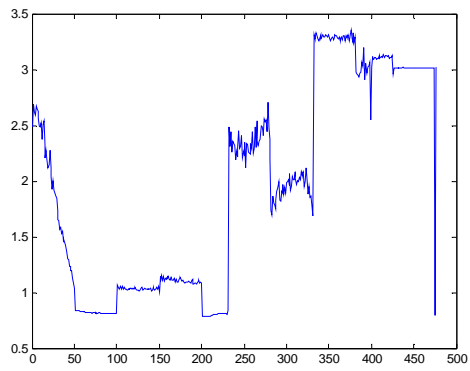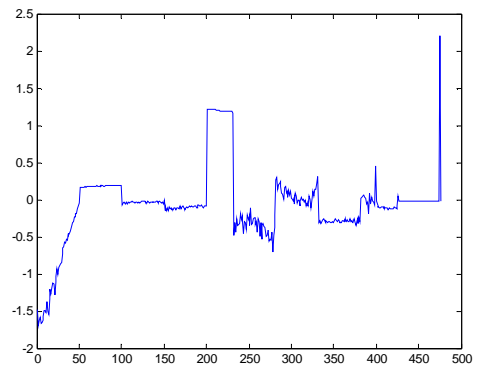
Figure 5.8: Network 3, 5 Neuron Average Unnormalized Numeric Network, a) training set results, b) training set error, c) test set results, d)test set error, e) bad set results, f) bad set error

82

Table 5.3: Network 3 Error Statistics

Network 3	Max error	Accuracy
Training set	~0.75	>96%
Test set	~1.1	>89%
Bad set	~2.2	>85%

Although the supporting data was lost, the graphs in figure 5.8 and the approximated accuracies in table 5.3 show that Network 3 outperforms all of the normalized numeric output networks.

2) *Network 4*: Network 4 is a representative great training result for chemistry detection networks with numeric outputs using unnormalized data, its training and testing results are displayed in figure 5.9, 5.10, and table 5.4 below. Network 4 has 10 neurons in its hidden layer, it took 32 training epoch to reach a MSE of 0.000618, figure 5.9 displays all 32 training epochs.
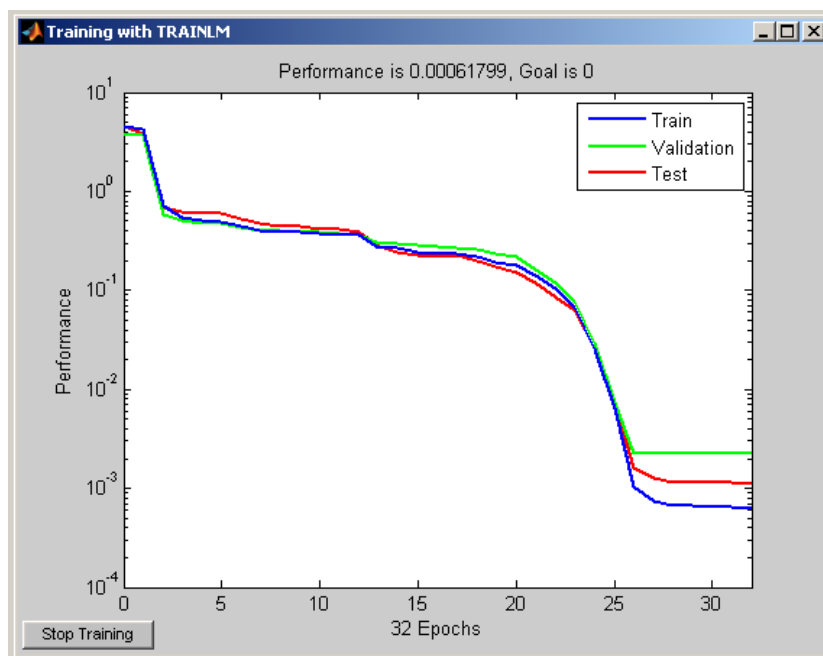

Figure 5.9: Network 4 Training Window

83
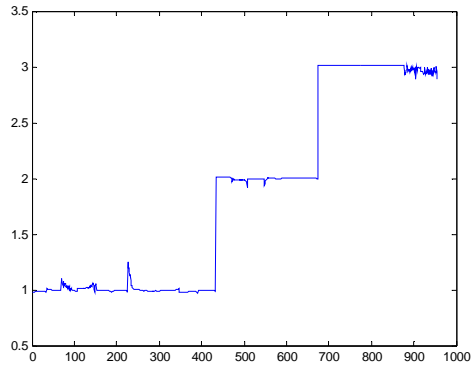
a)
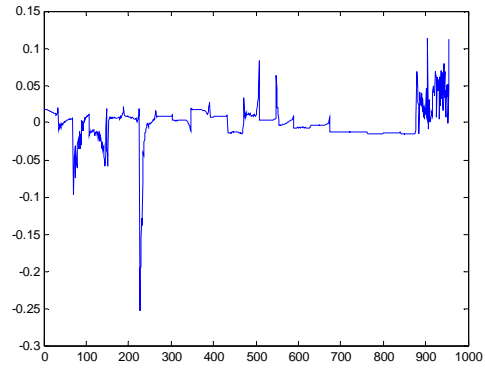
b)
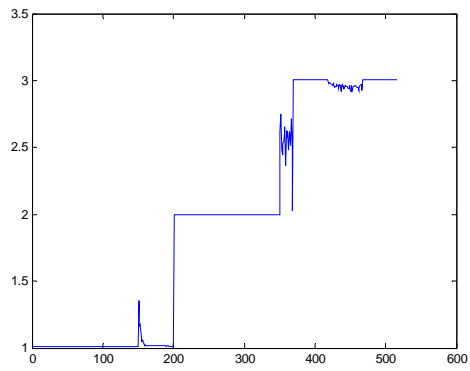
c)
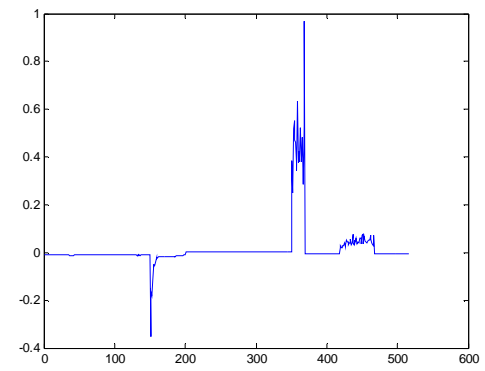
d)
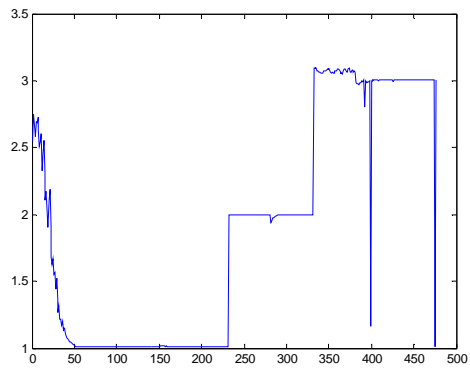
e)
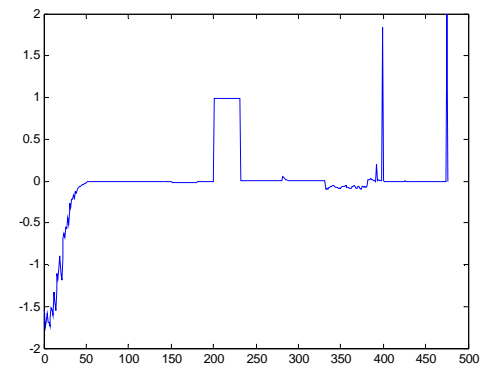
f)

Figure 5.10: Network 4, 10 Neuron Great Unnormalized Numeric Network, a) training set results, b) training set error, c) test set results, d)test set error, e) bad set results, f) bad set error

84

Table 5.4: Network 4 Error Statistics

Network 4	Mean error	Max error	Accuracy
Training set	0.0145	0.2539	100%
Test set	0.0282	0.9704	>94%
Bad set	0.1653	1.9913	>84%

Network 4 has very good overall performance. Visually, Network 4 has almost perfect performance except where detection errors occur. Statistically however, Network 4 is only about 5% more accurate that Network 3.

3) *Network 5*: Network 5 is a perfect training result for chemistry detection networks with numeric outputs using unnormalized data, its training and testing results are displayed in figure 5.11, 5.12, and table 5.5 below. Network 5 has 5 neurons in its hidden layer, it took 100 training epoch to reach a MSE of $3.14*10^{-12}$, figure 5.11 displays all 100 training epochs.
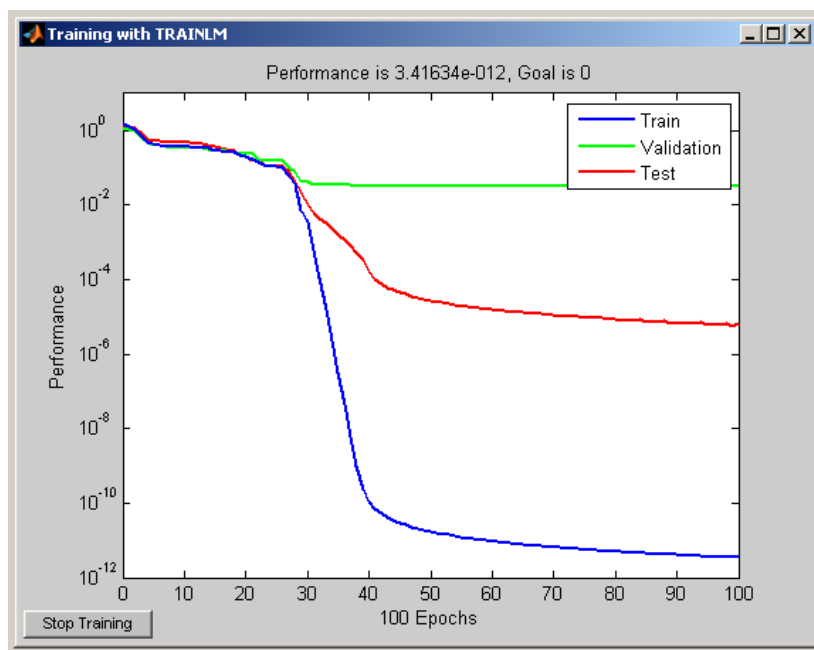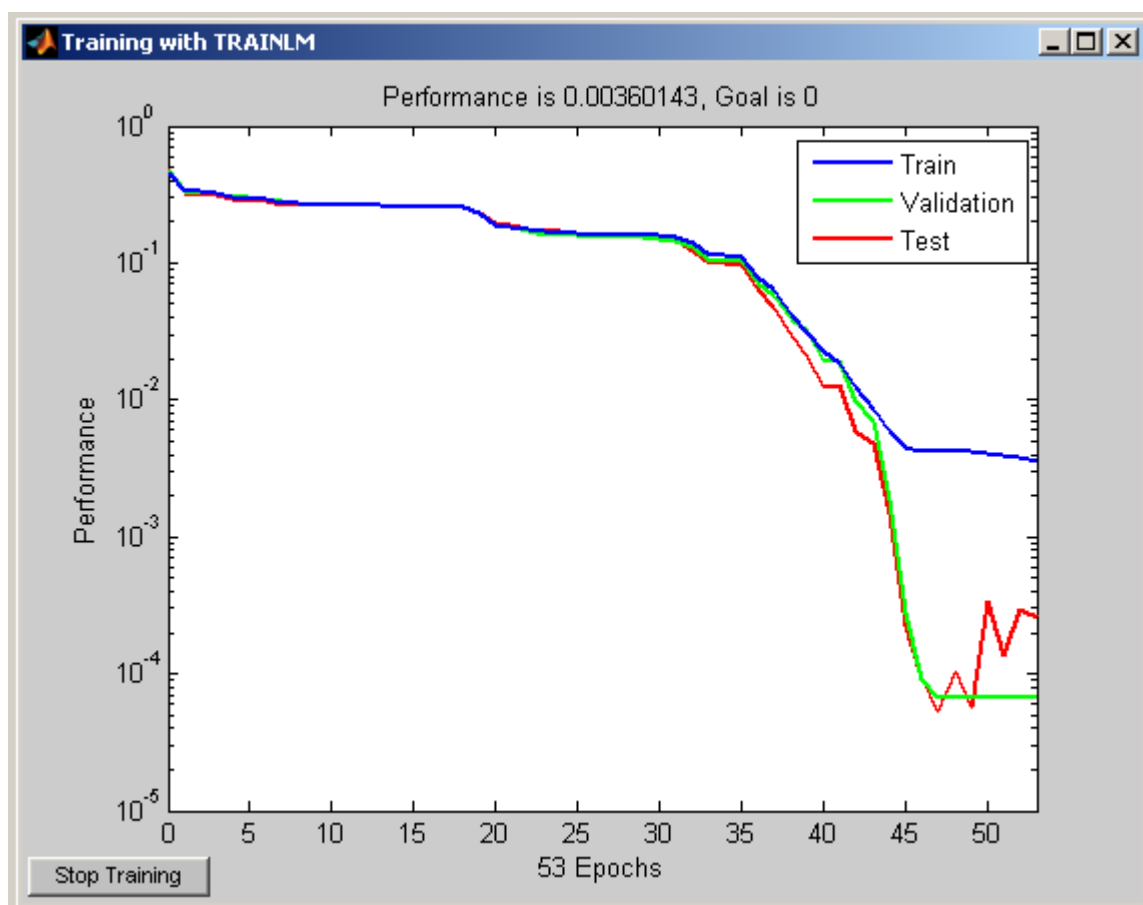

Figure 5.11: Network 5 Training Window
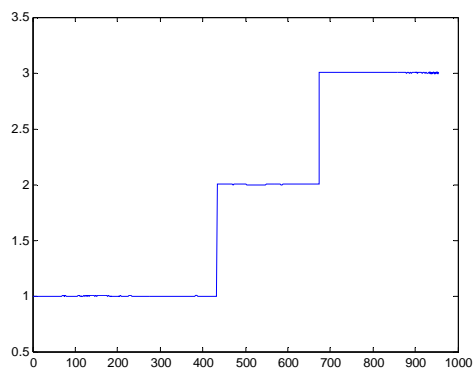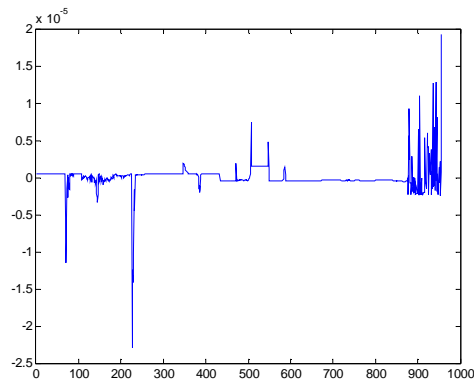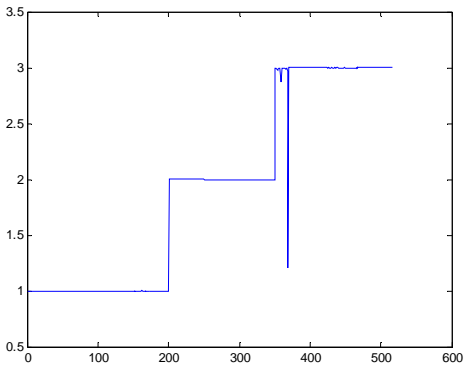
Figure 5.12: Network 5, 5 Neuron Perfect Unnormalized Numeric Network, a) training set results, b) training set error, c) test set results, d)test set error, e) bad set results, f) bad set error

Table 5.5: Network 5 Error Statistics

Network 5	Mean error	Max error	Accuracy
Training set	8.0631e-007	2.2928e-005	100%
Test set	0.0039	1.7967	>98%
Bad set	0.1497	2.0000	>88%

Network 5 has extremely good results, as figure 5.12 and table 5.5 show, Network 5 has almost 100% accuracy except over known bad data. Network 5's results are similar to Network 4's except with perfectly smooth output, even on errors, and with fewer errors overall. Even though Network 5 is a rare occurrence, its results are similar enough to Network 4's that both would be acceptable choices. Also, Network 5's almost perfect performance except over bad data is offered as evidence that chemistry detection can be used as SOH indicator to detect bad batteries, these results will become more apparent as the same detection errors are repeatedly made by all chemistry detection networks.

Final results show that numeric output format is valid when used with unnormalized data. While the normalized networks gave average results at best, unnormalized networks gave exceptional to near perfect performance with fewer required training attempts. Also, testing has revealed no preference for the number of neurons in the hidden layer, as the 5, 10, and 20 neuron versions have all generated good results in one test or the other; because of this lack of preference combined with the perfect 5 neuron network for the unnormalized tests, 5 neurons are generally the best. One interesting result is that the best normalized network correctly identified the

first set of NiMH batteries while none of the unnormalized networks were able to; similar results are present throughout the chemistry detection research, where some Bad sets are almost always incorrect, like the first SLA plot, while some sets are only occasionally incorrect, like the first NiMH plot, this is most likely due to different defects in the different battery sets, or reflect different SOH levels, but these results will be explored in future SOH work.

5.2.5   *Binary Chemistry Detection Design Criterion*

This section will review the research results for the chemistry detection networks with binary output. Three different transfer functions were selected for evaluation, linear, log sigmoid, and tan sigmoid. The tan sigmoid functions is the single most common transfer function for hidden neurons, its primary function is to accept an infinitely wide input range and output numbers between +/- 1. The log sigmoid function is the second most common transfer function for hidden neurons, it also accepts an infinite input range but it outputs numbers between zero and one. The linear transfer function is really a unity operator, a linear function with a slope of one whose output equals its input; the weights and bias for this layer set the true slope and offset for this function. The linear function is the most common output function when a wide range of output values are desired, as in the numeric output networks.

The results of each transfer function will be display in order, log, tan, and then linear; only the log sigmoid set will use both normalized and unnormalized, the rest use only unnormalized because it offered superior results. All binary ANNs use the same

data as in figure 5.1; sample neural network models for each output are displayed in figure 5.13, though the hidden layer will vary between 5, 10, and 20 neurons.

a)

b)

c)
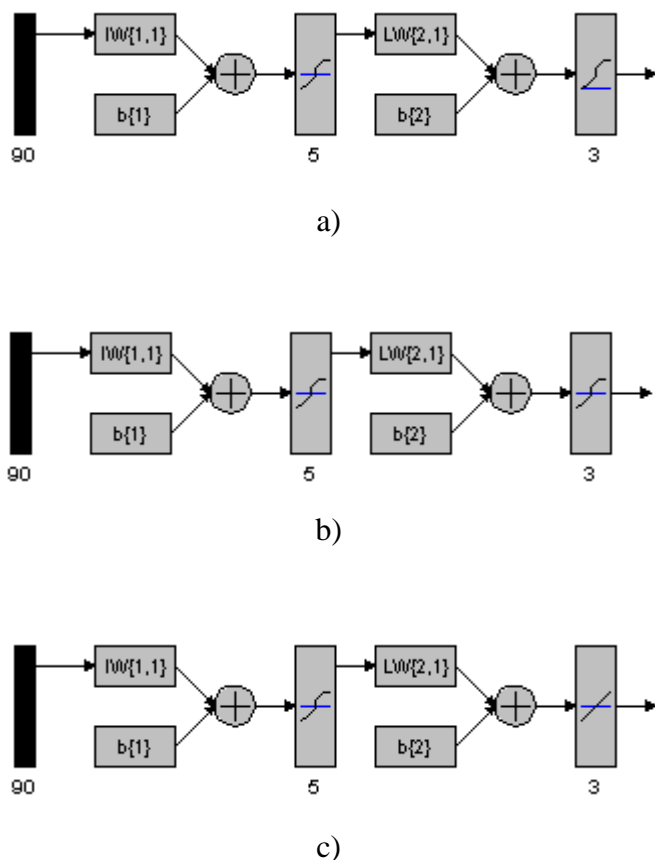
Figure 5.13: Sample Binary Chemistry Detection Models, a) log sigmoid output, b) tan sigmoid output, c) linear output

5.2.6   *Normalized Binary Log Sigmoid Chemistry Detection*

This third section analyzes chemistry detection networks using the binary output format with log sigmoid transfer functions using normalized input data. Network 6 is a representative of an average network while Network 7 is a perfect example, on average, most networks will look like Network 6 after training but many retraining will generate one like Network 7

1) *Network 6*: Network 6 is an average training result for chemistry detection networks with binary log sigmoid outputs using normalized data, its training and testing results are displayed in figure 5.14, 5.15 and table 5.6 below. Network 6 has 5 neurons in its hidden layer, it took 71 training epoch to reach a MSE of 0.0652, figure 5.14 displays all 71 training epochs.
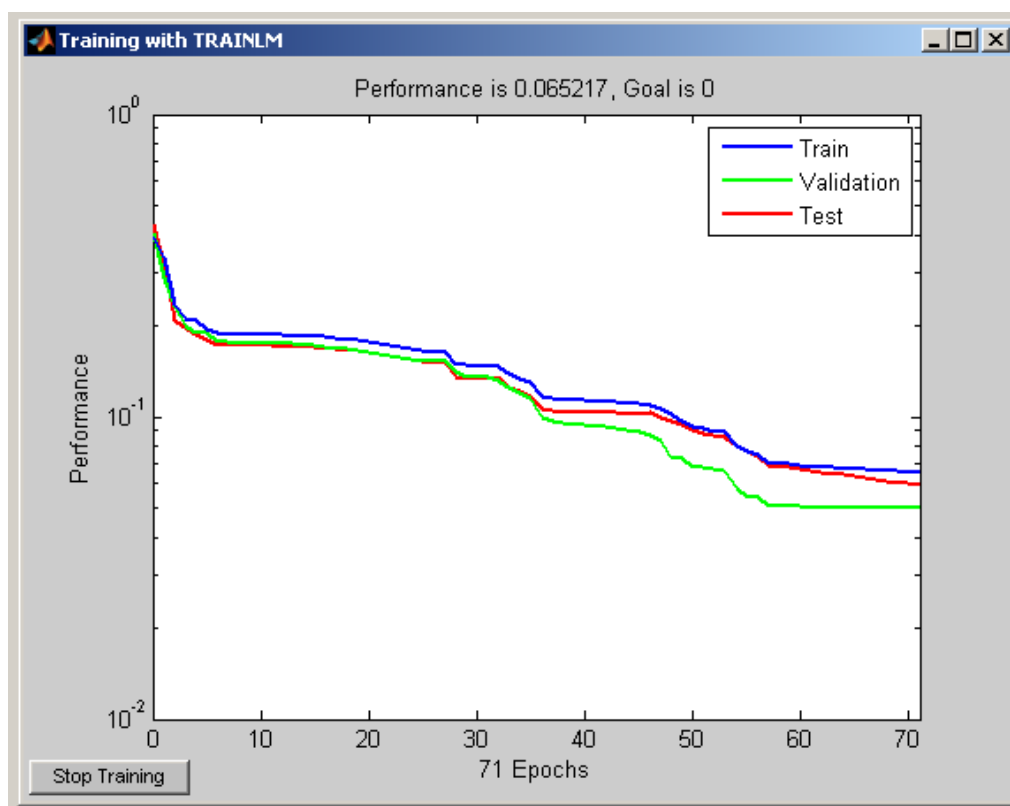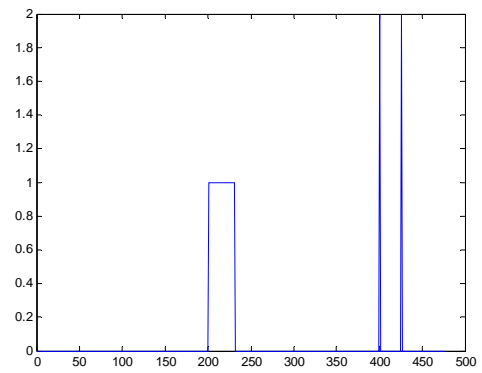

Figure 5.14: Network 6 Training Window
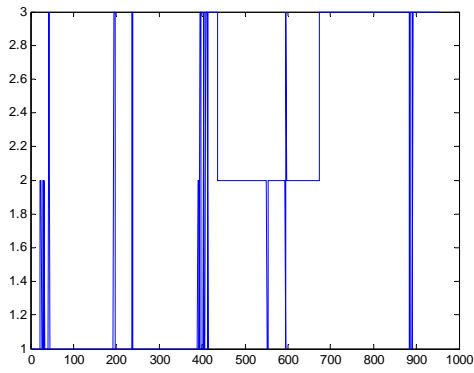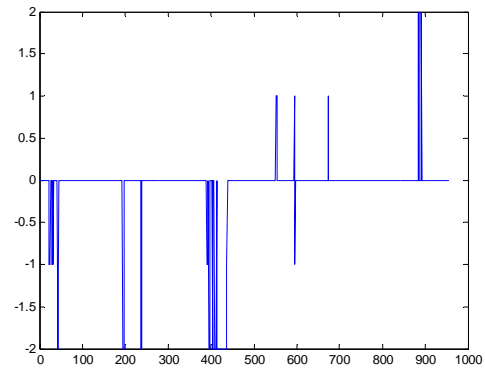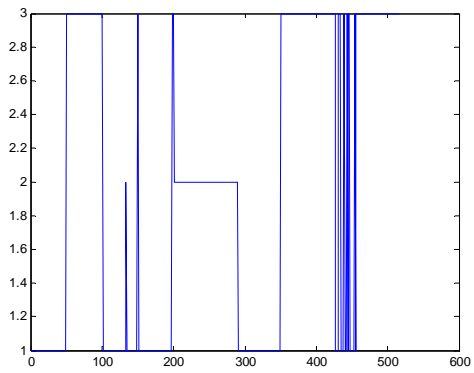
Figure 5.15: Network 6, 5 Neuron Average Normalized Binary Log Network, a) training set results, b) training set error, c) test set results, d)test set error, e) bad set results, f) bad set error

91

Table 5.6: Network 6 Error Statistics

Network 6	Accuracy	Type of detection errors
Training set	93.72%	all massive quantization errors
Test set	73.69%	all massive quantization errors
Bad set	88.45%	all massive quantization errors

Network 6 shows good performance, though not as good as Network 3, the unnormalized numeric average example. As table 5.6 indicates, all of the errors are due to quantization, which explains the random and oscillatory nature of the errors. Although Network 6 experiences massive quantization errors in regions of known error and on battery set borders, it shows relatively minor quantization elsewhere. Also, while Network 6 has similar Bad set accuracy as all previous networks, it manages to correctly identify all known Bad set trouble spots including the notorious SLA set.

2) *Network 7*: Network 7 is a perfect training result for chemistry detection networks with binary log sigmoid outputs using normalized data, its training and testing results are displayed in figure 5.16, 5.17 and table 5.7 below. Network 7 has 5 neurons in its hidden layer, it took 91 training epoch to reach a MSE of 0.000289, figure 5.16 displays all 91 training epochs.
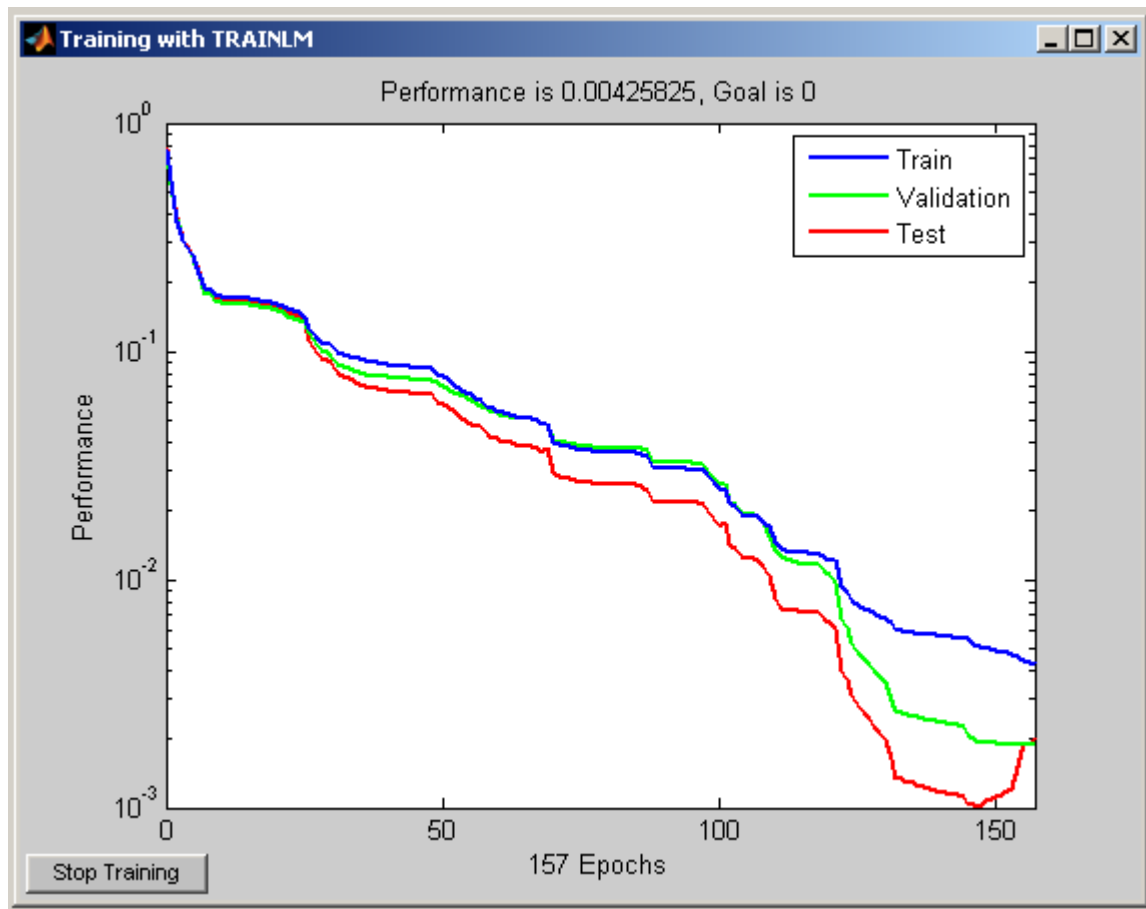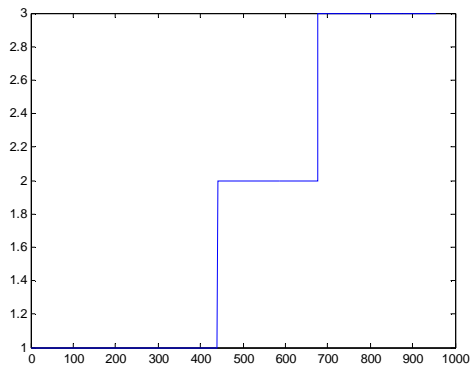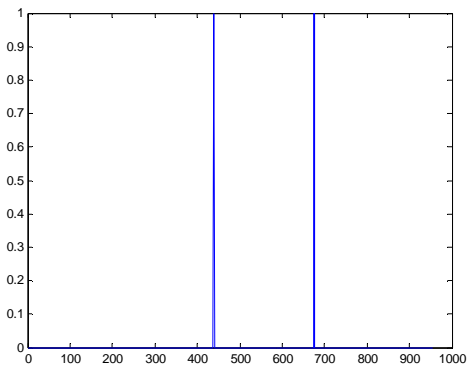
Figure 5.16: Network 7 Training Window
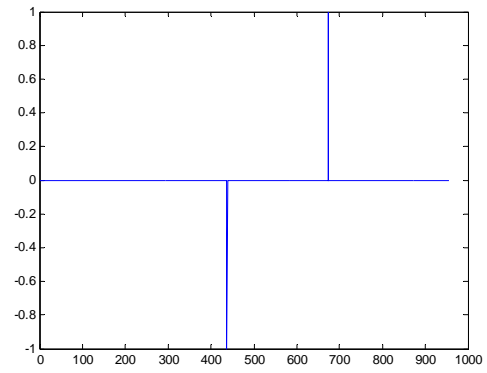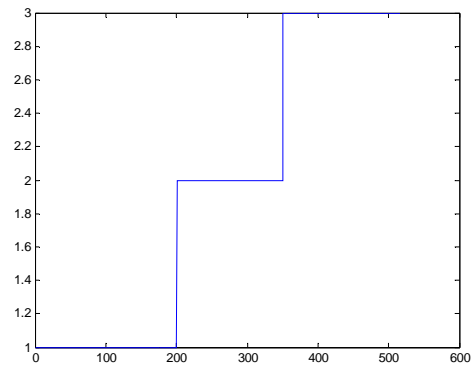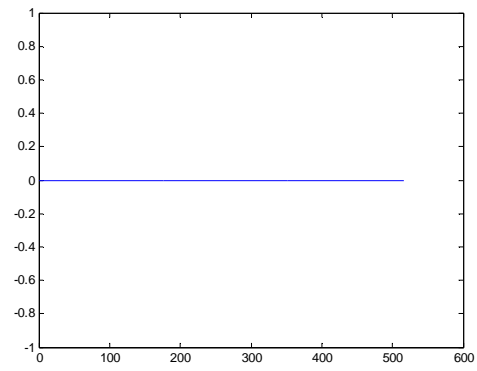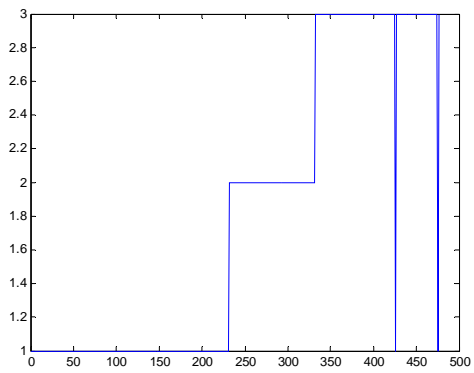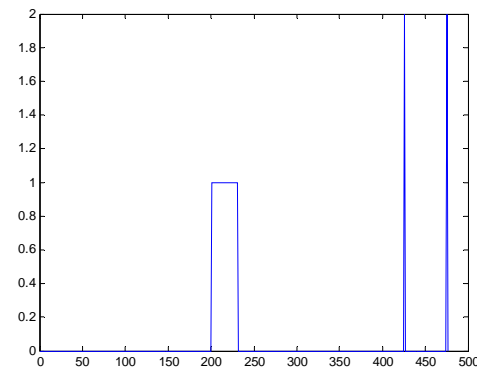
Figure 5.17: Network 7, 5 Neuron Perfect Normalized Binary Log Network, a) training set results, b) training set error, c) test set results, d)test set error, e) bad set results, f) bad set error

94

Table 5.7: Network 7 Error Statistics

Network 7	Accuracy	Type of detection errors
Training set	99.79%	2 classification errors, near perfect quantization
Test set	100%	very good to near perfect quantization throughout
Bad set	93.07%	all classification errors, near perfect quantization

Network 7 has almost perfect performance in all respects. With near perfect quantization except in common error regions, and even in the error regions the worst quantized output resembles [0.6, 0.001, 0.906], which still has a 0.3 margin of error. The Test set had near perfect quantization throughout.

These results show overall promising results for log sigmoid binary outputs, but the network training errors were unusually high. The average Network 6 had a 0.06 error, which would generally be unacceptable, whereas the extremely rare Network 7 had a 0.0002 error, which is common for most average or good networks but is extremely high for most perfect networks which generally have 10^{-6} or lower MSE. Also, while one perfect network was generated, the majority of the networks were like Network 6 and it was very hard to get a training error below Network 6's.

5.2.7   *Unnormalized Binary Log Sigmoid Chemistry Detection*

This fourth section analyzes chemistry detection networks using the binary output format with log sigmoid transfer functions using unnormalized input data. Network 8 is a sample average network while Network 9 is a sample great network, on average, most networks will look like Network 8 after training but a few retraining will generate one like Network 9

95

1) *Network 8*: Network 8 is an average training result for chemistry detection networks with binary log sigmoid outputs using unnormalized data, its training and testing results are displayed in figure 5.18, 5.19 and table 5.8 below. Network 8 has 5 neurons in its hidden layer, it took 53 training epoch to reach a MSE of 0.0036, figure 5.18 displays all 53 training epochs.
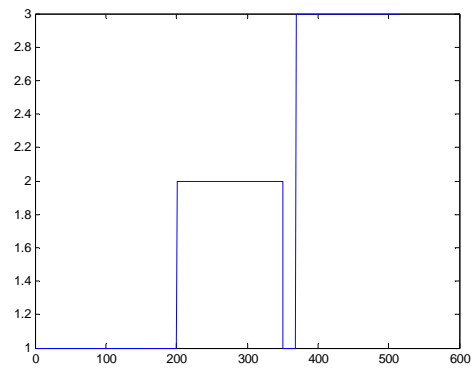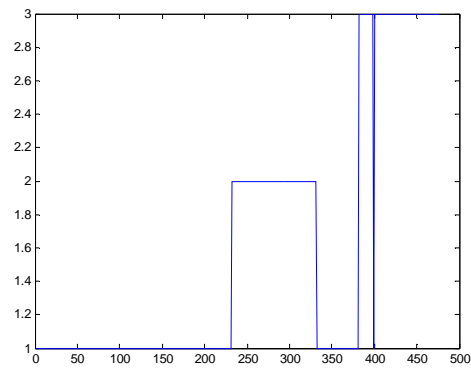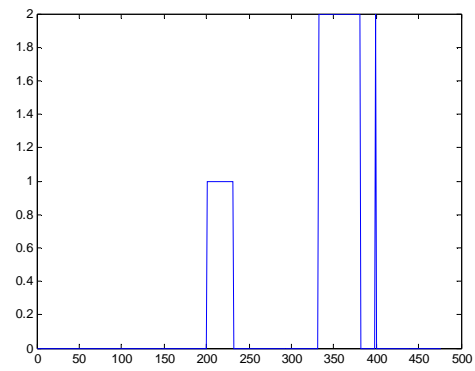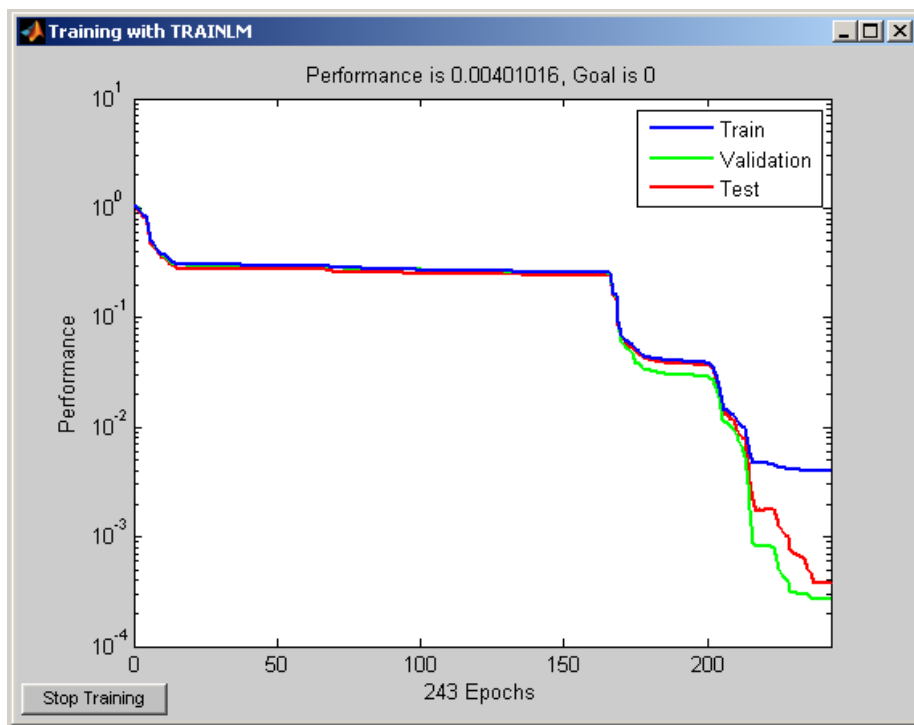

Figure 5.18: Network 8 Training Window
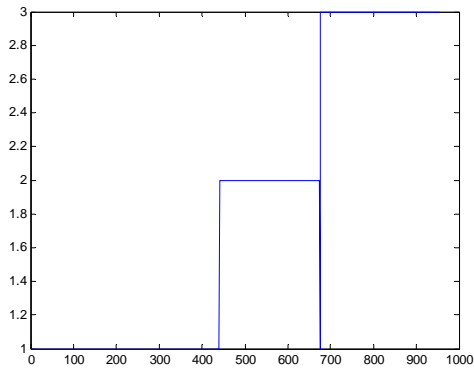
a)
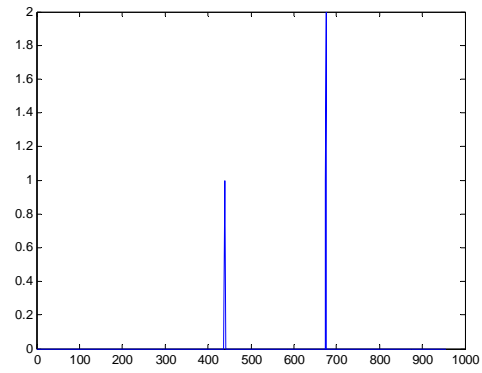
b)
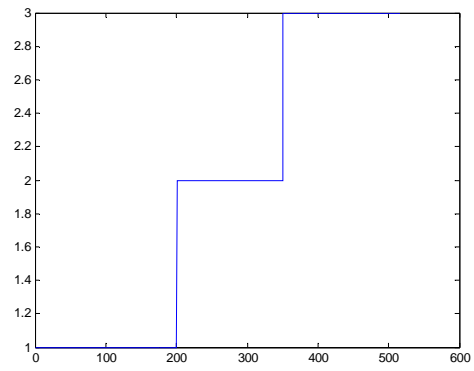
c)
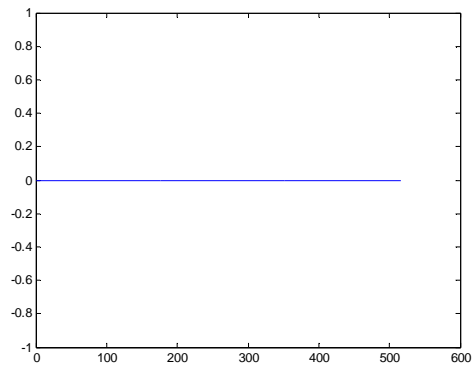
d)
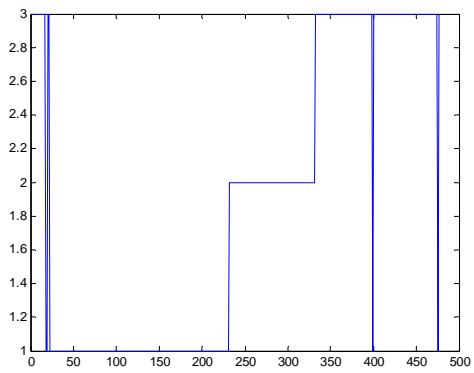
e)
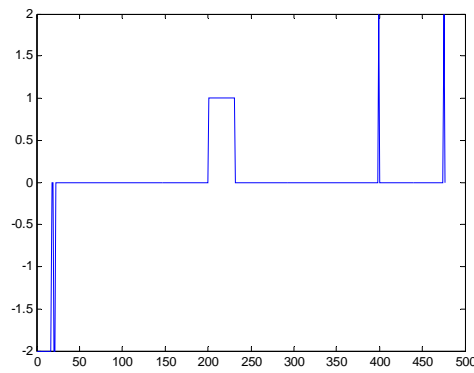
f)

Figure 5.19: Network 8, 5 Neuron Average Unnormalized Binary Log Network, a) training set results, b) training set error, c) test set results, d)test set error, e) bad set results, f) bad set error

97

Table 5.8: Network 8 Error Statistics

Network 8	Accuracy	Type of detection errors
Training set	99.37%	6 classification errors, near perfect to perfect quantization
Test set	100%	very good to near perfect quantization throughout
Bad set	89.08%	Half classification half quantization, near perfect quantization

Network 8 showed very good performance, almost as good as the perfect Network 7, but with higher amounts of quantization in error regions, which caused more errors in Training and Bad sets. However, Network 8 regularly showed perfect [1,0,0] quantization in trouble free spots, but it also showed perfect quantization in the first SLA set in the Bad set, which were its only classification errors in the Bad set.

2) *Network 9*: Network 9 is an above average training result for chemistry detection networks with binary log sigmoid outputs using unnormalized data, its training and testing results are displayed in figure 5.20, 5.21 and table 5.8 below. Network 9 has 20 neurons in its hidden layer, it took 64 training epoch to reach a MSE of 0.003117, figure 5.20 displays all 64 training epochs.
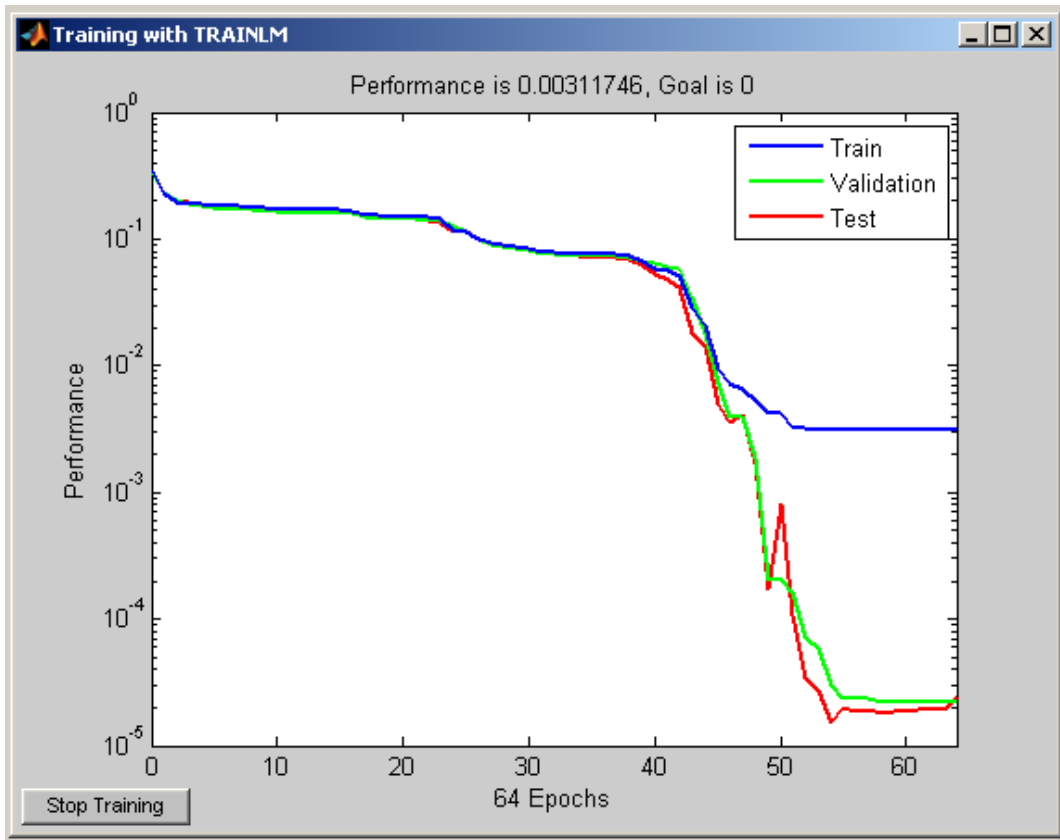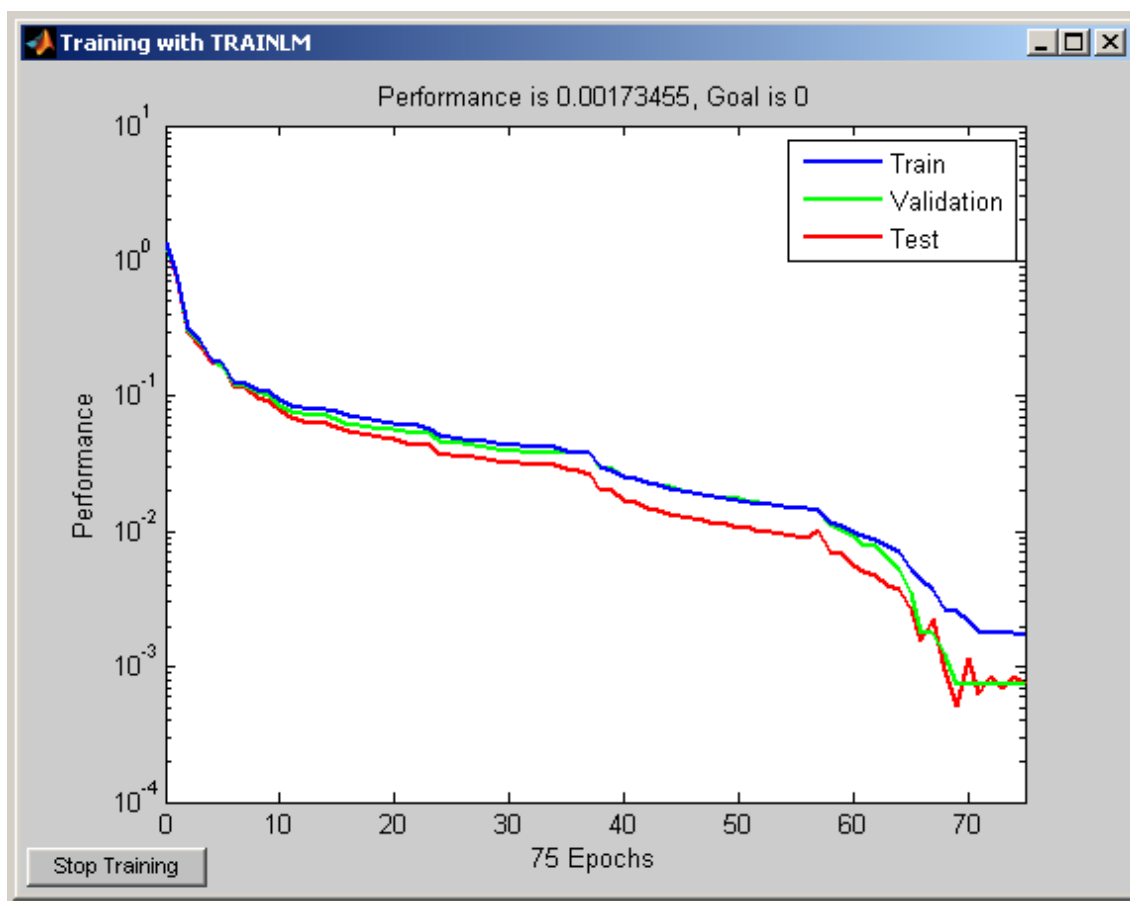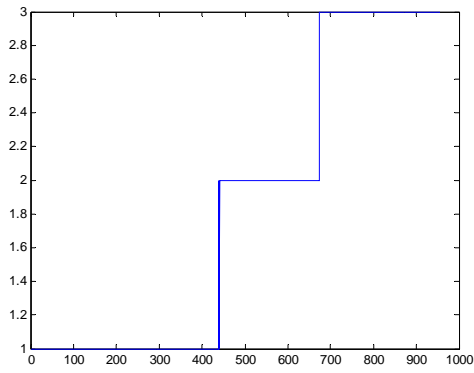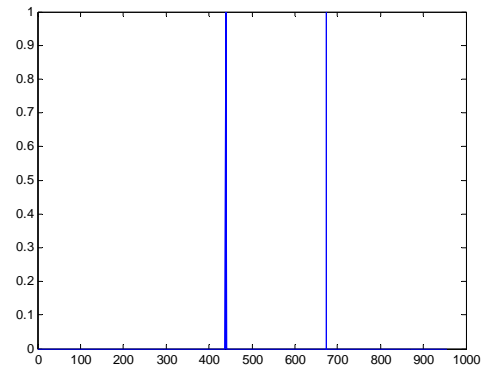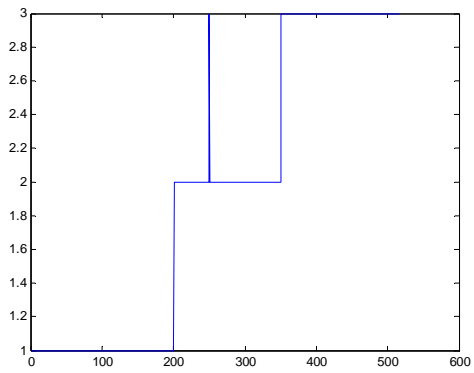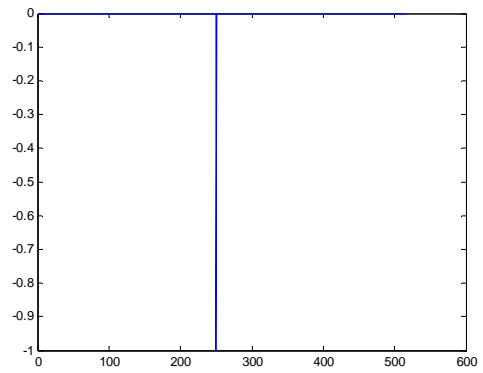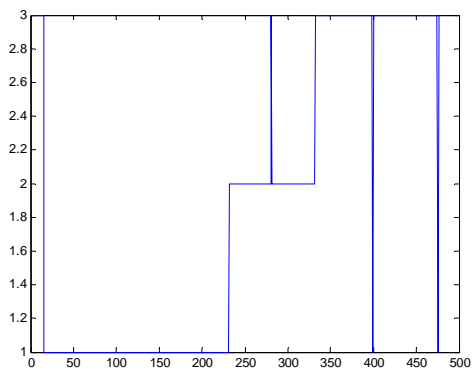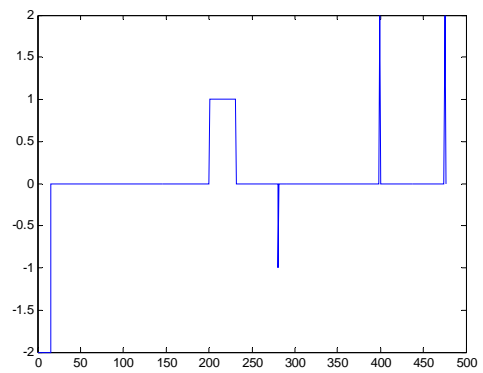
Figure 5.20: Network 9 Training Window
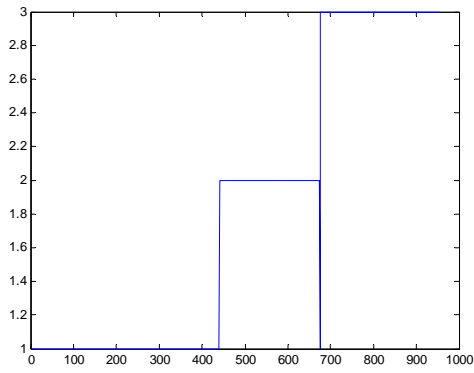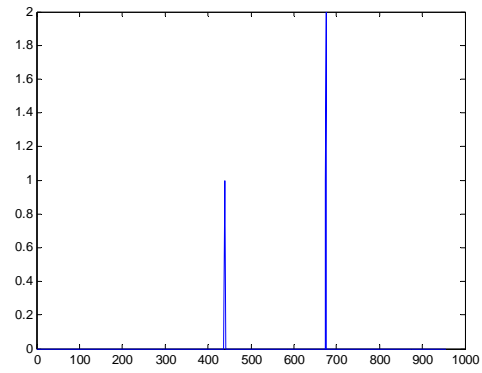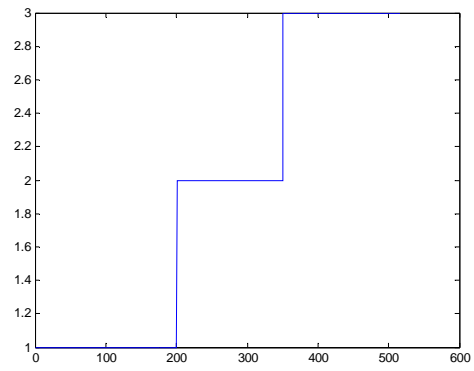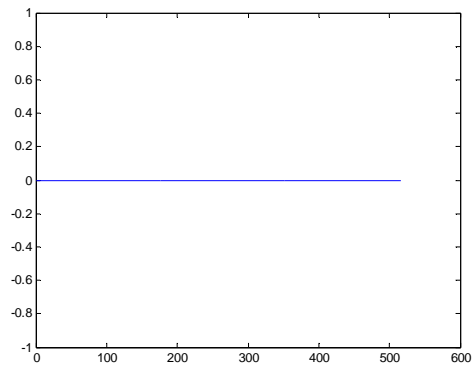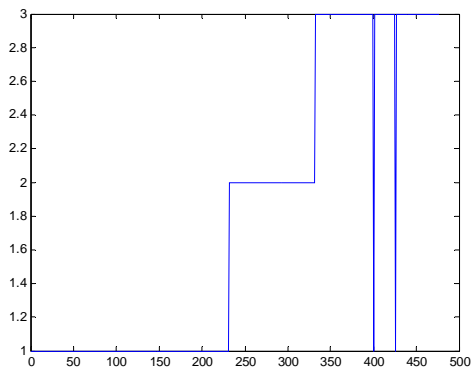
Figure 5.21: Network 9, 20 Neuron Good Unnormalized Binary Log Network, a) training set results, b) training set error, c) test set results, d)test set error, e) bad set results, f) bad set error

100

Table 5.9: Network 9 Error Statistics

Network 9	Accuracy	Type of detection errors
Training set	99.37%	6 classification errors, near perfect to perfect quantization
Test set	100%	very good to near perfect quantization throughout
Bad set	93.07%	most classification 2 quantization, near perfect quantization

Network 9 is almost identical to Network 8 but better quantization prevented the extra detection errors in the Bad set.

Overall results for unnormalized log sigmoid output show near perfect results in the average network. One interesting result from the training logs shows that although the training MSE was about 0.003 on average, the test and validation errors were generally two orders of magnitude below them; these unusually low test and validation errors explain the generally exceptional accuracy and suggest that a perfect network could be generated, though such a perfect network is only likely to have a 0.3% improvement in the Training and Bad sets based on previous performance.

Final results show that the binary log sigmoid output format performs exceptionally well with both normalized and unnormalized input data. However, the normalized networks required a perfect set to generate the same performance as an average unnormalized network, making unnormalized the superior choice for all detection networks. Also, testing has again revealed no preference for the number of neurons in the hidden layer, leaving the 5 neuron networks as the best choice. All binary log sigmoid network generally had the same performance except Network 6, whose generally poorer quantization caused it to have the lowest overall accuracy but almost 100% detection accuracy on the known error spots in the Bad set that all other

101

networks usually fail at; this unusual result warrants further research in future SOH work.

5.2.8   *Unnormalized Binary Tan Sigmoid Chemistry Detection*

This fifth section analyzes chemistry detection networks using the binary output format with tan sigmoid transfer functions using unnormalized input data. Network 10 is a representative of an average network while Network 11 is an above average example, on average, most networks will look like Network 10 after training but one or two retraining will generate one like Network 11

1) *Network 10*: Network 10 is an average training result for chemistry detection networks with binary tan sigmoid outputs using unnormalized data, its training and testing results are displayed in figure 5.22, 5.23 and table 5.10 below. Network 10 has 10 neurons in its hidden layer; it took 157 training epoch to reach a MSE of 0.004258, figure 5.22 displays all 157 training epochs.
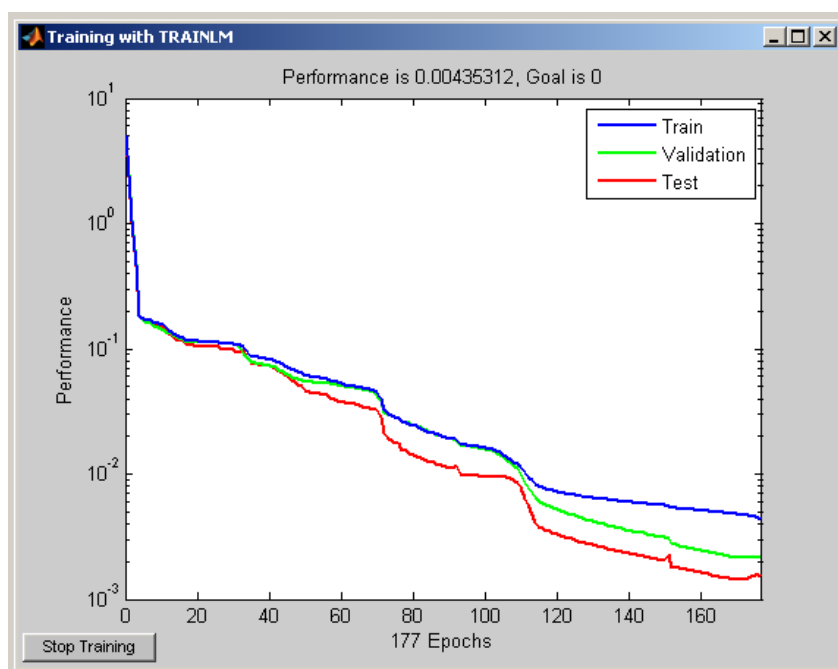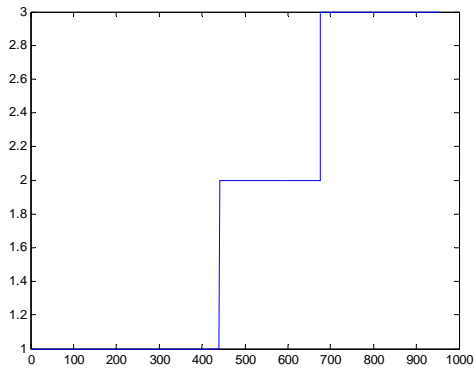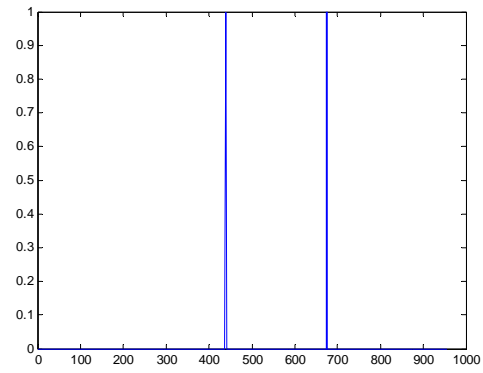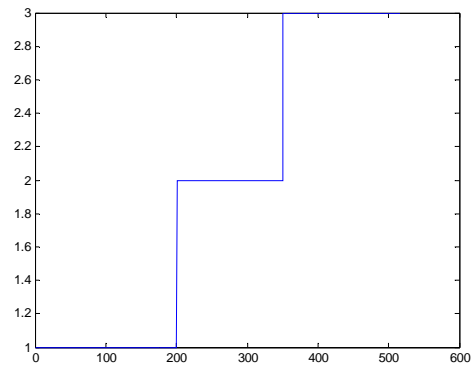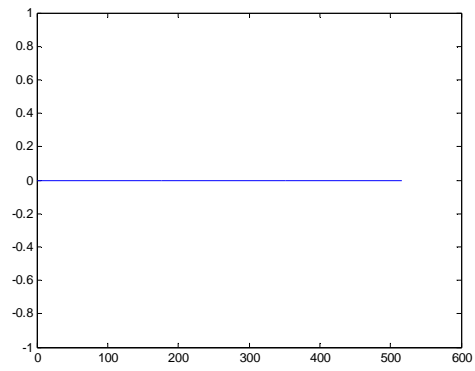
Figure 5.22: Network 10 Training Window
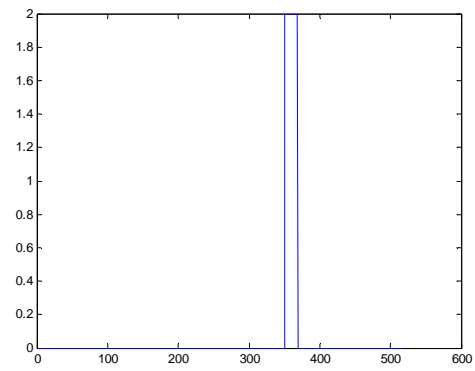
Figure 5.23 Network 10, 10 Neuron Average Unnormalized Binary Tan Network, a) training set results, b) training set error, c) test set results, d)test set error, e) bad set results, f) bad set error

104

Table 5.10: Network 10 Error Statistics

Network 10	Accuracy	Type of detection errors
Training set	99.37%	all classification errors, no quantization errors present at all
Test set	96.32%	all quantization errors, but good quantization otherwise
Bad set	82.77%	Half quantization half classification, good quantization else

Network 10 performs the same as the log sigmoid networks but with less quantization in the Bad and Test sets causing lower accuracy.

2) *Network 11*: Network 11 is an above average training result for chemistry detection networks with binary tan sigmoid outputs using unnormalized data, its training and testing results are displayed in figure 5.24, 5.25, and table 5.11 below. Network 11 has 10 neurons in its hidden layer, it took 243 training epoch to reach a MSE of 0.00401, figure 5.24 displays all 243 training epochs.
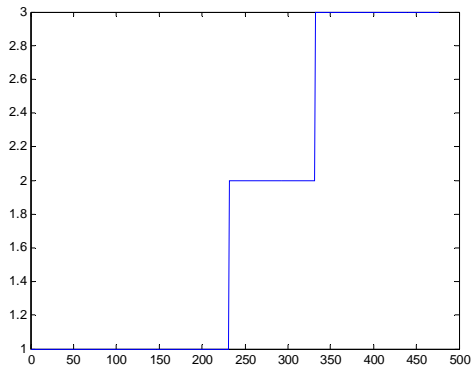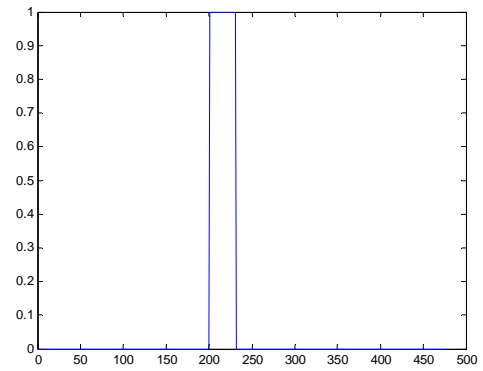

Figure 5.24: Network 11 Training Window
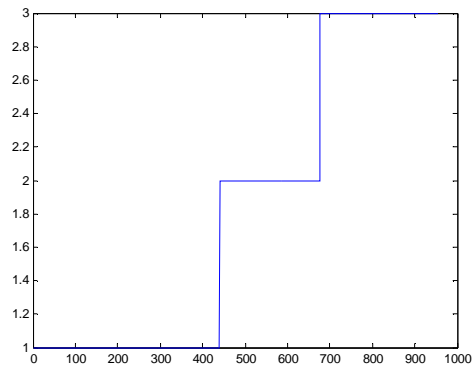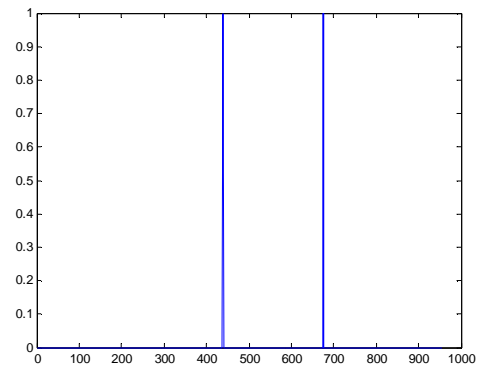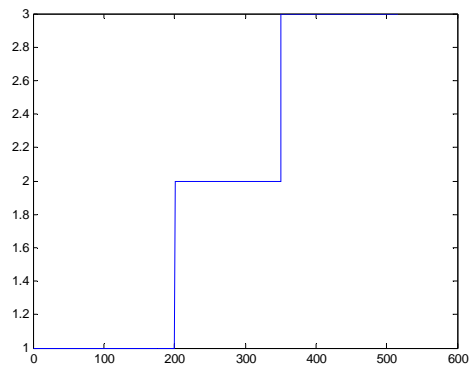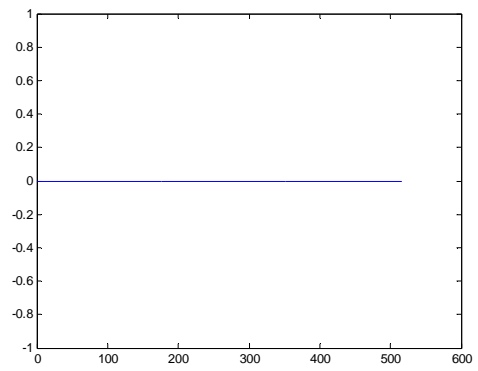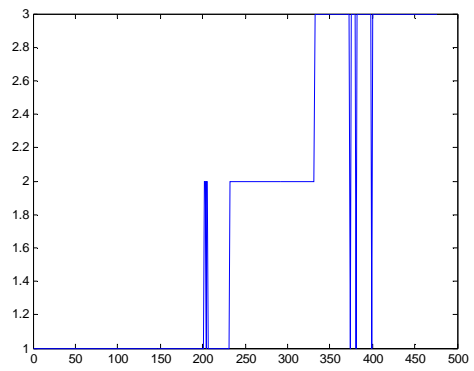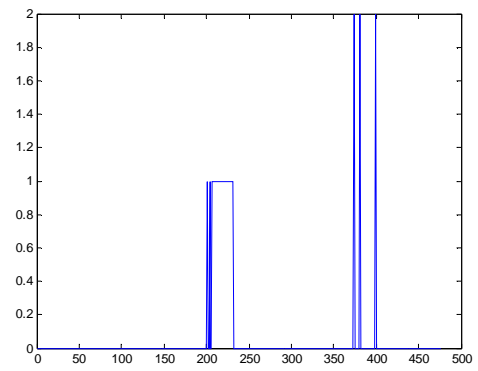
Figure 5.25: Network 11, 10 Neuron Good Unnormalized Binary Tan Network, a) training set results, b) training set error, c) test set results, d)test set error, e) bad set results, f) bad set error

106

Table 5.11: Network 11 Error Statistics

Network 11	Accuracy	Type of detection errors
Training set	99.37%	all classification errors, no quantization errors present at all
Test set	100%	All generally of .99 .06 .001 form
Bad set	93.70%	all quantization errors, general imperfect quantization

Network 11 performs exactly like the good log sigmoid networks except for higher quantization error in the Bad set that actually improves accuracy. Although both Networks 10 and 11 have similar MSE, Network 11 has significantly lower testing and validation MSE similar to the unnormalized log sigmoid networks.

Final results show that the binary tan sigmoid output format performs comparatively well with log sigmoid output format. However, the tan sigmoid networks average performance was slightly less effective. Network 11's high Bad set performance was the result of unusual quantization error caused by negative numbers of the [-.9, .01,-.9] type that resulted in 0.01 turning into a 1 because it was the only positive number; this unusual result wasn't generally repeatable and is regarded as a fluke, though this does establish a pattern of quantization errors causing correct classifications. Despite the similar performance of the log sigmoid and tan sigmoid networks, the log sigmoid is considered better due to its higher average accuracy and lack of negative numbers.

5.2.9 *Unnormalized Binary Linear Chemistry Detection*

This sixth section analyzes chemistry detection networks using the binary output format with linear transfer functions using unnormalized input data. Network 12 is a representative of an average network while Network 13 is an above average example,

107

on average, most networks will look like Network 12 after training but one or two retraining will generate one like Network 13

1) *Network 12*: Network 12 is an average training result for chemistry detection networks with binary linear outputs using unnormalized data, its training and testing results are displayed in figure 5.26, 5.27, and table 5.12 below. Network 12 has 5 neurons in its hidden layer, it took 75 training epoch to reach a MSE of 0.001734, figure 5.26 displays all 75 training epochs.
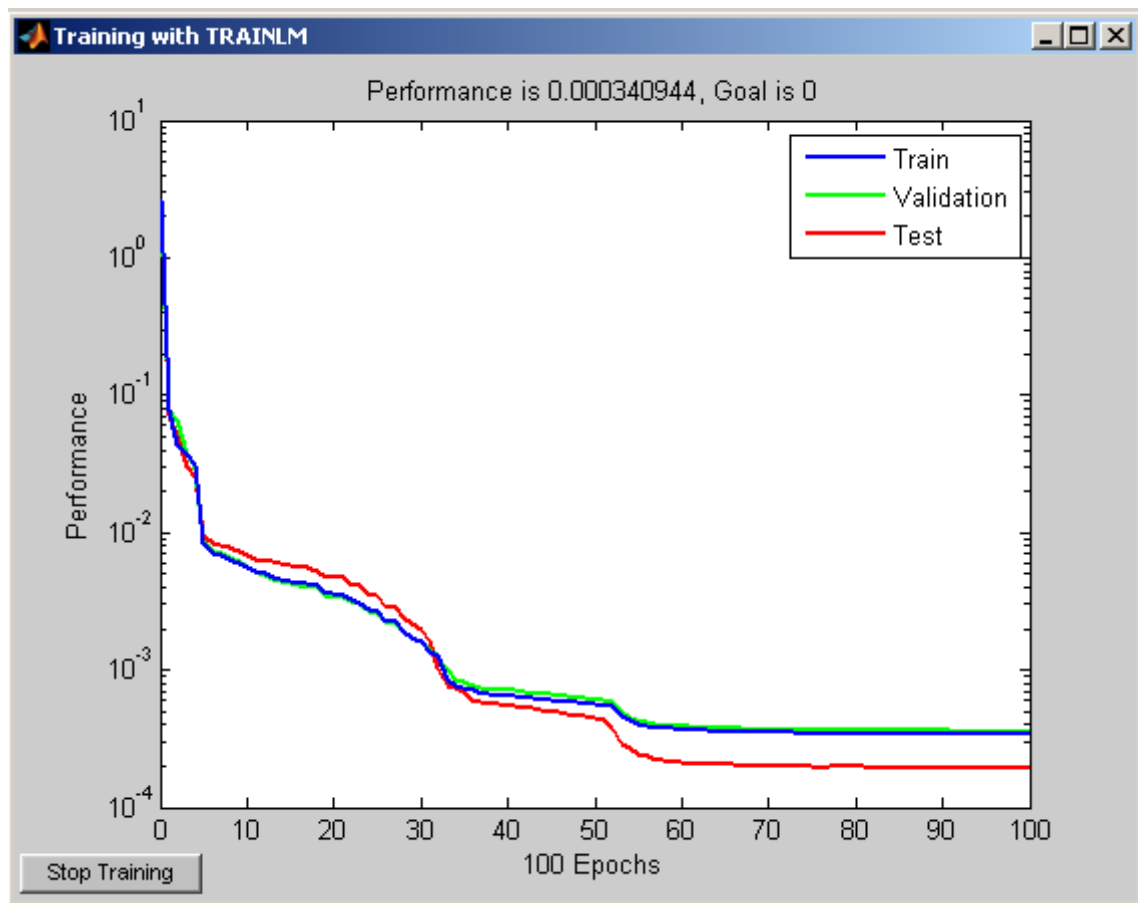

Figure 5.26: Network 12 Training Window

108

Figure 5.27: Network 12, 5 Neuron Average Unnormalized Binary Linear Network, a) training set results, b) training set error, c) test set results, d)test set error, e) bad set results, f) bad set error

Table 5.12: Network 12 Error Statistics

Network 12	Accuracy	Type of detection errors
Training set	99.69%	all quantization errors, decent quantization elsewhere
Test set	99.81%	1 quantization error, unusual [-.05,-.2,1.35] form
Bad set	89.71%	all classification errors, general imperfect quantization

Network 12 provides great results only slightly below par with other binary networks. Due to the nature of linear output, Network 12 has less than perfect quantization and slightly negative outputs, the best outputs look like [1.01,-.0001,-.01]

2) *Network 13*: Network 13 is a good training result for chemistry detection networks with binary linear outputs using unnormalized data, its training and testing results are displayed in figure 5.28, 5.29, and table 5.13 below. Network 13 has 20 neurons in its hidden layer, it took 177 training epoch to reach a MSE of 0.00435, figure 5.28 displays all 177 training epochs.
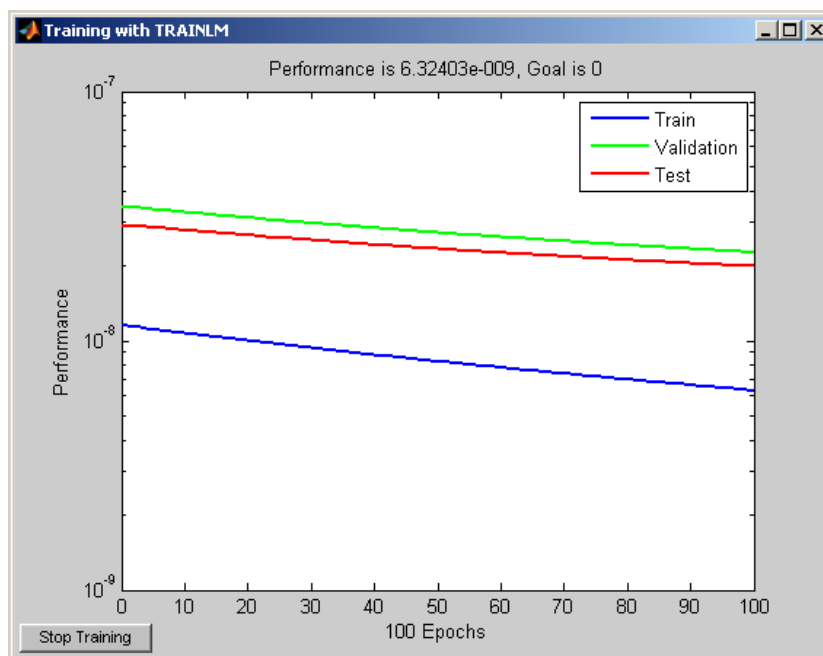

Figure 5.28: Network 13 Training Window

110

Figure 5.29: Network 13, 20 Neuron Good Unnormalized Binary Linear Network, a) training set results, b) training set error, c) test set results, d)test set error, e) bad set results, f) bad set error

111

Table 5.13: Network 13 Error Statistics

Network 13	Accuracy	Type of detection errors
Training set	99.37%	All classification errors, decent quantization
Test set	100%	Poor quantization
Bad set	93.47%	All quantization errors, of [13,0,-12] form

Although Network 13 has better performance than Network 12, its accuracy is due to very poor quantization in general, which tends to overload outputs in order to generate proper results.

Final results indicate that although binary linear output network have comparable performance to other binary output networks, they generally have poorer quantization and negative outputs. Ultimately unnormalized log sigmoid is the best.

5.2.10 *Chemistry Detection Final Results*

In the end, the chemistry detection research has identified that binary output format, neural networks with log sigmoid transfer functions using unnormalized input data has the overall best performance. As indicated by Network 8 and Network 9, unnormalized log sigmoid networks have consistently high performance with near perfect quantization. And although some networks had slightly higher performance in one set or another, the log sigmoid networks had the highest consistency. In terms of hidden layer neuron count, no particular value distinguished itself so the smaller 5 neuron is the best by default.

5.3 Experimental Results SOC Estimation

5.3.1   *SOC Estimation Design Considerations*

The second half of the ANN method is SOC estimation. Because SOC estimation requires a linear output for its sweep of possible SOC values, the only design considerations are the number of hidden layer neurons and whether or not to use normalized input data. This part of the research is divided into three sections, one for each chemistry, and each subsection tests normalized and unnormalized input data for each chemistry. All three chemistry networks share the same basic neural network model shown in figure 5.30 below, though the hidden layers have 5, 10, or 20 neurons
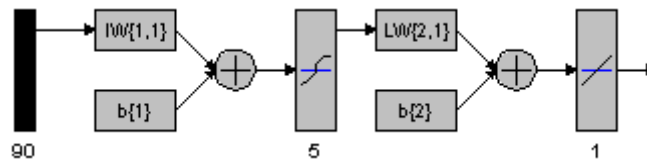
Figure 5.30: Sample SOC Estimation Neural Network Model

5.3.2   *Li-Ion SOC Estimation Setup*

The first SOC subsection is the Li-Ion SOC estimation research. Figure 5.31 below shows the three datasets used for Li-Ion SOC estimation, figure 5.31.a is the training set, 5.31.b is the test set that contains mostly clean data, and 5.31.c is the bad set that contains all remaining data sets not used in the first two including irregular ones due to damaged batteries or measurement errors. These dataset are not randomized so

that the results for each individual battery set can be evaluated. Additionally, the perfectly linear SOC plots demonstrate Li-Ion battery's constant power output.

a)

b)

c)
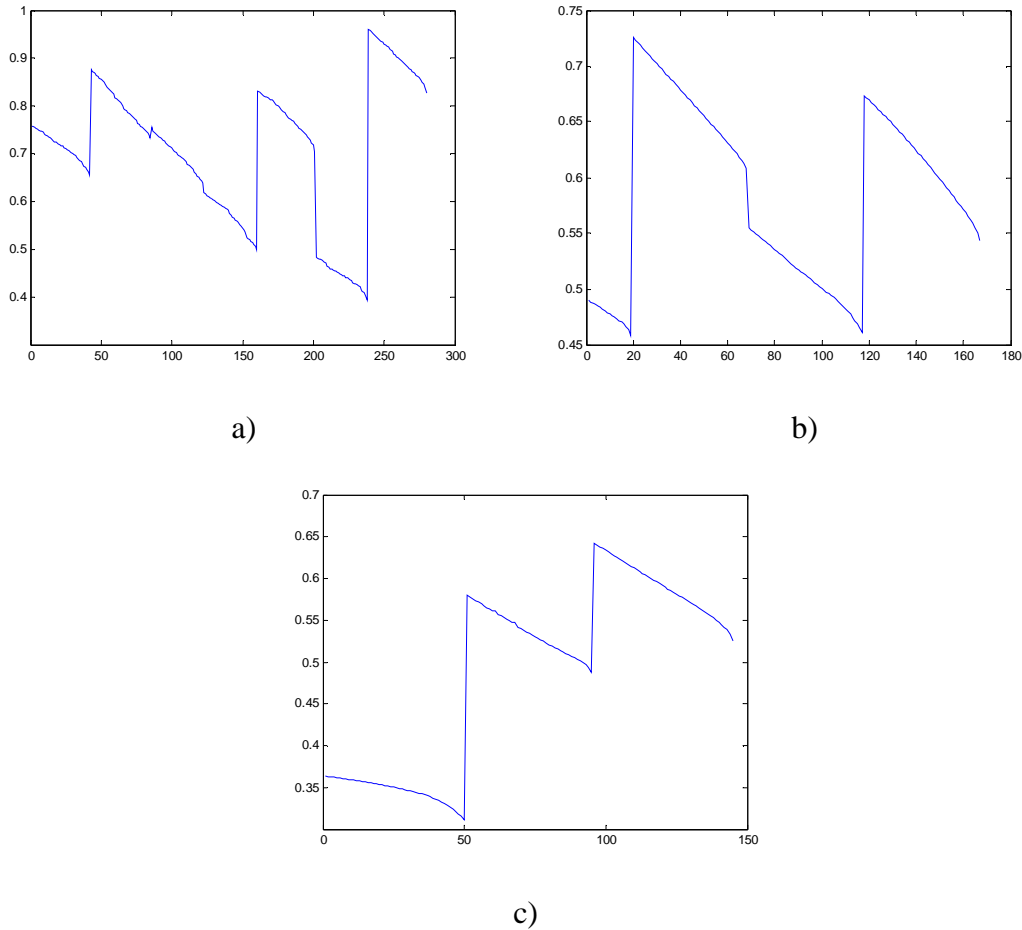
Figure 5.31: Original Li-Ion SOC Estimation Plots, a) Training set, 280 samples, b) Test set, 167 samples, c) Bad set, 145 samples

5.3.3   *Normalized Li-Ion SOC Estimation Research*

This section analyzes Li-Ion SOC estimation using normalized input data. Network 14 is a representative of an average network while Network 15 is a perfect example, on average, most networks will look like Network 14 after training but a dozen retraining will generate one like Network 15, which is rare but easily obtainable.

114

1) *Network 14*: Network 14 is an average training result for Li-Ion SOC estimation networks using normalized data, its training and testing results are displayed in figure 5.32, 6.33, and table 5.14 below. Network 14 has 5 neurons in its hidden layer, it took 100 training epoch to reach a MSE of 0.000340, figure 5.32 displays all 100 training epochs.
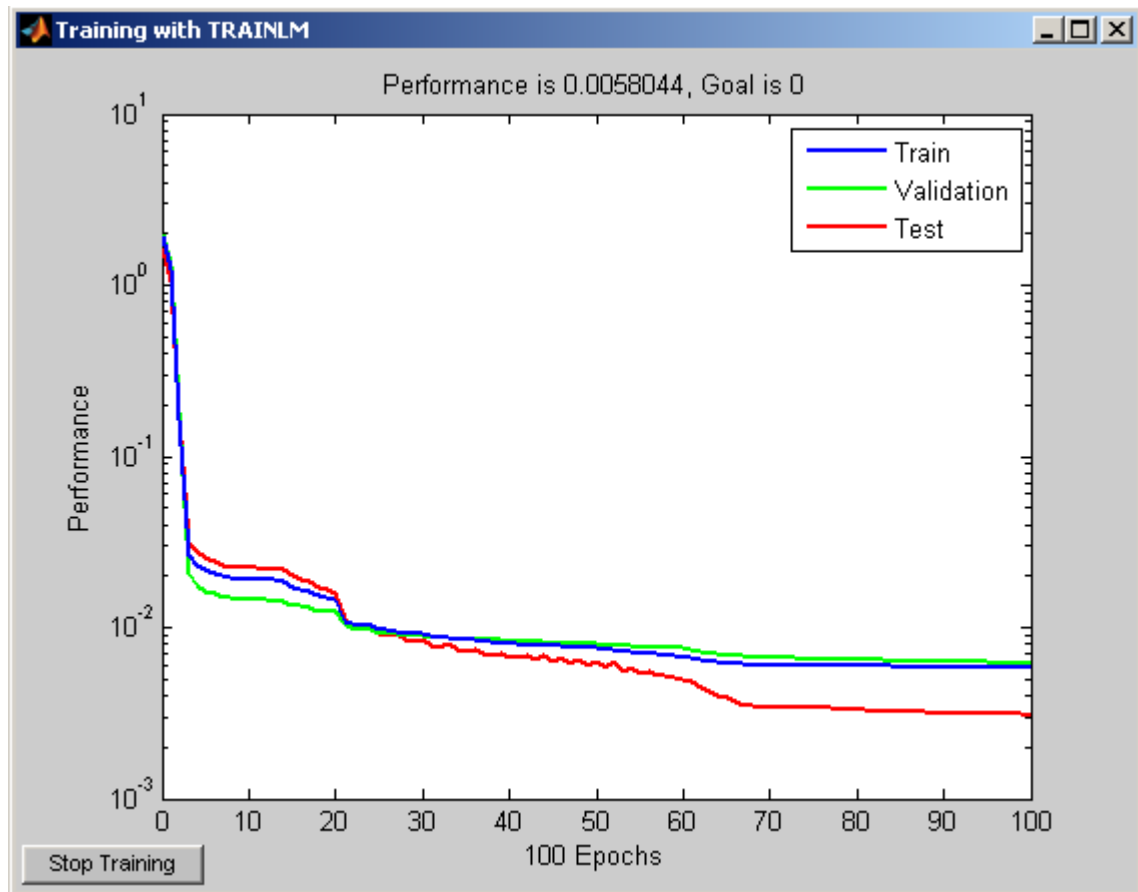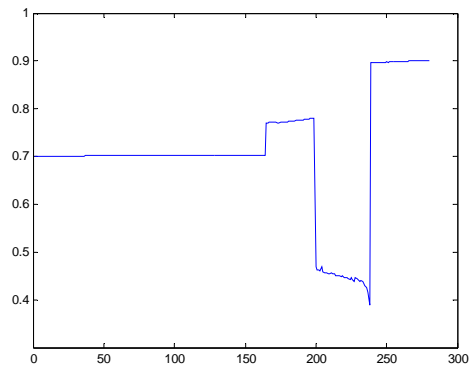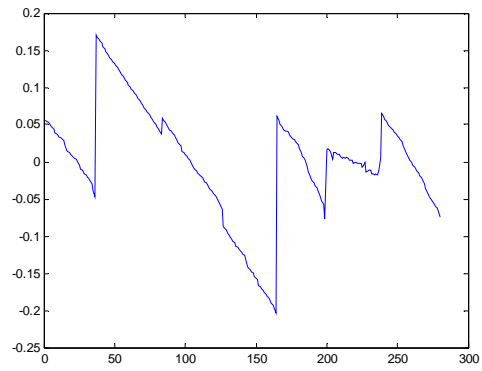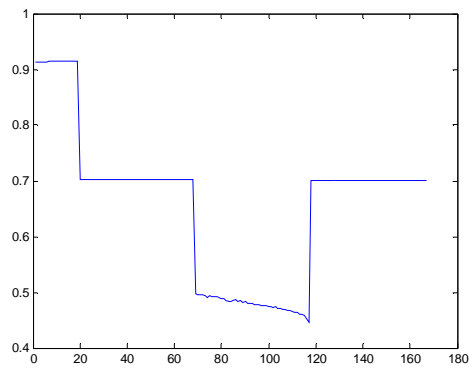

Figure 5.32: Network 14 Training Window
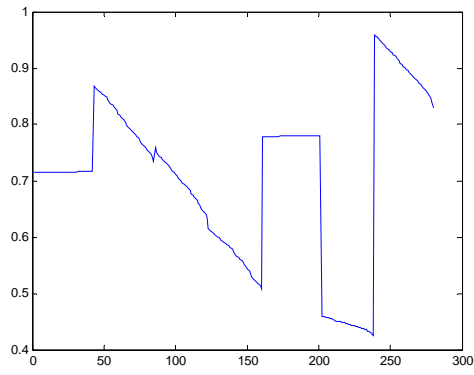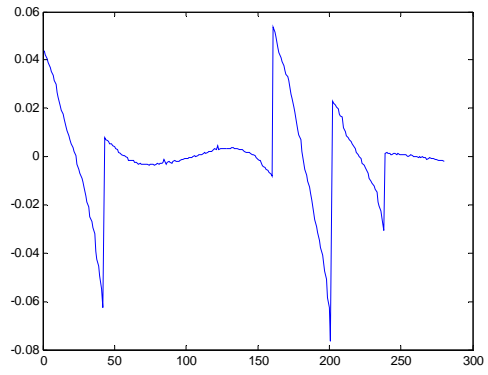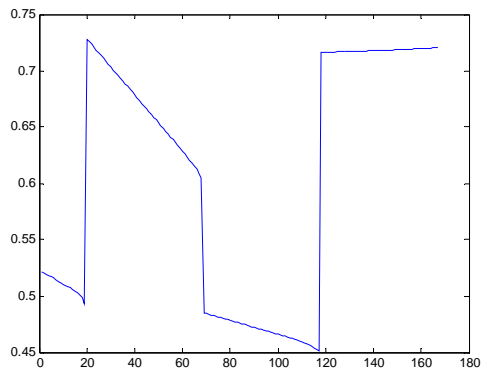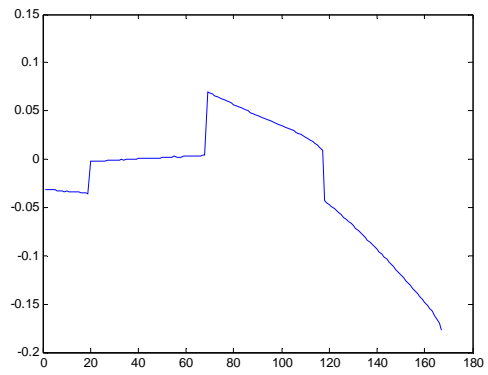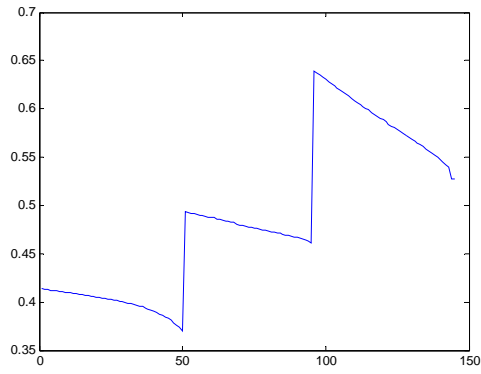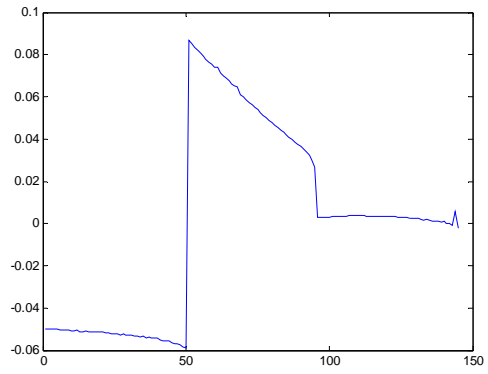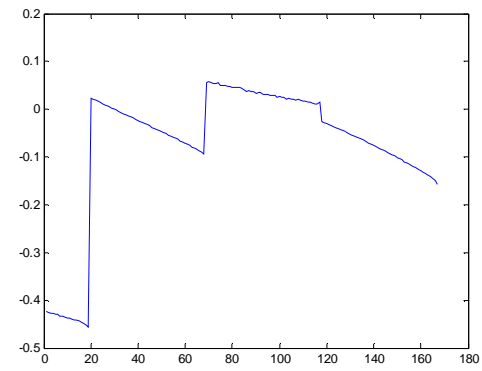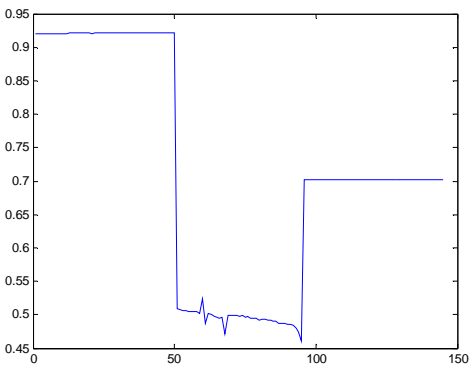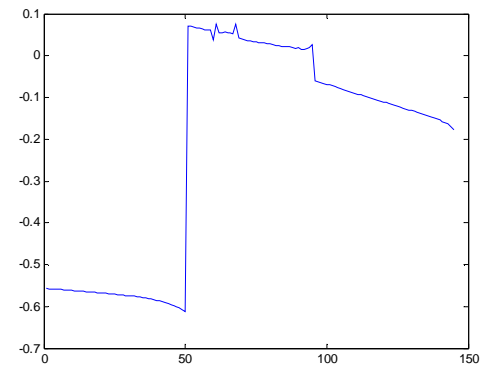
Figure 5.33 Network 14, 5 Neuron Average Normalized Li-Ion SOC Network, a) training set results, b) training set error, c) test set results, d)test set error, e) bad set results, f) bad set error

116

Table 5.14: Network 14 Error Statistics

Network 14	Mean error	Max error
Training set	0.0109	0.0764
Test set	0.0472	0.1774
Bad set	0.0369	0.0865

Network 14 does a reasonable job at modeling the SOC outputs but generally has a hard time modeling the perfectly linear regions. Although the 4.72% average SOC error is somewhat acceptable, the 17.74% max error isn't.

2) *Network 15*: Network 15 is a perfect training result for Li-Ion SOC estimation networks using normalized data, its training and testing results are displayed in figure 5.34, 5.35, and table 5.15 below. Network 15 has 20 neurons in its hidden layer, it took 900 training epoch to reach a MSE of $6.32*10^{-9}$ and it can go lower, figure 5.34 displays the last 100 training epochs.

Figure 5.34: Network 15 Training Window
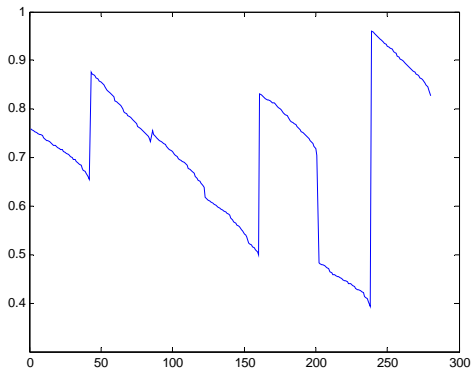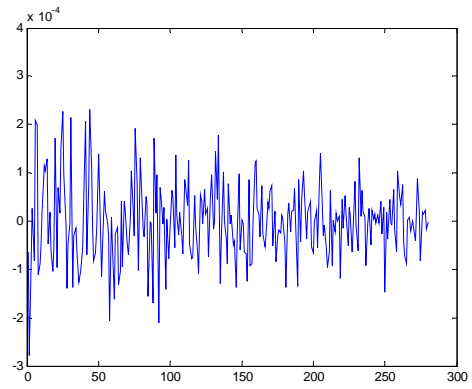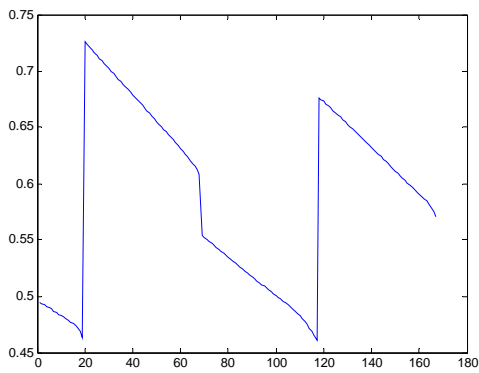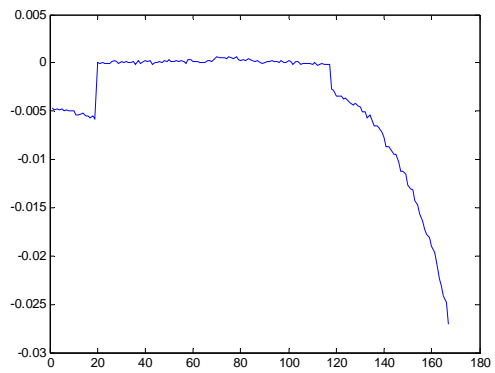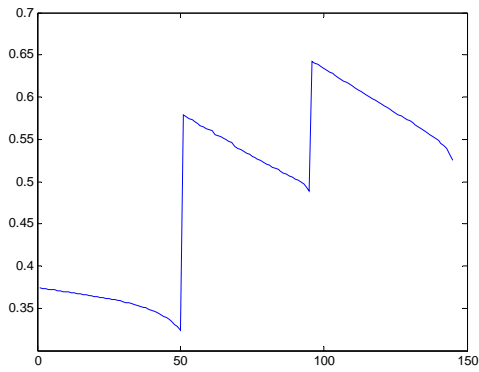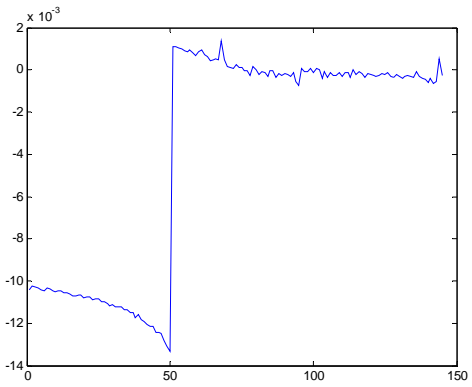
Figure 5.35: Network 15, 20 Neuron Perfect Normalized Li-Ion SOC Network, a) training set results, b) training set error, c) test set results, d)test set error, e) bad set results, f) bad set error

118

Table 5.15: Network 15 Error Statistics

Network 15	Mean error	Max error
Training set	8.0868e-005	3.8101e-004
Test set	0.0045	0.0317
Bad set	0.0037	0.0121

Network 15 is an extremely perfect network, with average error less than 0.5% and a maximum 3.17% error over a notoriously difficult region shown in figure 5.35.d. Network 15's error plots are consistent with the error patterns usually seen on the higher accuracy networks, though the error magnitude is greatly reduced. Even though Network 15 is a perfect example, it is only the second perfect network generated for Li-Ion.

Overall results show that Li-Ion SOC networks with normalized input data can perform extremely well but they require a very low training MSE in order to properly fit the unusual linear curves. However, extensive testing on hidden layer neuron count showed no preference as each neuron count generated a perfect network; network accuracy is solely dependent on training MSE.

5.3.4   *Unnormalized Li-Ion SOC Estimation Research*

This section analyzes Li-Ion SOC estimation using unnormalized input data. Network 16 is the average network example; countless testing has generated networks that are all similar to Network 16.

1) *Network 16*: Network 16 is an average training result for Li-Ion SOC estimation networks using unnormalized data, its training and testing results are displayed in figure 5.36, 5.37, and table 5.16 below. Network 16 has 5 neurons in its

hidden layer, it took 100 training epoch to reach a MSE of 0.0058, figure 5.36 displays

all 100 training epochs.
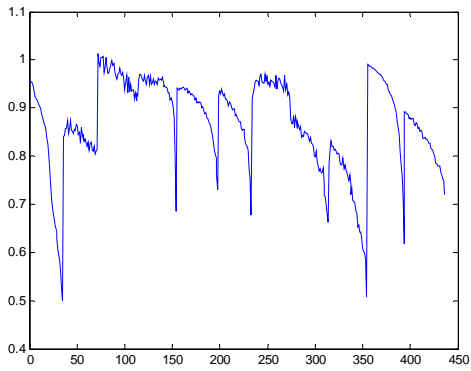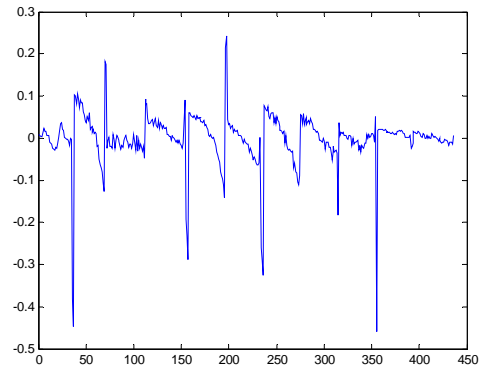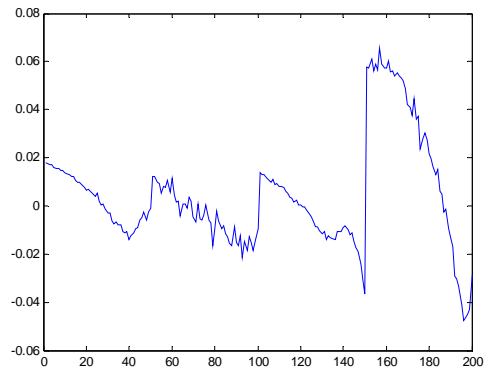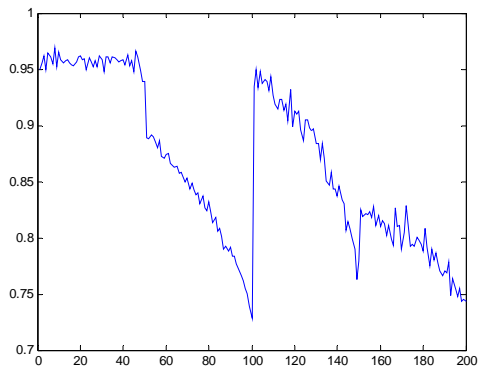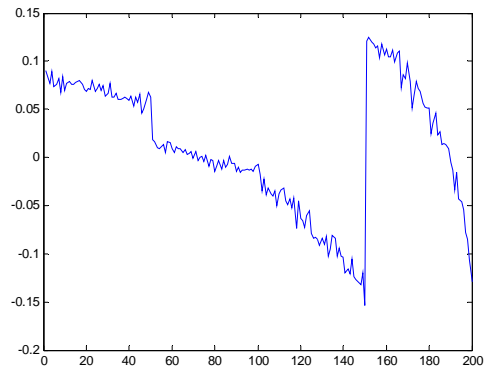

Figure 5.36: Network 16 Training Window

Figure 5.37: Network 16, 5 Neuron Average Unnormalized Li-Ion SOC Network, a) training set results, b) training set error, c) test set results, d)test set error, e) bad set results, f) bad set error

121

Table 5.16: Network 16 Error Statistics

Network 16	Mean error	Max error
Training set	0.0556	0.2029
Test set	0.0961	0.4565
Bad set	0.2495	0.6113

Unfortunately, Network 16's dismal performance is extremely common for unnormalized Li-Ion SOC estimation networks. It was believed that the Li-Ion SOC ANNs would benefit from unnormalized data in the same way the chemistry detection ANNs did, but unnormalized input data only served to generate flat SOC curves with huge offset errors, no valid reason was found to explain this result. Also, performance results were universally bad regardless of hidden layer neuron count.

The final results show that a neural network for Li-Ion SOC estimation can have excellent accuracy and modeling performance as long as it is trained to an extremely low MSE using only normalized input data. Experiments showed that MSEs below 10^{-5} were required for reasonable performance, though the max error on the Test set tended to be high outside without perfect networks due to the troublesome plot. In terms of hidden layer neuron count, the higher neuron count networks tended to generate more perfect networks with lower MSE, but the total number of perfect networks isn't large enough to draw a definite conclusion.

5.3.5   NiMH SOC Estimation Setup

The second SOC subsection is the NiMH SOC estimation research. Figure 5.38 below shows the three datasets used for NiMH SOC estimation, figure 5.38.a is the training set, 5.38.b is the test set that contains mostly clean data, and 5.38.c is the bad

set that contains all remaining data sets not used in the first two including irregular ones due to damaged batteries or measurement errors. These dataset are not randomized so that the results for each individual battery set can be evaluated. Additionally, the nonlinear, exponentially decreasing SOC plots demonstrate NiMH's declining power output with declining SOC, and the sharp SOC changes show that NiMH batteries gain the majority of their power in the first few minutes of charging, this is the basis of rapid battery chargers.
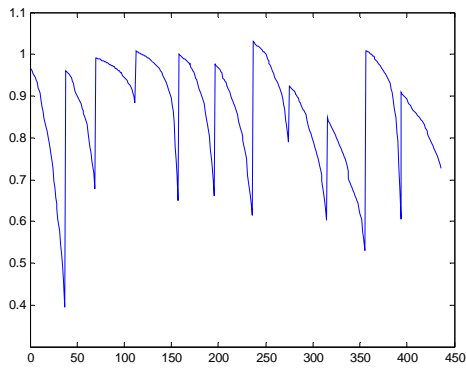
a)
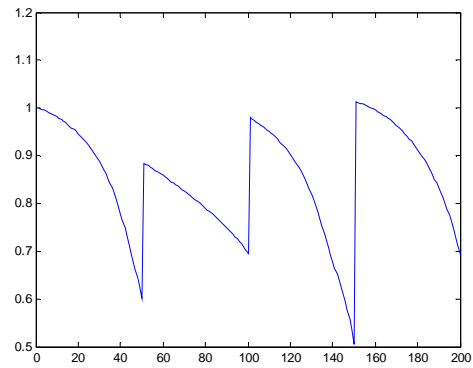
b)
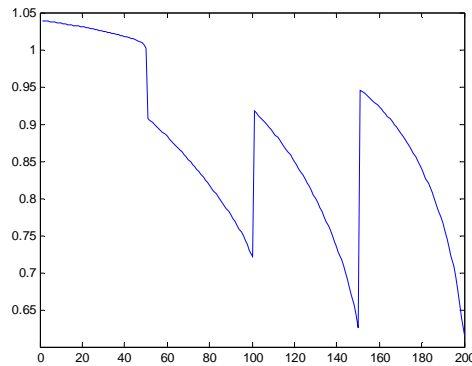
c)

Figure 5.38: Original NiMH SOC Estimation Plots, a) Training set, 436 samples, b) Test set, 200 samples, c) Bad set, 200 samples

5.3.6   *Normalized NiMH SOC Estimation Research*

This section analyzes NiMH SOC estimation using normalized input data. Network 17 is the average network example, countless testing has generated networks that are all similar to Network 17, they usually range between 0.006 and 0.004 MSE.

1) *Network 17*: Network 17 is an average training result for NiMH SOC estimation networks using normalized data, its training and testing results are displayed in figure 5.39, 5.40, and table 5.17 below. Network 17 has 5 neurons in its hidden layer, it took 93 training epoch to reach a MSE of 0.00404, the lowest achieved for normalized inputs, figure 5.39 displays all 93 training epochs.
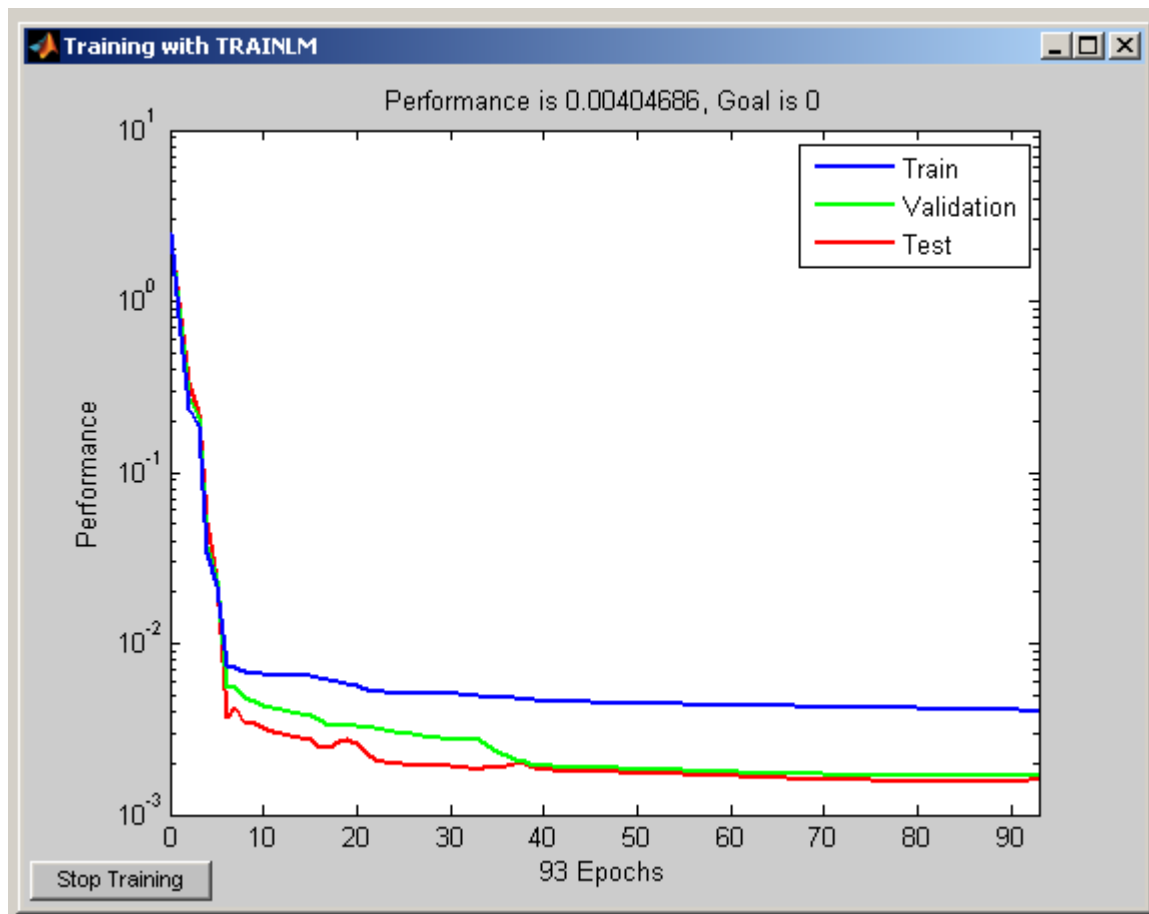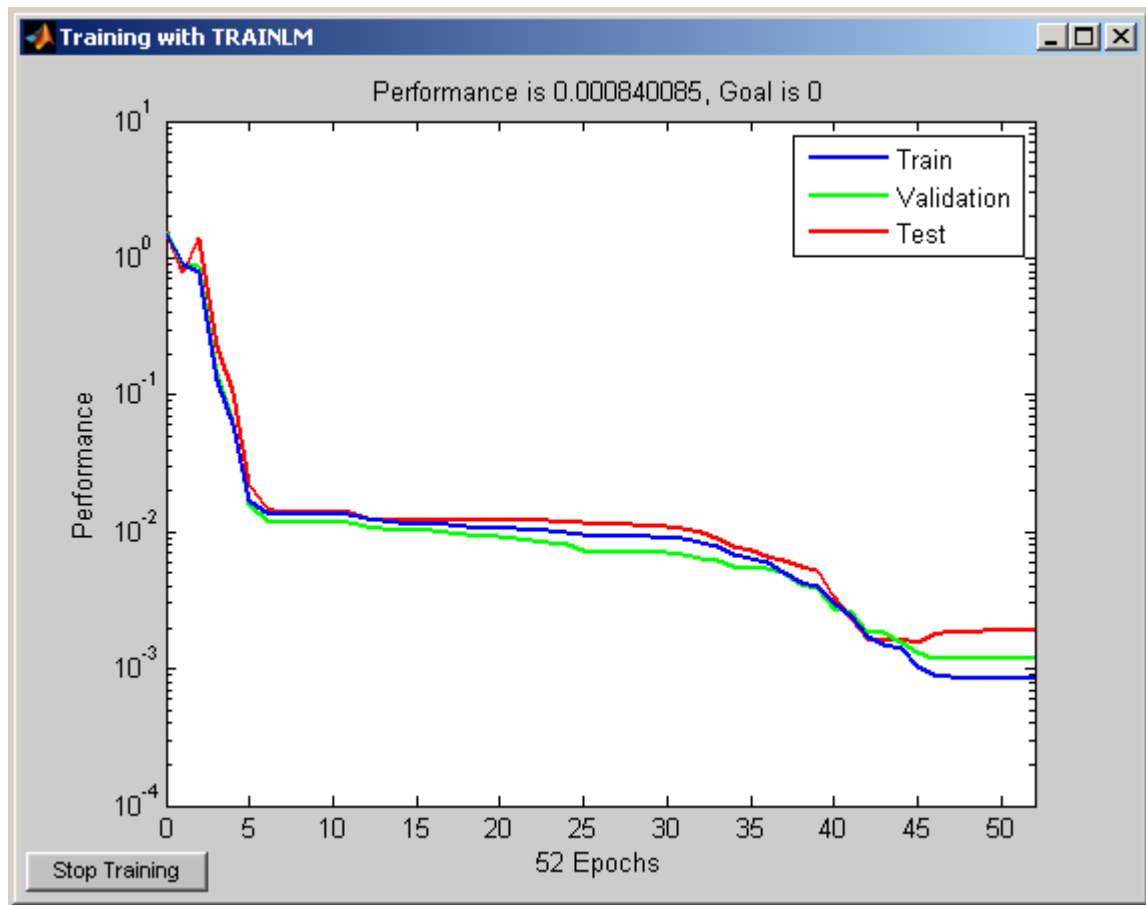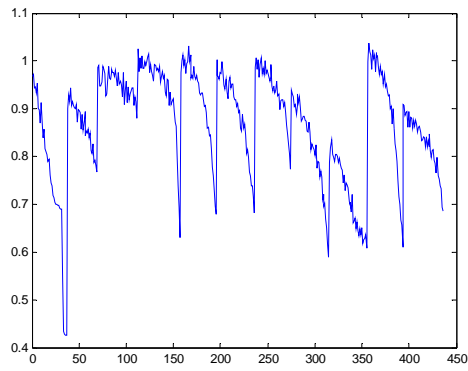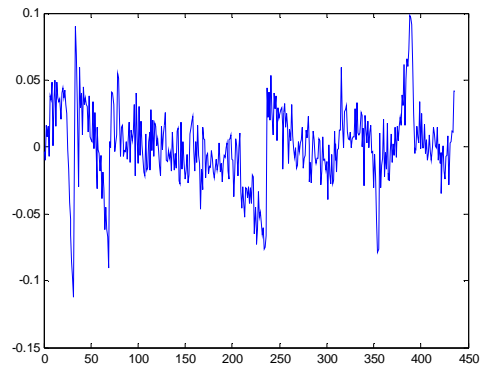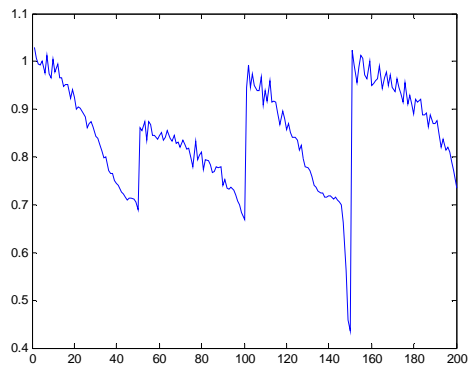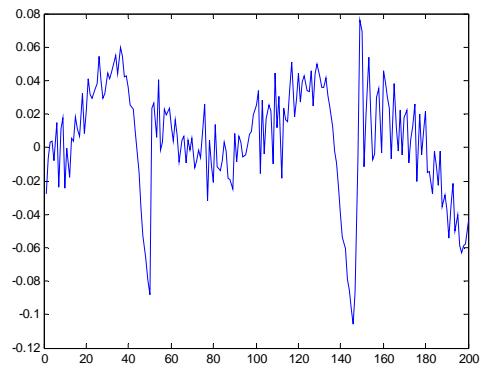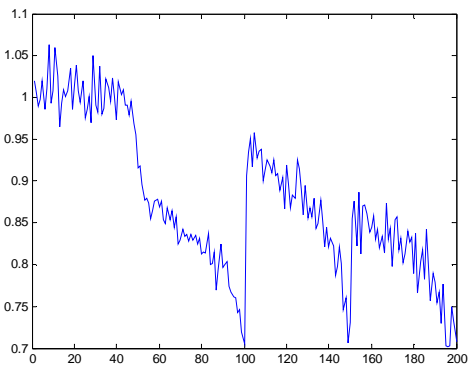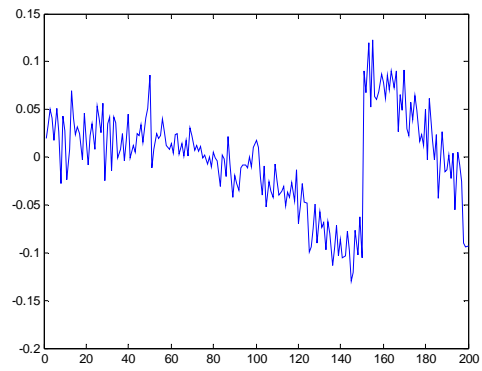

Figure 5.39: Network 17 Training Window

124

a)

b)
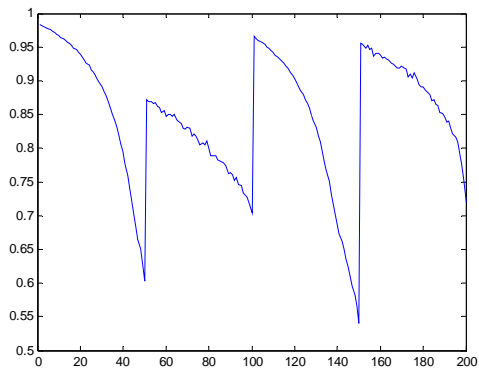
c)

d)

e)

f)

Figure 5.40: Network 17, 5 Neuron Average Normalized NiMH SOC Network, a) training set results, b) training set error, c) test set results, d)test set error, e) bad set results, f) bad set error

125

Table 5.17: Network 17 Error Statistics

Network 17	Mean error	Max error
Training set	0.0344	0.4586
Test set	0.0165	0.0656
Bad set	0.0562	0.1534

Network 17 has adequate performance overall, but it has poor performance on difficult tasks, such as modeling the sharp SOC changes in the Training set or the difficult batteries in the Bad set. Ultimately, the generally average performance of normalized NiMH ANNs is due to the relatively high training MSE. As usual, no hidden layer neuron count preference was in evidence.

5.3.7   *Unnormalized NiMH SOC Estimation Research*

This section analyzes NiMH SOC estimation using unnormalized input data. Network 18 represents an average network while Network 19 is a good network, on average, most networks will look like Network 18 after training but a couple retraining will generate one like Network 19.

1) *Network 18*: Network 18 is an average training result for NiMH SOC estimation networks using unnormalized data, its training and testing results are displayed in figure 5.41, 5.42, and table 5.18 below. Network 18 has 5 neurons in its hidden layer, it took 52 training epoch to reach a MSE of 0.00084, figure 5.41 displays all 52 training epochs.
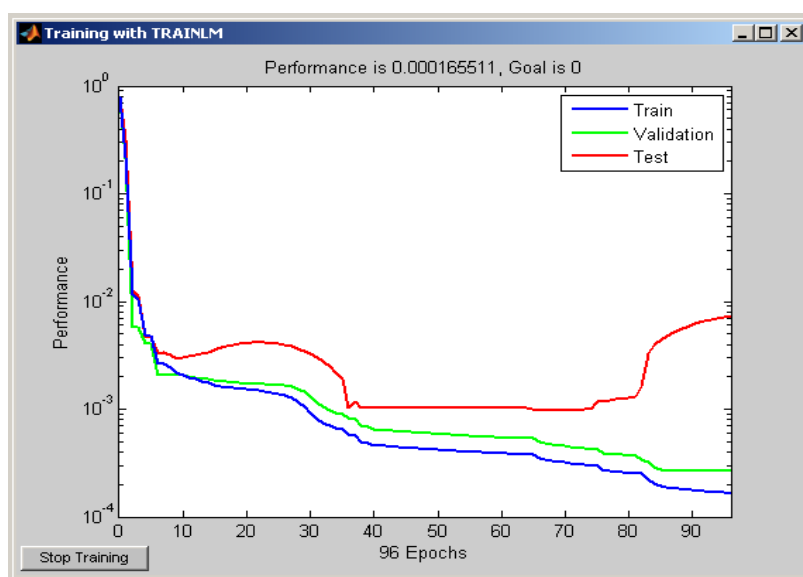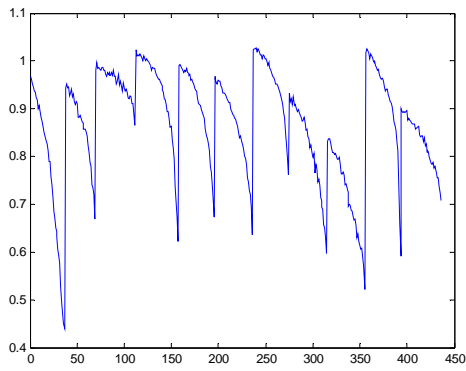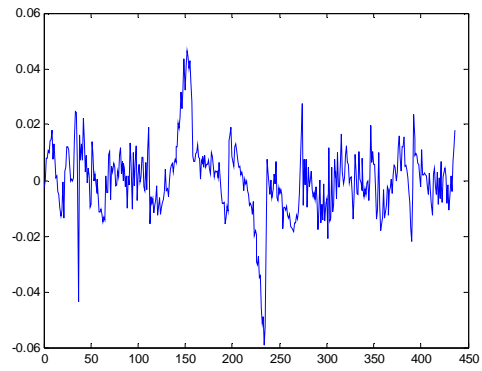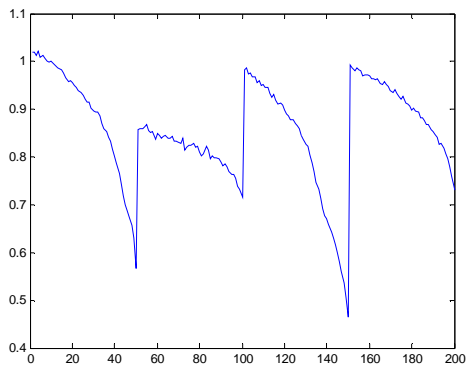
Figure 5.41: Network 18 Training Window

Figure 5.42: Network 18, 5 Neuron Average Unnormalized NiMH SOC Network, a) training set results, b) training set error, c) test set results, d)test set error, e) bad set results, f) bad set error

128

Table 5.18: Network 18 Error Statistics

Network 18	Mean error	Max error
Training set	0.0212	0.1125
Test set	0.0261	0.1056
Bad set	0.0389	0.1302

Network 18 has a good overall performance, similar to Network 17's but with lower max error due to better SOC drop and Bad set battery modeling. The high max errors are due mainly to poor drop performance, although Network 18 has improved over Network 17 it still needs more improvement to be acceptable.

2) *Network 19*: Network 19 is a good training result for NiMH SOC estimation networks using unnormalized data, its training and testing results are displayed in figure 5.43, 5.44, and table 5.19 below. Network 19 has 5 neurons in its hidden layer, it took 96 training epoch to reach a MSE of 0.000165, figure 5.43 displays all 96 training epochs.

Figure 5.43: Network 19 Training Window
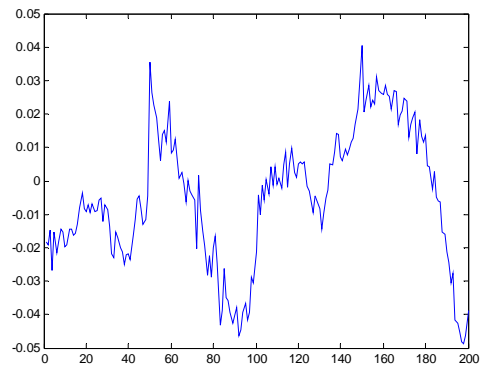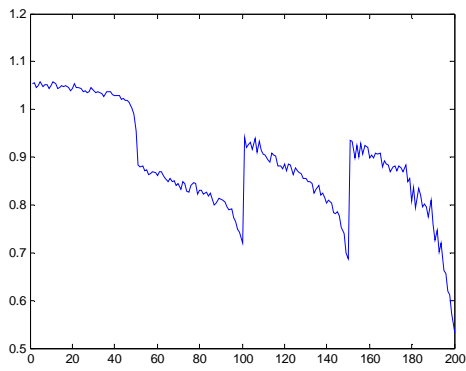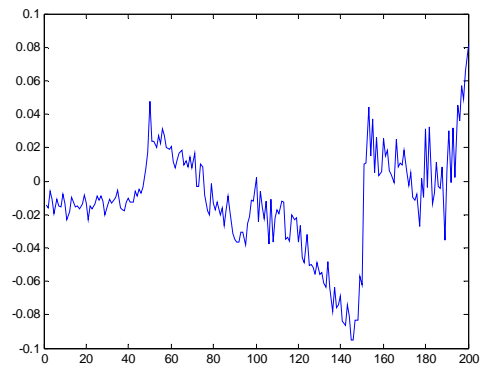
Figure 5.44: Network 19, 5 Neuron Good Unnormalized NiMH SOC Network, a) training set results, b) training set error, c) test set results, d)test set error, e) bad set results, f) bad set error

130

Table 5.19: Network 19 Error Statistics

Network 19	Mean error	Max error
Training set	0.0091	0.059
Test set	0.0166	0.0486
Bad set	0.0244	0.0951

Network 19 has great overall performance, with approximately half the mean and max error of Network 18. This improvement is due to Network 19's four times smaller MSE. Network 19 offers an acceptable level of performance with a 2.44% average SOC error.

Final results show that NiMH SOC networks have an acceptable level of performance in general, but more so using unnormalized data due to the smaller MSE. No definitive reason can be found to explain why unnormalized data performs better; all of the networks have similar SOC waveforms and similar mean errors. In terms of hidden layer neuron count, all counts performed identically and only training MSE determines network accuracy. Unfortunately 0.001 is the smallest MSE generated, no perfect networks exist.
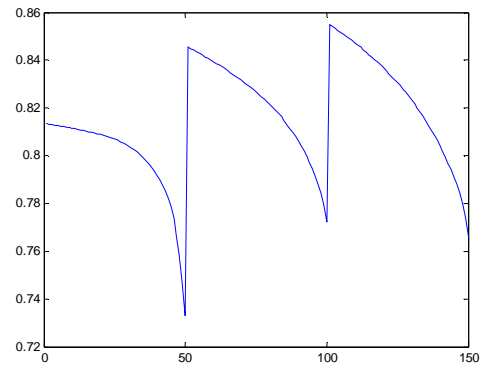
5.3.8   *SLA SOC Estimation Setup*

The third SOC subsection is the SLA SOC estimation research. Figure 5.45 below shows the three datasets used for SLA SOC estimation, figure 5.45.a is the training set, 5.45.b is the test set that contains mostly clean data, and 5.45.c is the bad set that contains all remaining data sets not used in the first two including irregular ones due to damaged batteries or measurement errors. These dataset are not randomized so that the results for each individual battery set can be evaluated. Additionally, the

131
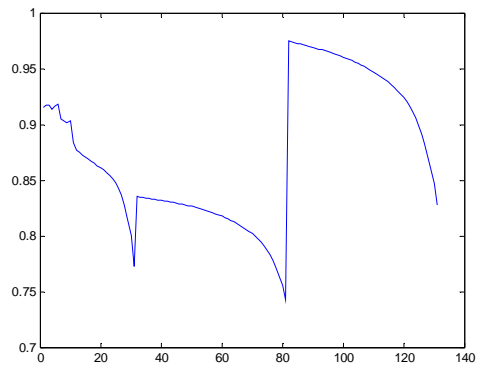
nonlinear decreasing SOC plots demonstrate SLA's declining power output with declining SOC.
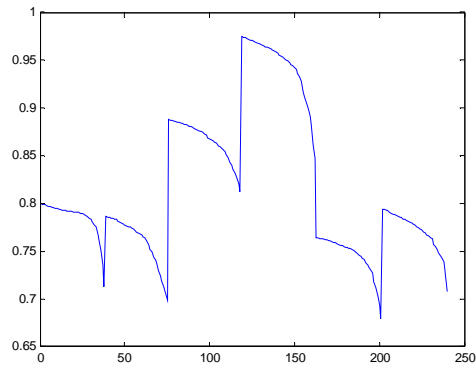
a)   b)

c)

Figure 5.45: Original SLA SOC Estimation Plots, a) Training set, 240 samples, b) Test set, 150 samples, c) Bad set, 131 samples

5.3.9 *Unnormalized SLA SOC Estimation Research*

This section analyzes SLA SOC estimation using unnormalized input data. Network 20 represents an average network while Network 21 is a good network, on average, most networks will look like Network 20 after training but a few retraining will generate one like Network 21.

1) *Network 20*: Network 20 is an average training result for SLA SOC estimation networks using unnormalized data, its training and testing results are displayed in figure 5.46, 5.47, and table 5.20 below. Network 20 has 5 neurons in its hidden layer, it took 166 training epoch to reach a MSE of $1.838*10^{-6}$, figure 5.46 displays all 166 training epochs.
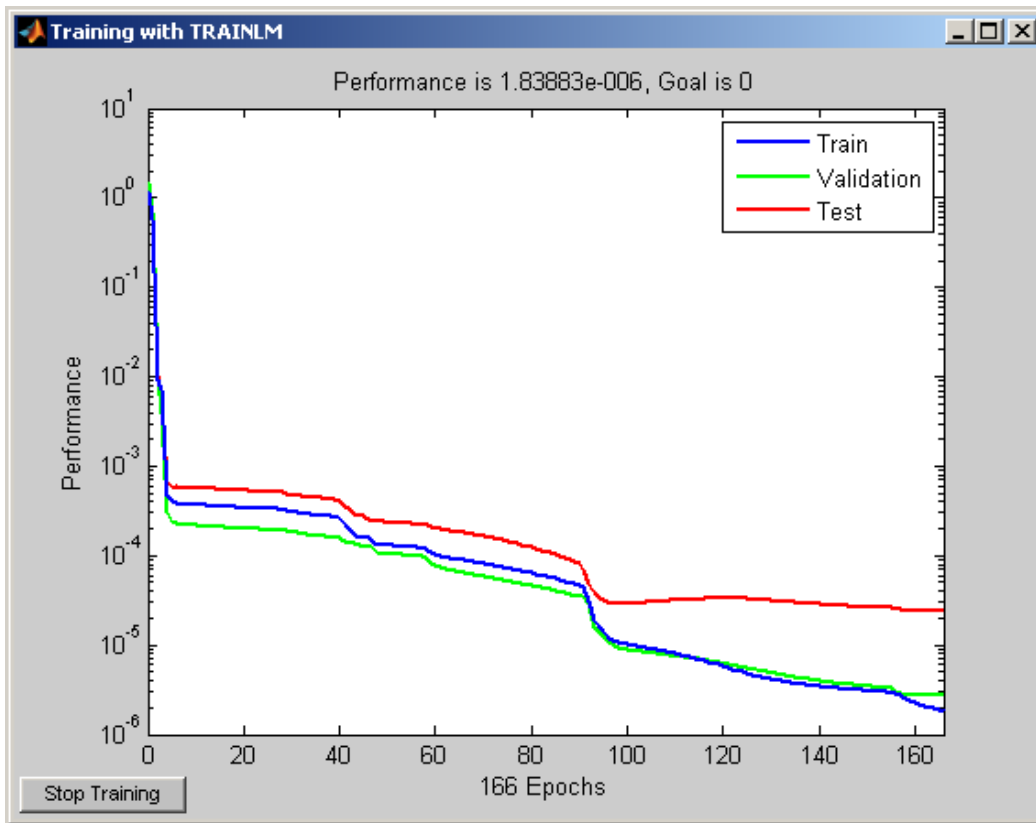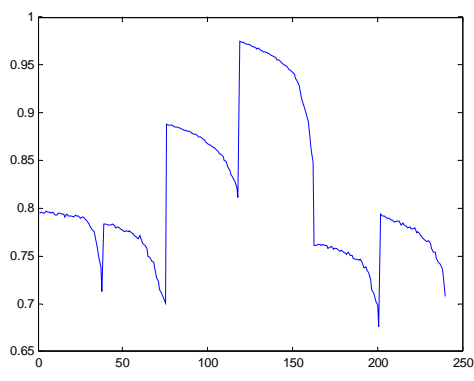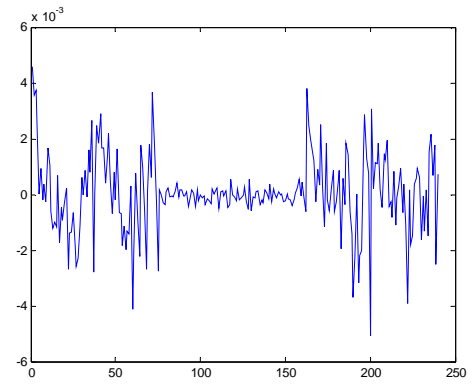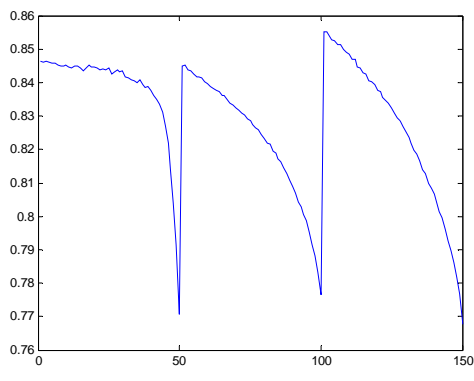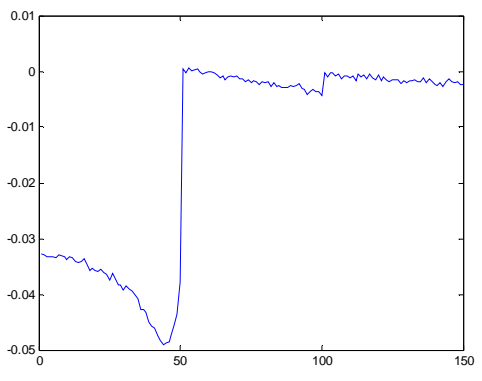

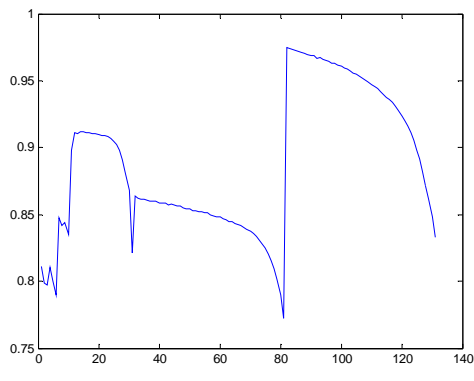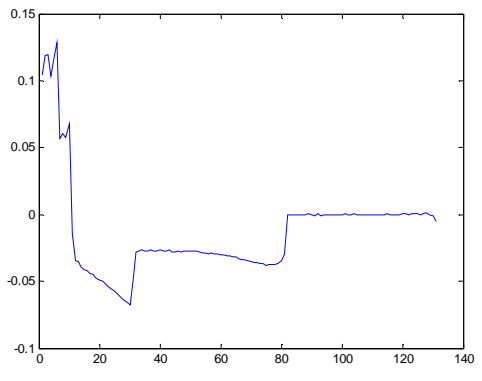Figure 5.46: Network 20 Training Window

a)

b)

c)

d)

e)

f)

Figure 5.47: Network 20, 5 Neuron Average Unnormalized SLA SOC Network, a) training set results, b) training set error, c) test set results, d)test set error, e) bad set results, f) bad set error

134

Table 5.20: Network 20 Error Statistics

Network 20	Mean error	Max error
Training set	9.2204e-004	0.0051
Test set	0.0139	0.0491
Bad set	0.0268	0.1281

Network 20 has a very good performance, with a small mean error and reasonably small max error except on the notorious distorted waveform of the Bad set. Neglecting that terrible waveform, Network 20 has less than 0.05 max error on the Bad set as well.

2) *Network 21*: Network 21 is a good training result for SLA SOC estimation networks using unnormalized data, its training and testing results are displayed in figure 5.48, 5.49, and table 5.21 below. Network 21 has 10 neurons in its hidden layer, it took 209 training epoch to reach a MSE of 7.465*10^-7, figure 5.48 displays all 209 training epochs.
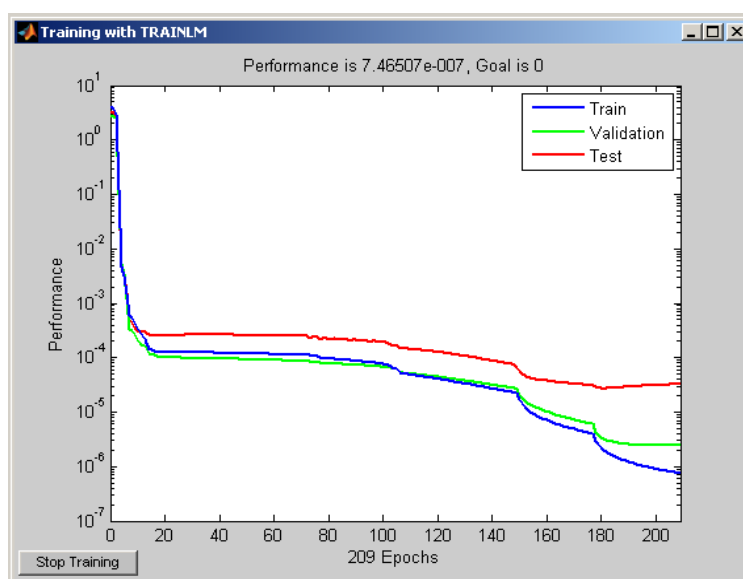

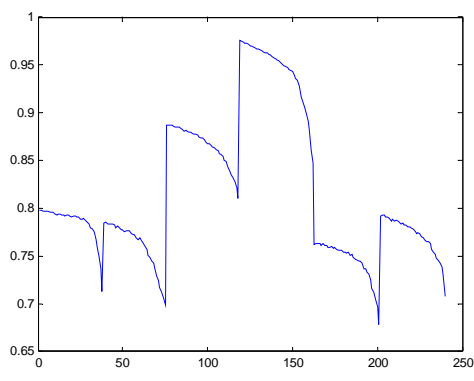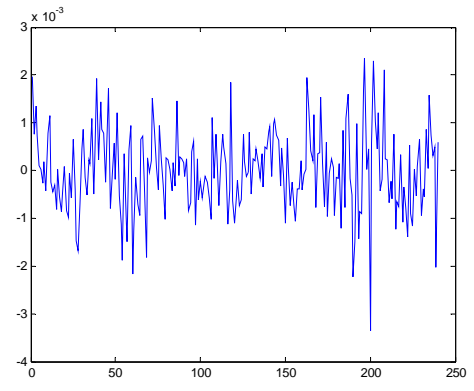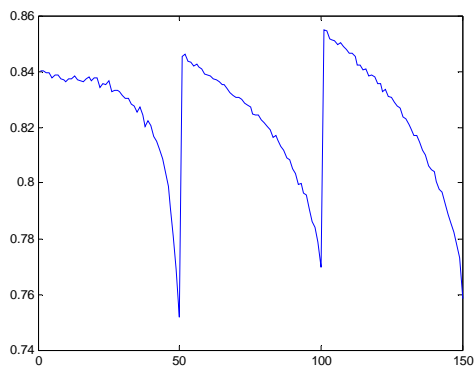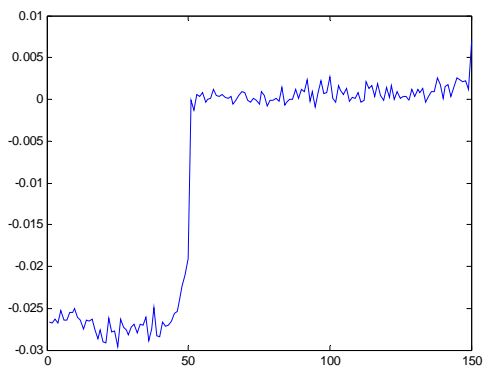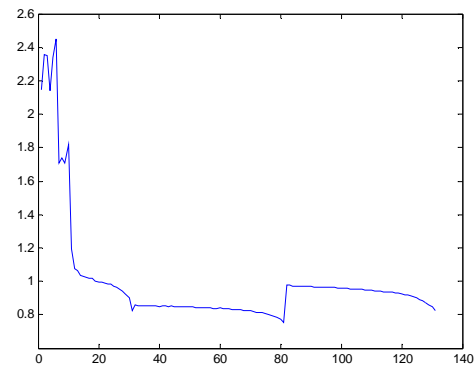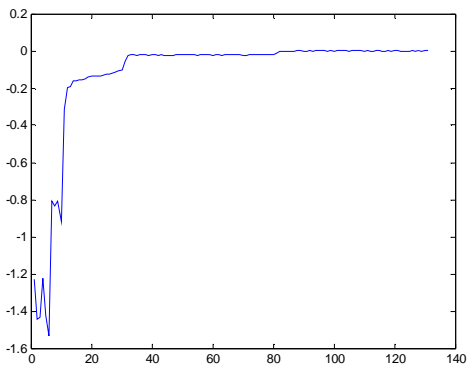Figure 5.48: Network 21 Training Window

Figure 5.49: Network 21, 10 Neuron Good Unnormalized SLA SOC Network, a) training set results, b) training set error, c) test set results, d)test set error, e) bad set results, f) bad set error

136

Table 5.21: Network 21 Error Statistics

Network 21	Mean error	Max error
Training set	6.7327e-004	0.0033
Test set	0.0094	0.0296
Bad set	0.1200	1.53

Network 21 has very good performance, with an extremely small 0.94% mean error and 2.96% max error. The results for the Bad set are misleading because the extremely high max error is skewing the mean error results; and although the distorted set is blown out of proportions, the remaining plots have almost zero max error.

The results for unnormalized SLA SOC estimation show that SLA networks have very good performance in general but find it especially difficult to model the distorted waveform in the Bad set.

5.3.10 *Normalized SLA SOC Estimation Research*

This section analyzes SLA SOC estimation using normalized input data. Network 22 represents an average network while Network 23 is a perfect network, on average, most networks will look like Network 22 after training but several retraining will generate one like Network 23.

1) *Network 22*: Network 22 is an average training result for SLA SOC estimation networks using normalized data, its training and testing results are displayed in figure 5.50, 5.51, and table 5.22 below. Network 22 has 10 neurons in its hidden layer, it took 176 training epoch to reach a MSE of $1.399*10^{-5}$, figure 5.50 displays all 176 training epochs.
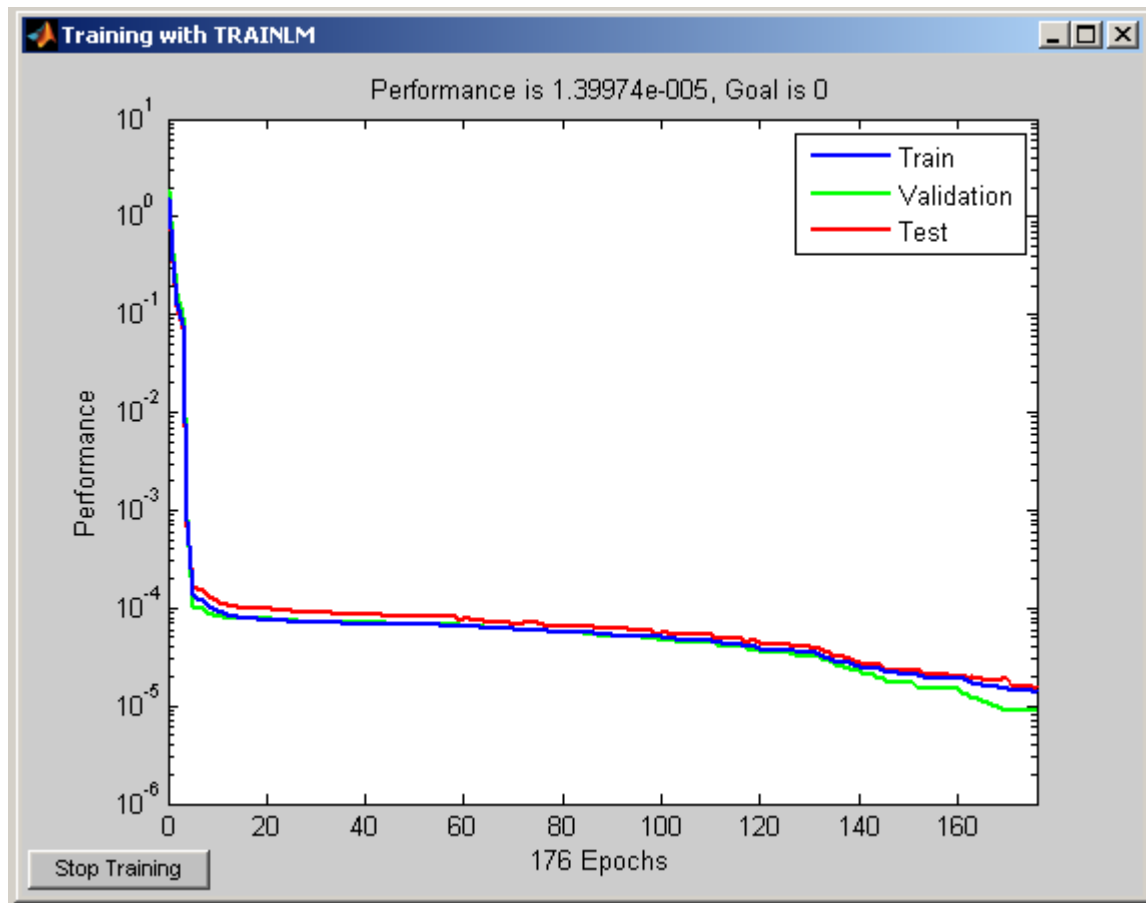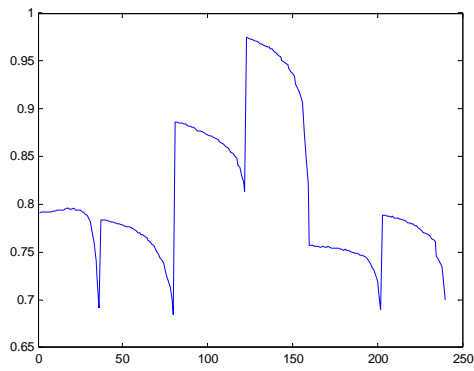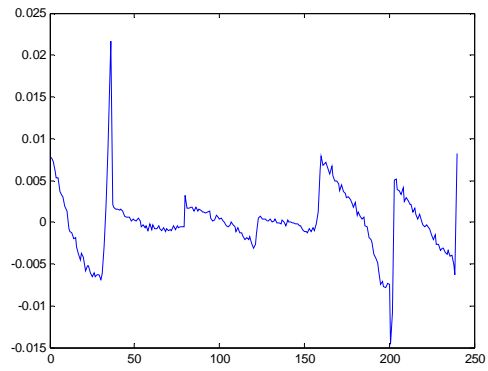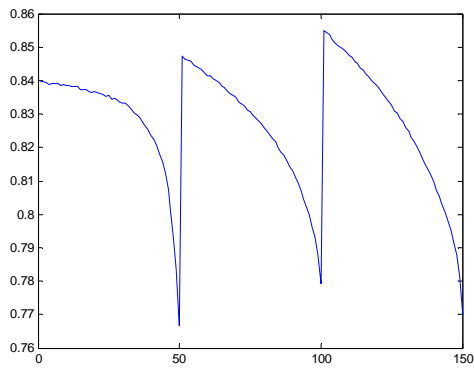
Figure 5.50: Network 22 Training Window

Figure 5.51: Network 22, 10 Neuron Average Normalized SLA SOC Network, a) training set results, b) training set error, c) test set results, d)test set error, e) bad set results, f) bad set error

139

Table 5.22: Network 22 Error Statistics

Network 22	Mean error	Max error
Training set	0.0025	0.0217
Test set	0.0121	0.0361
Bad set	0.0211	0.0683

Network 22 shows a remarkable improvement over the unnormalized SLA SOC networks. Although the Training set max error is higher, Network 22 is able to model the distorted waveform extremely well. These results are even more remarkable considering that Network 22 has a MSE ten times higher that Network 20.

2) *Network 23*: Network 23 is a perfect training result for SLA SOC estimation networks using normalized data, its training and testing results are displayed in figure 5.52, 5.53, and table 5.23 below. Network 23 has 5 neurons in its hidden layer, it took 743 training epoch to reach a MSE of 9.159*10^-10, figure 5.52 displays all 743 training epochs.

Figure 5.52: Network 23 Training Window

140
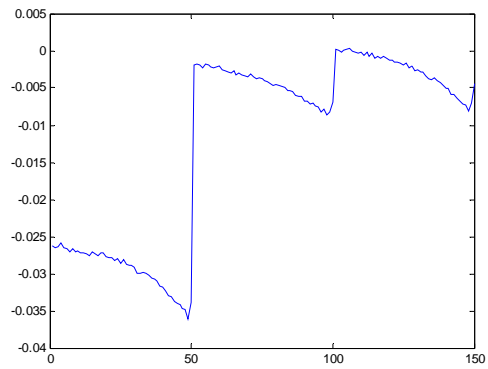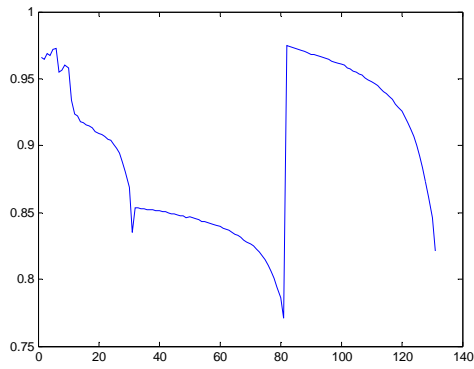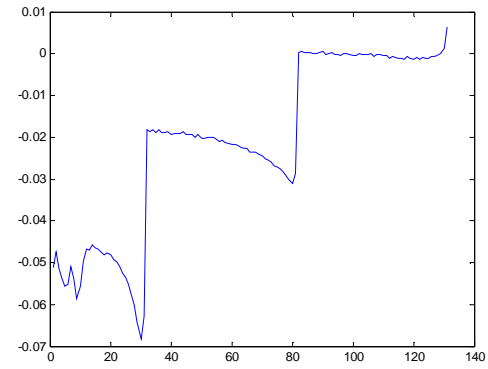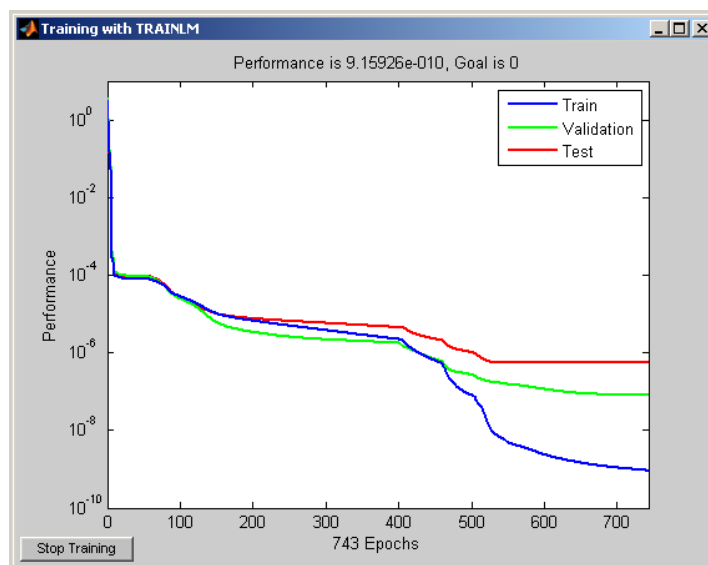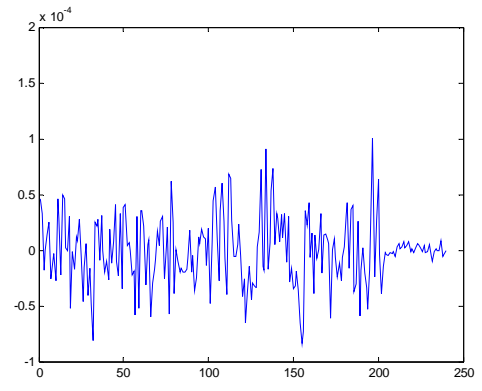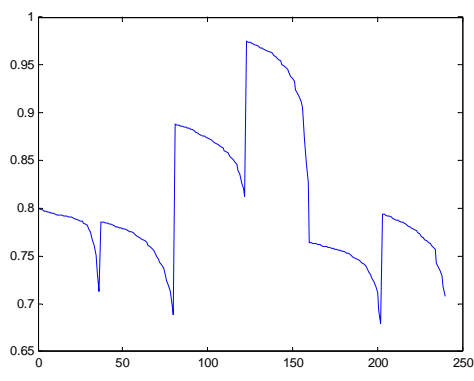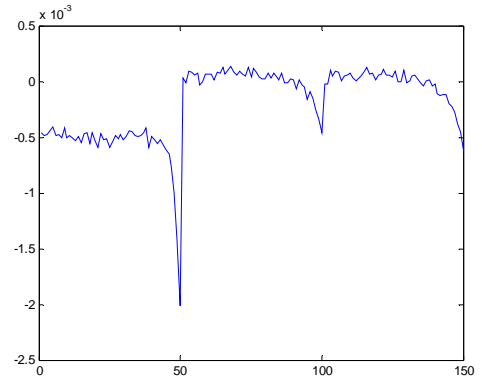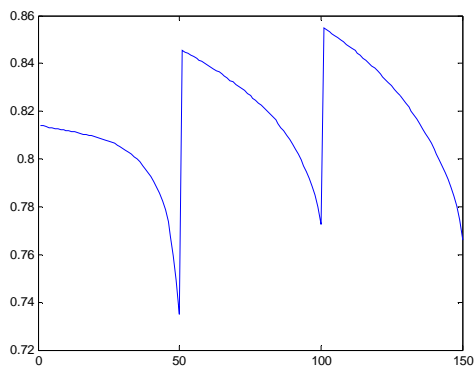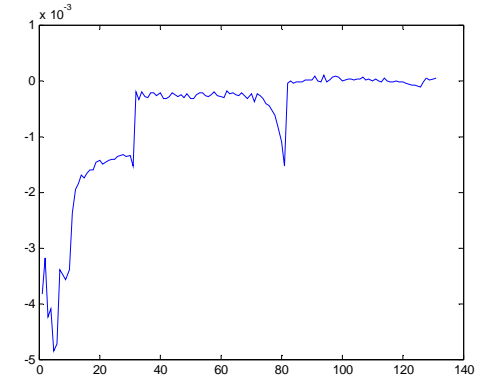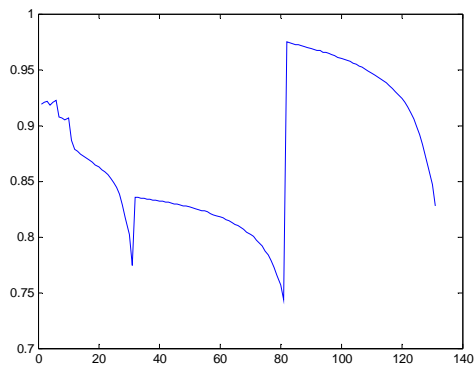
Figure 5.53: Network 23, 5 Neuron Perfect Normalized SLA SOC Network, a) training set results, b) training set error, c) test set results, d)test set error, e) bad set results, f) bad set error

Table 5.23: Network 23 Error Statistics

Network 23	Mean error	Max error
Training set	2.2867e-005	0.0001
Test set	2.4561e-004	0.002
Bad set	6.8875e-004	0.0048

Network 23 has practically perfect performance, with an absolute maximum error of 0.48% on the distorted waveform. Although this network is a perfect example, it took relatively few retrains to generate it, and based on the overall low training MSEs this network is not a rare result.

Final results show that all SLA SOC networks do remarkably well in general, though the normalized versions perform even better due to their superior Bad set modeling. The overall high accuracy of these networks is due to their extremely low average training MSE. And as usual, no distinction can be made between hidden layer neuron counts.

5.3.11 *Conclusions for SOC Estimation Research*

The final results for SOC estimations show that results ranging from average to exceptional can be achieved with a well trained network using normalized input data. A case by case review shows that Li-Ion and SLA networks had a remarkable performance improvement using normalized input data while the NiMH network had a moderate decrease in performance, so overall normalized input data is the best choice for all chemistry types. Concerning NiMH SOC network performance, NiMH's all around mediocre performance is surprising considering how well the Li-Ion and SLA networks performed; usually Li-Ion is the most difficult because of its relatively flat

voltage profile, but even the heavily distorted SLA plot had overall better performance when normalized data was used. In all likelihood, the NiMH tests suffered from low quality sample data.

5.3.12 *Conclusions for Neural Network Method*

Final results for the complete ANN method show greater than 93% accurate chemistry detection and less than 2.44% average SOC error over damaged batteries, while healthy batteries have almost 100% accurate chemistry detection and less than 1.6% average SOC error. These results are excellent overall, but as the chemistry detection networks show, the maximum accuracy is ultimately limited by the quality of testing data available. However, the Neural Network method's consistent inability to correctly identify the same known bad battery sets is actually an asset that indicates this method's potential in future SOH research. In the mean time, using larger, error free training sets or designing a network around a specific target battery will remove most of the intentional errors and result in a far more powerful and precise battery detection and monitoring system.

CHAPTER 6

CONCLUSIONS AND FUTURE WORK

6.1 Conclusions

The present paper represents a new battery identification method in which the type of chemistry, number and state-of-health for the cells within a battery package can be precisely monitored. Using analytical and artificial neural networks in an experimental setup, claims of the proposed method have been verified. This method can form the central part of a health monitoring and battery management system in an EV or HEV system. Of the methods presented here, the neural network shows the most promise, due to its high accuracy and repeatability, but all methods performed well and can be improved with further research. Improving upon the MSE method simply requires performing the arduous calibration process in order to find the optimal error weights. Improving on the Hybrid method and further improving on the Statistical Analysis method all require a more robust and reliable line fitting algorithm than the default one provided by LabView; one that is specifically tailored to the range of possible batteries, or at least able to maintain the proper shape. While the Neural Network method works great, its performance can easily be improved with a larger and cleaner training data and by adding current and temperature inputs which will extend the operating range. In regards to fixed battery SOC determination, the performance of

144

each method can be improved by redesigning the system around the target battery instead of using samples from a wide variety of cell counts and capacities.

To improve upon the hybrid method and to further improve the MSE method, we need to develop a more robust line-fitting program that is specifically tailored to our target parameter ranges. While the Neural Network method works great, its performance can be improved with more training data and by adding current and temperature inputs which will extend the operating range

6.2 Future work

The discoveries made during this research offer tremendous potential for future work. The foremost of which is the research and development of a SOH estimation method to add to the Neural Network Method. But other potential research projects include: modifying the proposed methods for a fixed battery system, adapting the methods away from a fixed charging cycle to a variable or random charging cycle, and adding Kalman filters and other advanced data collection techniques to improve the quality of the data collected. However, now that this research has provided proof of concept, future research can reduce or remove the purposely defective battery data that was included in this project; by removing these defective data sets, all future work is likely to demonstrate a dramatic increase in accuracy and reliability.

REFERENCES

[1] bq2000 datasheet, http://focus.ti.com/lit/ds/symlink/bq2000.pdf

[2] D. Rutz and R. Jansen, "BioFuel Technology Handbook". WIP Renewable Energies, February 2007.

[3] S. Grewal and S.A. Grant, "A Novel Technique for Modeling the State of Charge of Lithium Ion Batteries Using Artificial Neural networks," *INTELEC 2001*, 14-18 Oct 2001 Conf. Pub. No. 484.

[4] David Linden, Thomas B. Reddy (ed). Handbook Of Batteries 3rd Edition. McGraw-Hill, New York, 2002 ISBN 0-07-135978-8 page 23.1

[5] David Linden, Thomas B. Reddy (ed). Handbook Of Batteries 3rd Edition. McGraw-Hill, New York, 2002 ISBN 0-07-135978-8 page 23.7

[6] United States Patent 5,948,567

[7] Case History, "In Search of the Perfect Battery," The Economist print edition, Mar 6, 2008

[8] David Linden, Thomas B. Reddy (ed). Handbook Of Batteries 3rd Edition. McGraw-Hill, New York, 2002 ISBN 0-07-135978-8 page 29.2

[9] David Linden, Thomas B. Reddy (ed). Handbook Of Batteries 3rd Edition. McGraw-Hill, New York, 2002 ISBN 0-07-135978-8 page 29.6

[10] I. Buchmann, "The nickel-based battery, its dominance and the future," Battery University.com

[11] S. Vorkoetter, "Choosing and Using Nickel-Metal-Hydride (NiMH) Rechargeable Batteries," Stefanv.com

[12] D. DeCoster, "NiMH Batteries Projected to Replace Flywheels For Critical Bridge Time Applications" *Battery Power: Products and Technology*, vol 11 issue 1, Feb 2007

[13] P. Rybski, "NiMH Batteries, Chevron Patents and the Future of Plug-in Hybrid Cars" SEA.com

[14] M. Whittingham, "Electrical Energy Storage and Intercalation Chemistry." *Science*. Vol. 192. no. 4244, pp. 1126 – 1127, 11 June 1976

[15] M.M. Thackeray, W.I.F. David, P.G. Bruce, J.B. Goodenough, "Lithium insertion into manganese spinels, Materials Research Bulletin," Volume 18, Issue 4, April 1983, Pages 461-472, ISSN 0025-5408

[16] A. K. Padhi, K. S. Nanjundaswamy, and J. B. Goodenough, "Phospho-olivines as Positive-Electrode Materials for Rechargeable Lithium Batteries" J. Electrochem. Soc. 144, 1188

[17] David Linden, Thomas B. Reddy (ed). Handbook Of Batteries 3rd Edition. McGraw-Hill, New York, 2002 ISBN 0-07-135978-8 page 35.2

[18] M. Silberberg, *Chemistry: The Molecular Nature of Matter and Change*, 4th Ed. New York (NY): McGraw-Hill Education. p 935. 2006.

[19] "Rechargeable Lithium Batteries." Electropaedia.com

http://www.mpoweruk.com/lithiumS.htm#lto

[20] J. Geraci, "Using the Cell Broadband Engine to Compute an Electrochemical Battery Model" Technical Report (MIT, Research Laboratory of Electronics), 721 http://hdl.handle.net/1721.1/37586

[21] Doyle, M., Fuller, T. and Newman, J. "Modeling of Galvanostatic Charge and Discharge of a Lithium/Polymer/Insertion Cell," Journal of the Electrochemical Society; vol. 140, no. 6; June 1993; pp. 1526-1533.

[22] R.C. Kroeze, P.T Krein. "Electrical battery model for use in dynamic electric vehicle simulations," Power Electronics Specialists Conference, 2008. PESC 2008. IEEE, vol., no., pp.1336-1342, 15-19 June 2008

[23] Miyamoto, H.; Morimoto, M.; Morita, K., "On-line SOC Estimation of Battery for Wireless Tram Car," *Power Electronics and Drive Systems, 2007. PEDS '07. 7th International Conference on*, vol., no., pp.1624-1627, 27-30 Nov. 2007

[24] MatLab Neural Network Toolbox User's Guide www.mathworks.com/access/helpdesk/help/pdf_doc/nnet/nnet.pdf

[25] Samangkool, K.; Premrudeepreechacharn, S., "Maximum power point tracking using neural networks for grid-connected photovoltaic system," *Future Power Systems, 2005 International Conference on*, vol., no., pp.4 pp.-4, 18-18 Nov. 2005 URL: http://ieeexplore.ieee.org/stamp/stamp.jsp?arnumber=1600488&isnumber=33649

[26] Cai, C.H.; Du, D.; Liu, Z.Y., "Battery state-of-charge (SOC) estimation using adaptive neuro-fuzzy inference system (ANFIS)," *Fuzzy Systems, 2003. FUZZ '03. The 12th IEEE International Conference on*, vol.2, no., pp. 1068-1073 vol.2, 25-28 May

2003

URL: http://ieeexplore.ieee.org/stamp/stamp.jsp?arnumber=1206580&isnumber=27148

[27] Shen, W.X.; Chan, C.C.; Lo, E.W.C.; Chau, K.T., "Adaptive neuro-fuzzy modeling of battery residual capacity for electric vehicles," *Industrial Electronics, IEEE Transactions on*, vol.49, no.3, pp.677-684, Jun 2002

URL: http://ieeexplore.ieee.org/stamp/stamp.jsp?arnumber=1005395&isnumber=21696

[28] Chenghui Cai; Dong Du; Zhiyu Liu; Jingtian Ge, "State-of-charge (SOC) estimation of high power Ni-MH rechargeable battery with artificial neural network," *Neural Information Processing, 2002. ICONIP '02. Proceedings of the 9th International Conference on*, vol.2, no., pp. 824-828 vol.2, 18-22 Nov. 2002

URL: http://ieeexplore.ieee.org/stamp/stamp.jsp?arnumber=1198174&isnumber=26965

[29] Singh, P.; Kaneria, S.; Broadhead, J.; Wang, X.; Burdick, J., "Fuzzy logic estimation of SOH of 125Ah VRLA batteries," *Telecommunications Energy Conference, 2004. INTELEC 2004. 26th Annual International*, vol., no., pp. 524-531, 19-23 Sept. 2004

URL: http://ieeexplore.ieee.org/stamp/stamp.jsp?arnumber=1401519&isnumber=30390

149

BIOGRAPHICAL INFORMATION

Matthew Ragsdale was born in Dallas, Texas in 1984. He completed his undergraduate studies at the University of Texas at Arlington and received his B. S. degree in Electrical Engineering in May 2007. He continued on as a graduate student at the University of Texas at Arlington in order to work under Dr. Babak Fahimi in the Renewable Energy and Vehicular Motion Lab while pursuing his Masters degree in Electrical Engineering. His current research interests include Battery Management, Renewable Energy, Power Electronics, and Microcontrollers.